Spring 2016

Thermal characterization of phase change materials for thermal energy storage

Rami Mohammad Reda Saeed

THERMAL CHARACTERIZATION OF PHASE CHANGE MATERIALS FOR THERMAL ENERGY STORAGE

by

RAMI MOHAMMAD REDA SAEED

A THESIS

Presented to the Faculty of the Graduate School of the

MISSOURI UNIVERSITY OF SCIENCE AND TECHNOLOGY

In Partial Fulfillment of the Requirements for the Degree

MASTER OF SCIENCE IN NUCLEAR ENGINEERING

2016

Approved by

Joshua P. Schlegel, Advisor
Carlos H. Castano
Lokeswarappa Dharani

ABSTRACT

The study provides a valuable and useful database for Phase Change Materials (PCMs) for Thermal Energy Storage (TES) applications. Only a few existing studies have provided an overall investigation of thermophysical properties of PCMs in this detailed manner. Several organic PCMs, namely Myristic acid, Capric Acid, Lauryl Alcohol, Palmitic acid and Lauric acid, have been characterized after being carefully selected to cover wide range of TES applications. Insights and information gained from this work will be applied toward the design and modelling of many low temperature thermal energy storage applications. The study experimentally investigated uncertainty of thermal characterization of PCMs by DSC analysis and the various thermal events and effects that occur when PCMs are tested in a DSC. The optimum measurement condition was found to be at a heating rate of 3°C/min and a sample mass of 7.5 mg. Furthermore, the study discovered a novel PCM eutectic mixture of 60% Methyl Palmitate (MP) and 40% Lauric Acid that can be readily adapted to large-scale industrial production to help improve the performance of energy systems, particularly in buildings. Further effort has been devoted to develop a final formulation of the PCM eutectic mixture characterized by a solid to gel phase transformation using Methyl hydroxyethyl cellulose as a gelling/thickening agent, and an enhanced thermal performance using Nano-graphene platelets (NGPs). The corresponding enhancement when 10% of NGPs was added was as follows: thermal conductivity was increased by about 97.7%, the specific heat capacity was increased by 52% for solid phase and 64% for liquid phase, the thermal diffusivity increased by 42% for solid phase and 54% for liquid phase.

ACKNOWLEDGMENTS

My deepest gratitude is to my advisor, Dr. Joshua Schlegel, who has always been a tremendous mentor and guardian at the same time. I am grateful to him for holding me to a high research standards and guiding me to meet those standards. Your knowledge and friendly nature makes me so proud to be known as your student. Beside my advisor, my sincere thanks also goes to Dr. Sawafta, who provided me an opportunity to visit them as a trainee, and who gave access to their laboratory and research facilities. Special thanks to Dr. Castano, for his advice, support, and encouragement. I have never met a friendly person like you. My sincere thanks to the rest of my committee: Dr. Dahrani and Dr. Lee for their insightful comments and suggestions.

I would also like to thank my friends, Hakim, Otoom, Aziz, Majdi, and Sachin for their support and encouragement during my graduate studies in the U.S. I had a wonderful time all these years because of you. I have to give a special mention for the best brother and friend I have ever known, Saif. Thank you for all the concern, support and strength all these years.

I would like to thank my family to whom this thesis is dedicated to. Thank you for all of the sacrifices that you've made on my behalf, you have always been inspiring and I never would have made it here without you. Last but not least, I have to give a special mention for the support given by the best person in my life, Safaa. There are no proper words to convey my deep gratitude for you. Even from a distance, you have been a constant source of love, support, strength, and encouragement every day. There is no way to express how much it meant to me to have you in my life.

TABLE OF CONTENTS

LIST OF ILLUSTRATIONS

Page

LIST OF TABLES

Page

1. INTRODUCTION

1.1. OBJECTIVES

The study aimed to provide a valuable and useful database for Phase Change Materials (PCMs) for low temperature Thermal Energy Storage (TES) applications. Only a few existing studies provided an overall investigation of the thermophysical properties of PCMs in a detailed manner. The study characterized several PCMs that have been carefully selected to cover wide range of TES applications. The study also presents the state of the art methodologies and standards to characterize these materials with the highest accuracy. Moreover, systematic and rational approaches have been used to discover a novel enhanced energy storage material that holds promise to achieve attributes that other materials cannot achieve. A new eutectic PCM mixture was discovered and characterized for thermal energy storage in buildings. The prepared eutectic PCM mixture was further enhanced by adding gel, and by enhancing the overall thermal performance using nano-additives.

In recent decades the limited reserves of fossil fuel, the rapid growth of global energy consumption, and the increased environmental concerns of greenhouse gas emissions have shed the light on the importance of effectively utilizing energy. For that reason developing new sources of energy has been the focus of extensive research in the last decade. However some of those energy sources can only provide energy intermittently. Thermal Energy Storage (TES) using Phase Change Materials (PCMs) provides an elegant solution, inexpensive method, and efficient energy storage that can improve the performance of energy systems and fill the gap between energy supply and energy demand; giving the possibility of conserving the energy.

In sections 3.1 to 3.5, wide range of PCMs were carefully selected to cover a wide range of applications. The aim was to determine the thermophysical properties accurately with experiment. The determination of these properties with that accuracy provides an invaluable database to predict the behavior of these materials in a thermal energy storage system.

Section 3.2 in particular, aimed to reveal state of the art methodologies when PCMs are characterized using a Differential Scanning Calorimetry (DSC). Reviewing the published data shows that different results for PCMs are reported in literature when it is characterized by DSC analysis. The study aimed to prove that these differences are not due to variability of materials, but due to problems with the measurement mode itself. In order to provide an alternative methodology for the existing standards and methods of calorimetry which were designed for other materials than PCMs, the study aimed to parametrically carry out several measurements with the goal of analyzing the sensitivity and resolution of the DSC measurement technique with PCMs, and revealing the optimum conditions.

In 2016 the U.S. Energy Information Administration (EIA) reported in their review that 41% of all energies are consumed for residential and buildings sector. Heating and cooling applications alone are responsible for 60% of that value [1]. Therefore, the demand for reducing the dependency on fossil fuels for thermal comfort in buildings is rising increasingly. PCMs are considered an ideal solution when incorporated into the building through wallboards, ceiling, floor, Air-conditioning systems, and even by incorporating them directly through gypsum mixture, cement paste, and mortar. Despite the great efforts devoted to study a variety of PCMs, TES using these materials is very challenging and

some targets cannot be met with the existing materials. Therefore the research conducted in Section 3.6 involves systematic and rational approaches to discover a novel enhanced energy storage material that hold promise to achieve attributes that other materials cannot achieve. The first goal in section 3.6.1 was to discover a new eutectic PCM mixture as a promising PCM for thermal regulation and TES applications, particularly to reduce energy consumption and temperature swing in buildings. The second goal in section 3.6.2 was to further enhance the proposed eutectic PCM mixture by: 1) making a novel eutectic PCM characterized by a gel phase transformation feature which solve numerous practical engineering problems when PCMs are used for TES applications in buildings. 2) Enhancing the overall thermal performance using nano-additives.

1.2. LITERATURE REVIEW

1.2.1. Thermal Energy Storage. Thermal Energy Storage (TES) provides an elegant and realistic solution for more efficient energy use in many areas where there is a mismatch between the energy supply and demand. There are three common ways to store thermal energy: sensible heat, latent heat and thermo-chemical energy [2, 3]. Regardless of the method used to store thermal energy, materials are always the key issue

1.2.1.1 Sensible heat. In sensible heat storage, thermal energy is stored or released by charging or discharging the material over a range of temperature without changing the phase during this process [4]. Charging occurs by raising the temperature of a solid or liquid, while heat is released when temperature decreases. The amount of stored energy

depends on the amount of storage material, the specific heat capacity, and the temperature change.

$$Q = m\int_{T1}^{T2} C_p.dT \tag{1}$$

Where Q is the sensible heat stored, m: the mass of storage material, T_1 and T_2 represent the temperature range, C_p: the specific heat capacity at constant pressure.

1.2.1.2 Latent heat. Energy storage by latent heat is very attractive due its high storage density at constant temperature corresponding to the phase transition temperature [5]. Unlike sensible heat storage, latent heat storage offers a higher storage capacity and can absorb and release heat at a constant temperature while it undergoes a phase change. This is illustrated in Figure 1.1. When heat is applied, the material stores heat as latent heat of fusion and its phase changes from solid to liquid. When the temperature drops, the heat is released and the material changes its phase from liquid to solid.

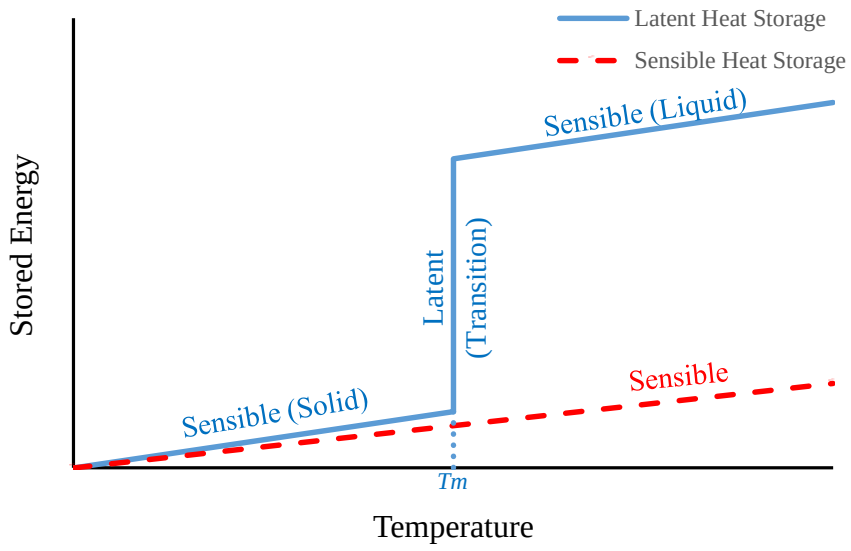

Figure 1.1. Performance comparison of latent heat and Sensible heat for TES.

Some latent heat storage materials like Phase change materials (PCMs) are capable of storing 5-14 times the heat per unit volume than conventional sensible storage materials such as water or rocks [6]. Compared to sensible heat storage, latent heat provides a huge energy storage capacity at a very narrow temperature range. For example, 1kg of ice at 0˚C requires 333kJ of energy, as a latent heat, to produce 1kg of water at 0˚C. The same amount of energy as a sensible heat is enough to raise the temperature of water from 0˚C to 80˚C. In order to determine the storage density of a latent heat storage system, the contributions of sensible heat over the entire temperature range of the process have to be considered in addition to the latent heat stored at the phase transition temperature [4]. The amount of energy stored for a latent heat storage system is given by:

$$Q = m\left[\int_{T1}^{Tm} C_{P\_Solid}.dT + \Delta h + \int_{Tm}^{T2} C_{P\_Liquid}.dT\right] \quad (2)$$

Where Q is the total thermal energy stored, the first term and last term represent the contributions of sensible heat of the solid and liquid phases, m: mass of storage material, T_1 and T_2 are the temperature range which the process operates, T_m: melting temperature, and Δh: latent heat of fusion.

1.2.1.3 Thermo-chemical energy. In thermo-chemical energy storage, thermal energy is stored and released by endothermic and exothermic reactions when molecular bonds are broken and reformed in a completely reversible chemical reaction [7]. The amount of stored energy is determined by the amount of storage material (m), the extent of conversion (a_r), and the heat of the reaction (Δh).

$$Q = ma_r\Delta h \quad (3)$$

Many processes that use thermo-chemical energy have been studied. However, thermal energy storage using this method is still very limited due to the high cost of such systems [8].

1.2.2. Classification of Phase Change Materials. PCMs, also called latent heat storage materials, are the most efficient method for latent heat TES. Energy per unit mass is stored during melting, and released during freezing at constant or narrow temperature range [2, 9]. PCMs have proven ability to improve the performance and reliability of thermal energy storage applications [10]. Recently PCMs have received great interest because of their high energy storage density and their ability to maintain a constant temperature while absorbing heat during melting and releasing heat when solidifying [9-12]. Specific interest has developed in the field of thermal management, solar energy systems, buildings, and greenhouses [12].

Any PCM that is used in a thermal energy storage system should meet several criteria related to thermophysical, kinetic, and chemical properties [13-15]: (1) Phase transition occurs within the desired operating temperature range of the system, so that the bulk of the added heat is stored as a latent heat within narrow temperatures; (2) high latent heat storage capacity; (3) high thermal conductivity to assist the absorption and release of energy in the storage system; (4) high specific heat capacity to provide additional sensible heat storage; (5) small volume changes in the phase transformation; (6) high density; (7) high nucleation rate to avoid supercooling of the liquid phase; supercooling is an effect in which the material exhibits a substantially lower freezing point than its melting point; (8) chemical stability and no degradation for large number of cycles; (9) non-toxicity; (10)

non-flammable; (11) no corrosion influence if used in certain structural materials; (12) relatively low cost and high availability.

Many PCMs do not fully meet all of these requirements for an ideal TES system. However, a wide range of technical and novel solutions have been developed. For instance, nanomaterial additives and metallic fins can be used to increase effective thermal conductivity [12, 16, 17]. Nucleating agents can help by suppressing the supercooling effect [18]. Many other new integrated containers and designs are currently of interest and still under development to avoid many potential problems [18].

A wide range of PCMs are currently available with varying thermal properties and and wide range of working temperature. Figure 1.2 shows the classification of Solid-Liquid PCM families; divided as Organic, Inorganic, and Eutectic [7].

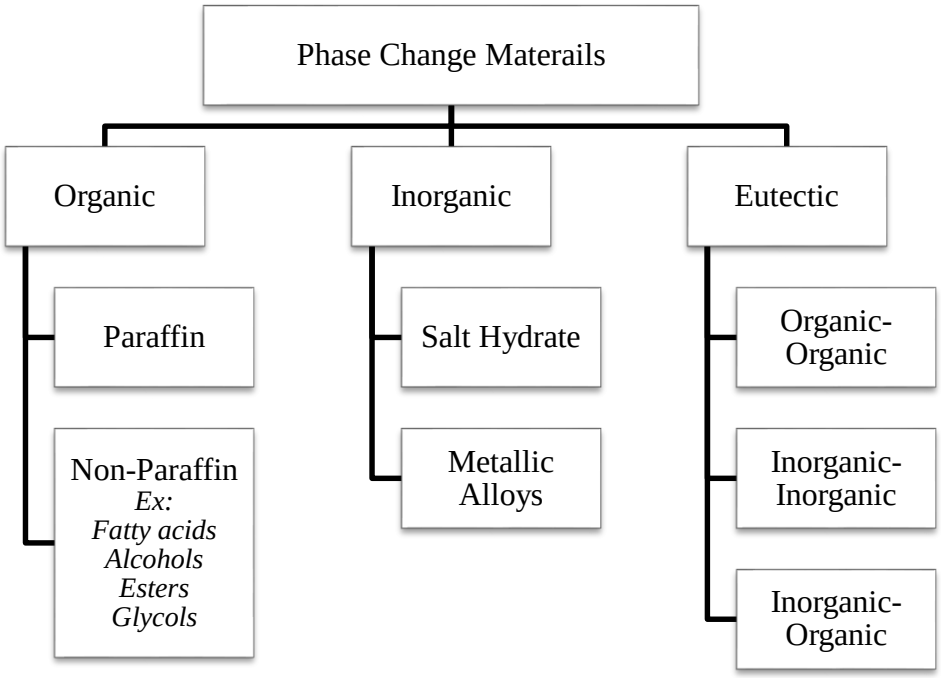

Figure 1.2. Classification of solid-liquid PCMs

1.2.2.1 Organic PCM. Organic PCMs are classified as Paraffin and Non-Paraffin. Paraffin consists of a saturated hydrocarbon chain of C_nH_{2n+2}. The length of the chain is directly proportional to the latent heat of fusion. Paraffins are known to be non-corrosive, non-toxic, have good stability upon cycling, and able to crystallize with little or no subcooling [18]. However, they also have low thermal conductivity, and high volume change for phase transition, are fairly flammable, and are non-compatible with plastic containers due to the chemical similarity which can lead to softening of some polymers [19].

The organic non-paraffin materials are the largest category of PCMs for TES [7]. Among the many types of non-paraffin organic PCMs, fatty acids have received interest recently as they are characterized by desirable thermophysical and kinetic properties. Fatty acids consist of a chain of $CH_3(CH_2)_{2n}COOH$ [20]. Compared to paraffins, fatty acids have a higher latent heat, smaller volume change for phase transition, sharp well-defined melting temperature, and reproducible behavior for melting and freezing [21, 22]. Fatty acids consist of one component, which helps to attain an ideal stability upon cycling [23]. Like Paraffins, fatty acids also have low thermal conductivity, are flammable at very high temperatures, and exhibit little or no supercooling [20].

Sugar Alcohols are organic PCMs which are characterized by the formula $HOCH_2[CH(OH)]_nCH_2OH$ [23]. These organic PCMs are new. Therefore, little information is available. They have a high density which gives them a higher latent heat of fusion compared to the other organic PCMs. However, they show some subcooling compared to other organic PCMs [24].

Esters, also known as fatty acid esters, can be produced from fatty acids combined with an alcohol. They are usually non-toxic, show no supercooling, and are available in large quantities for many commercial applications [25].

1.2.2.2 Inorganic PCM. Inorganic PCMs are classified as salt hydrates and metallic alloys. Inorganic PCMs usually have a higher heat of fusion than organic PCMs, with the exception of organic sugar alcohols [23]. Salt hydrates are inorganic PCMs that consist of salt and water in a crystal matrix when they solidify [20]. They have a high latent heat and a melting temperature range from 15 to 117°C [5]. Molten salts have a melting temperature range grom 250 to 1680 °C [26]. Salt hydrates are considered one of the most important PCM groups, and their applications in TES systems have been extensively studied by many researchers. The ease of availability and relatively low cost of salt hydrates make them very attractive for the commercial applications of TES [20, 27]. For instance, $CaCl_2.6H_2O$ and $Na_2SO_4.10H_2O$ are examples of salt hydrates that are widely available at a very low cost. Compared to other PCMs, they are characterized by a lower volume change during phase transition and a relatively high thermal conductivity in the range of 0.4 to 1 W/m.K [5, 20, 28]. One of the major drawbacks of salt hydrates is their instability upon cycling due the separation of water and salt, which causes a decrease in latent heat with time [6]. This problem can be solved by adding thickened compounds [5]. other problems of salt hydrates are supercooling and corrosiveness to metals [6].

Metallic alloys are inorganic PCMs of high thermal conductivity and relatively high heat of fusion compared to other PCMs. However, they have not been considered for commercial applications because of their weight drawbacks.

1.2.2.3 Eutectic PCM. Eutectic mixtures are used to get new PCMs with improved properties and with different melting temperature. They consist of a mixture of two or more PCM components – organic, or inorganic, or both – that melt and freeze simultaneously [20]. PCMs are also mixed to form a new eutectic PCM that melts at the same temperature but with a better melting behavior [5].

Eutectic mixtures are investigated by conducting several experiments until an ideal PCM mixture is found at the required melting temperature with a desirable "sharp" melting behavior and high enthalpy. If two or more components are found to have positive results, additional experiments are performed to find an optimum mixture and composition. This process is time consuming and requires a lot of work [5].

1.2.3. Applications of PCMs for Thermal Energy Storage. In this section, the use of PCMs in several applications of TES is presented. PCMs can reduce the operation cost, size, and capacity of many applications where thermal energy storage is applied. PCMs can play an important role in meeting an efficient and environmentally friendly usage of energy in various types of fields. For instance, the emissions of CO_2, SO_2, and NO_X from greenhouses that use PCMs for TES can be reduced by 40% [29]. Moreover, some cases, an energy savings of 50% can be obtained using PCMs in TES systems [18].

1.2.3.1 Nuclear thermal energy storage systems. Heat storage systems have been proposed in several studies for the accumulation of the excess heat generated by a nuclear reactor during low electricity demand [30-33]. For economic and reliable operation of the nuclear power plants, it is best to operate at the base-load condition or at constant power level. The nuclear reactor may be subject to variable electricity demand in an energy grid. The capacity factor can be negatively affected due the variable power demands, causing

economic penalties [33]. In this case, integrating a thermal energy storage system with the nuclear reactor will allow the nuclear reactors to meet the variation in power demand. During low electricity demand, the heat can be stored inside heat storage tanks equipped with PCMs of suitable phase transition temperature and thermal storage capacity. Lee et al. [31] proposed a similar idea but with the use of underground rock instead of PCM storage tanks. The heat can be extracted later during the peak demand hours and converted to electricity using a standard thermal plant. Among various technical options for thermal energy storage, PCMs are very attractive because of their high storage capacity around their phase transition temperature. Saeed et al. [33] coupled an advanced high temperature reactor to a thermal energy storage tank. Lithium chloride PCM was used as the thermal storage material. The thermal power of the nuclear reactor was kept at constant level as the demand is met from the energy stored in the TES tank. Figure 1.3 shows the block diagram for the proposed TES system.

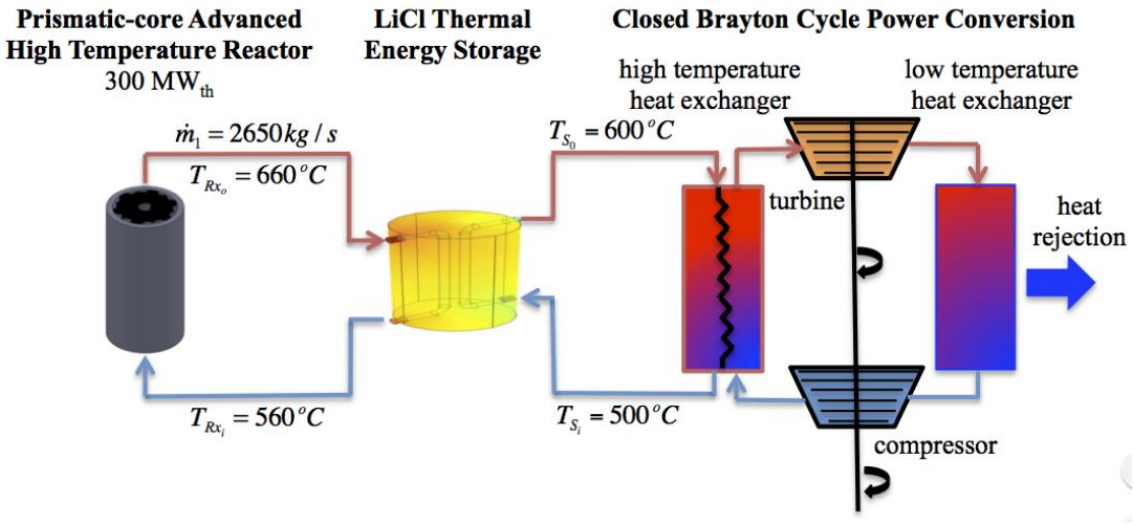

Figure 1.3. System block diagram for a nuclear reactor coupled with TES system taken from [33].

The study also demonstrated the inherent safety of such system during unplanned shutdown. The decay heat can be removed to the TES tank by natural circulation during loss of forced circulation. The reactor reached a shutdown state in less than half an hour, and the average temperature of the fuel and coolant were kept within safety limits during the transient.

Designing such heat storage devices and integrating PCM into the production cycle requires the use high temperature PCMs such as molten salts and their mixtures. These kinds of PCMs have a phase transition temperature range from 250 to 1680 °C, and heat of fusion from 68 to 1041 J/g [26].

1.2.3.2 Thermal storage in buildings. PCMs can contribute to regulate comfort temperature and lower the power consumption in buildings by storing energy during the day and releasing it at night. The energy can be stored either by using solar cells, wallboards, ceiling tiles or even by mixing PCMs within concrete walls. Commercial PCM wallboards and ceiling tiles are the most common method because of their simplicity and ease of installing. The use of PCMs through building structure is a passive thermal management method. It can help to maintain the room temperature within the comfort temperature range without the use of conventional mechanical cooling or heating system, or at least they can lower the electrical consumption of these systems by shifting the temperature peak hours and reducing the indoor temperature. Thereby, it contributes to reducing the peak power demand significantly.

The use of PCM wallboards or ceiling tiles coupled with a ventilation system that works at night as a discharge system can help to increase the TES efficiency of PCM. Figure 1.4 shows an example of such system.

Once the ambient temperature rises up to the melting temperature of the PCM, energy is absorbed and stored as a latent heat and the temperatures are maintained almost constant until the PCM fully melts. Ideally, the PCM only melts after absorbing its full latent heat capacity at constant temperature (melting temperature).

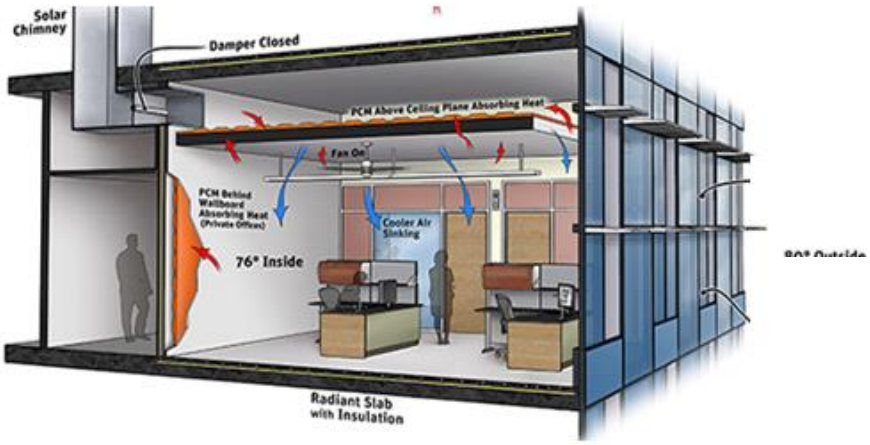

Figure 1.4. Schematic diagram of a house integrated with PCM ceiling tiles taken from reference [34]

A ventilation system at night can then be used to help discharge the PCM to start a new cycle the next day. A suitable PCM is chosen based on its melting temperature to suit a specific environment or application. Eutectic mixtures can help to find new PCMs that melt at the desired temperature if a pure PCM does not melt close to the required temperature. PCMs for TES in buildings has been studied by many researchers, and the use of this technique can reduce the cooling and heating energy between 14% and 87% based on selected parameters and environment [35].

In Figure 1.4, the thermal energy storage of a PCM is compared to other materials used for TES in buildings. Specifically, the latent heat storage capacity of Lauryl Alcohol as a PCM that melts at 23.83˚C with a heat of fusion of 216.5 kJ/kg is compared to the theoretical sensible heat storage capacity of rock and water. The specific heat capacity of concrete rock and water was assumed to be 0.750 kJ/(Kg.K) and 4.182 kJ/(kg.K), respectively. As clearly seen in Figure 1.5, for a system working in the temperature range of 20˚C where midpoint temperature is the PCM melting temperature, the PCM can store a total energy of 255.4 kJ/kg. Comparatively, the storage capacity of rock and water does not exceed 15.0 kJ/kg and 83.6 kJ/kg, respectively.

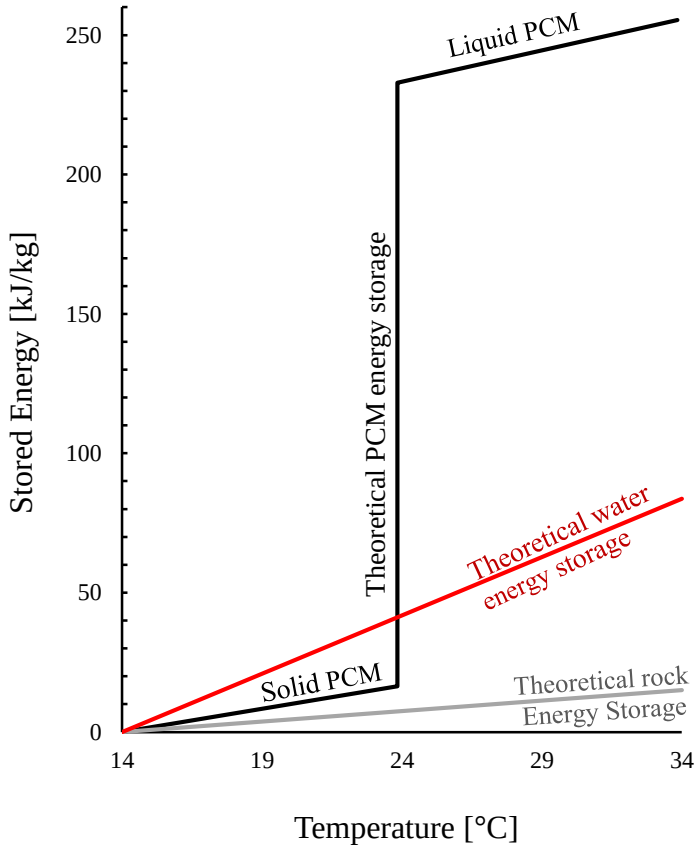

Figure 1.5. A comparison of the typical building material to PCM (Lauryl Alcohol) TES.

The correct choice of PCM is crucial. The used PCM must melt at the proper temperature with an appropriate storage capacity to yield the maximum performance and efficiency of the system. If an incorrect PCM is chosen, the phase change process may not be completed and the system will fail to store or release the total value of the heat of fusion.

1.2.3.3 Solar photovoltaic system. The energy generated from Photovoltaic (PV) panels depends on the intensity of the solar radiation, the quality of the panels in use, and the temperature of the panels [36]. The efficiency of generating energy from PV panels decreases with temperature. Only 10-20% of the incident solar radiation is converted into electric energy in PV panels; the rest is either reflected or causes overheating of the system [37]. The temperature rise of a PV modules is known to cause a decrease in power efficiency by 0.5% per kelvin above the standard test conditions (STC) of 25 °C. [38-40]. During the day, the temperature of a typical the PV panels may rise to 80°C or even higher, which accounts for about a 28% loss in solar to electrical conversion efficiency with respect to the STC.

Several studies have been devoted to the use of mechanical fans, water circulation, pumps, or other types of equipment that consume energy to enhance the free cooling and efficiency of PV panels. However integrating PCMs in PV panels provides a novel passive method solution to prevent overheating and remove heat from PV systems. Such PV-PCM systems are able to operate for a longer times within the desirable temperatures where higher efficiency is achieved. Even when compared to a natural ventilation methods, PCMs have a greater potential to enhance the efficiency of PV systems because they are not affected by the speed or direction of wind. Moreover, the excess and stored heat in a PCM can be utilized to provide heat to buildings or any other system when it solidifies.

Hasan et al. [41] developed a PV-PCM system to reduce PV temperature dependent power loss and to increase the conversion coefficient. The PV peak temperature was kept below 45°C, at solar intensity of 950 W/m^2. This peak temperature value is over 20°C lower than that of the PV system without PCM. In another study, Atkin and Farid [16] developed a novel design of PV-PCM consisting of a PCM infused graphite with external fins to improve heat sink at the rear side of the module as shown in Figure 1.6. It was shown that the overall efficiency can be increased by 13% using this thermal regulation system. Ma et al. [42] noted that the PV–PCM system can be extremely feasible from the economical side if integrated with a solar thermal system that can absorb the excess heat from the PV-PCM panels and discharge the stored heat in PCMs to provide building heat services.

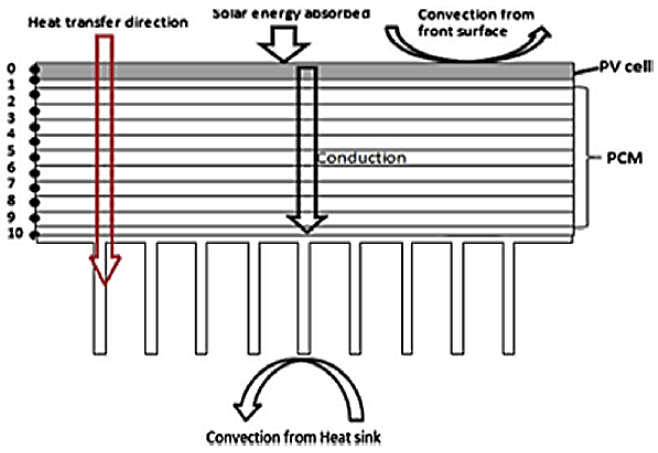

Figure 1.6. Sketch diagram of the experimental setup and PV panel configuration taken from [16].

1.2.3.4 Air conditioning applications. PCMs have been studied by many researchers for air conditioning units. PCM-based air conditioners consume less energy

than the conventional air conditioning systems. PCMs can increase the thermal performance by reducing the temperature of the air entering the evaporating coil when PCMs absorb heat during phase transition.

Chaiyat et al. [43] analyzed a PCM-based air conditioner. The results showed that PCMs can improve the thermal efficiency of the air conditioner and decrease the electrical consumption effectively.

Vakilaltojjar [44] introduced an air conditioning system in which cold air passes through a series of thin flat containers of PCMs. The study investigated the effect of PCM slab thickness and air gaps on the storage system performance. A better performance using a spherical capsule packed bed PCM for the air conditioning system was investigated by Fang et al. [45].

1.2.3.5 Solar water heating system. PCMs are integrated into solar energy collection systems to improve efficiency.

Prakash et al. [46] examined a solar water heating system containing a filled PCM layer at the bottom as shown in Figure 1.7. During the day the sun heats the water, which in turn transfers heat as latent heat in the PCM layer at the bottom.

At night or in the absence sun, the heat in PCM is discharged to water by injecting cold water to replace the hot water. The efficiency of such a system is limited by the poor heat transfer between the water and PCM.

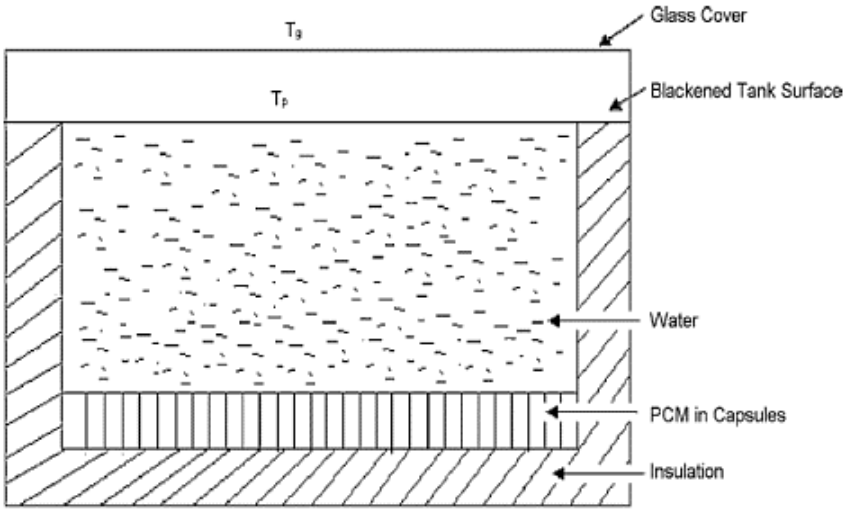

Figure 1.7. Solar water heating system [46]

Ghoneim [47] analyzed an enhanced design of such a storage system. A cylindrical storage tank containing several closed loop pipes was connected with a solar plate collector as shown in Figure 1.8. Such system can help to enhance the heat transfer between water and the PCM and reserve the heat for a much longer period of time.

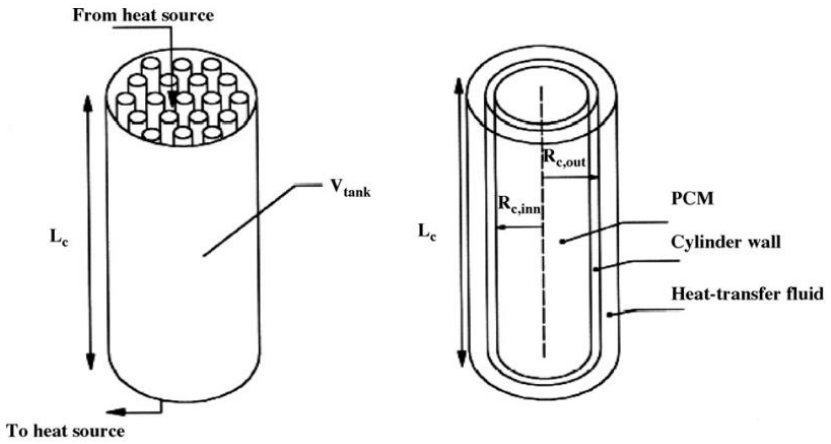

Figure 1.8. Cylindrical storage tank with PCM storage [7]

Several studies [47-51] have been done to compare the design of different size storage vessels and PCM storage materials of such solar heating system.

1.2.3.6 Biomedical applications. PCMs provide a very attractive solution for many biomedical applications in terms of thermal protection. For example, special bandages and textiles equipped with PCMs are used to maintain the skin temperatures within comfort range for burns and heat/cooling therapy [52]. Recently, many commercial products made hot or cold PCM pads to treat local pain have become available in the market. Mondieig et al. [53], proposed a device for thermal protection of biomedical products consisting of a double walled packaging system equipped with PCM, especially for the transportation or storage of blood elements. In an interesting study by Lv et al. [54], a new concept of thermal protection by PCMs during cryosurgery was presented. The healthy tissues near the cancerous tumor were protected from thermal injury using micro-encapsulated PCMs, which were delivered to the tissue by injection. Another novel study by Wang et al. [55] presented a bio-sensing technique using thermal probes of RNA aptamer-functionalized phase change nanoparticles for a highly sensitive and effective detection of thrombin. The PCM thermal probe absorbs heat and displays sharp thermal signal during the temperature scan. The existence and amount of thrombin can be detected by the position and area of the peaks.

1.2.3.7 Storage and transport of temperature sensitive products. Storage and transport containers are one of the most frequently used commercial applications of PCMs. The fields covered in temperature sensitive applications are much larger than storage and transportation of fresh food, medical products, and beverages. Azzouz et al. [56, 57] investigated the performance of a PCM-modified refrigerator. The use of PCM provides a

storage capacity that allows the system to work for 5-9 hours of continuous operation without a power supply, depending on the thermal load. The PCMs were tested in several thicknesses, thermal loads, and ambient temperatures. It was concluded that PCM-modified refrigerators have a 10-30% improved performance compared to conventional systems. Gin et al. [58] studied the effectiveness of PCMs in a freezer against heat loads like defrosting, loss of electrical power, and door openings. It was found that the presence of PCM during several heat loads reduces the temperature rise significantly, which also results in lower energy consumption. Furthermore Subramanian et al. [59] demonstrated that PCMs in domestic refrigerators can improve the quality of stored food by lowering the rate of hysteresis cycles.

The transport of temperature sensitive products in PCM containers is very efficient and helps to reduce energy expenses. PCM containers provide a clean and cheap tool for transportation trucks to regulate temperature and heat throughout the entire shipment period. Ahmed et al. [60] utilized PCM in transportation trucks to reduce heat transfer across the trailer walls. A 29.1% reduction in heat transfer was observed, causing a massive energy saving, and reducing the refrigeration system's size. This also led to longer operating life for the system equipment, and a reduced pollution from diesel driven cooling units. The transport of temperature sensitive food in special containers is another important application of PCM. This can be done by using special soft or rigid containers equipped with a PCM that melts at low temperatures [18]. The containers must be kept in a freezer for an adequate time until it solidify before they can be used to save food products. Because of the high latent heat of PCM it can hold food products at the required temperature for a long time without the need of an external source of energy.

1.2.3.8 Electronics. Thermal management using PCM based cooling systems has a great potential to be used in electrical devices and ships, that do not operate for long continues periods. Such PCM based cooling systems can maintain the temperature of electronics and prevent overheating [61, 62]. Kandasamy et al. [61] analyzed the thermal performance of a novel PCM thermal management system for cooling typical portable electronic devices. A PCM package was designed to meet the heat dissipation, cost, and size requirements of the device. Yin et al. [63] analyzed the thermal management and performance of composite PCM in a passive electronic cooling system. The system insured a greater reliability against the thermal shock of high heat flux. The heat transfer coefficient in this system was found to be 3 times greater than those cooling systems without PCM. In another work, Tan et al. [64] studid a PCM based heat storage unit for the cooling of mobile electronic devices. The PCM-based system maintained the temperature of chips within the comfort temperature range for 2 hours of transient operation. The configurations allowed the electronics to operate at a high power dissipation for a longer period time.

1.2.3.9 Other applications. If one tries to compile an overview of the applications of thermal energy storage using PCM, one would be impressed by the variety of possible technical solutions and the large number of applications that are under development. For instance, PCM are proposed for a special thermal cooling vest used by athletes, that helps them perform better and feel more comfortable, reducing the risk of dehydration and fatigue, and controlling the body temperature [65]. Another application that is under development is the PCM integrated concrete wall. The PCM wall effectively captures the incident solar radiation on the wall and is very effective in shifting the peak loads [66]. The use of PCM in walls also helps to attain a higher thermal energy storage using a thinner

wall structure. Apart from the opaque parts of buildings, PCM was also proposed in special PCM-filled glass windows [67]. Compared to air filled windows, the PCM-filled windows are more thermally effective and capable of filtering out the thermal radiation. PCMs have also been used to extend the lifespan of Lithium-ion batteries to avoid the overheating problems which significantly decrease their lifespan [68]. PCMs were also used for cooling applications of electric and combustion engines [69]. The use of PCMs has been implemented in vehicles for thermal comfort by companies like BMW [70]. Thermal control using PCM has also been implemented in spacecraft thermal systems [71], solar cookers [72], and greenhouses [73].

2. EXPERIMENTAL METHODS AND MATERIALS

2.1. PHASE CHANGE MATERIALS

Seven heat storage materials have been selected for this study. Myristic acid (99% purity), Capric acid (99% purity), Lauryl Alcohol (99% prutiy), Palmitic acid (99% Purity), Lauric acid (99% Purity), and Methyl palmitate (99% prutiy) were procured from Sigma Aldrich. A eutectic mixture of 60% Methyl palmitate and 40% Capric acid were prepared. The chemical data of the PCMs and their thermal properties are given in various references which are collected by the National Institute of Standards and Technology (NIST) and shown in Table 2.1 [74].

Table 2.1. Compositions and chemical data for the selected PCMs

Name	Scientific Name	Molecular Formula	CAS Number	Melting Temp. [°C]	Melting Enthalpy [J g^{-1}]
Myristic Acid	Tetradecanoic acid	$C_{14}H_{28}O_2$	544-63-8	53.96	197.96
Capric acid	n-Decanoic acid	$C_{10}H_{20}O_2$	334-48-5	31.19	162.86
Lauryl Alcohol	1-Dodecanol	$C_{12}H_{26}O$	112-53-8	24.00	215.83
Palmitic Acid	Hexadecanoic acid	$C_{16}H_{32}O_2$	57-10-3	62.47	211.99
Lauric Acid	Dodecanoic acid	$C_{12}H_{24}O_2$	143-07-7	43.92	181.45
Methyl palmitate	Methyl hexadecanoate	$C_{17}H_{34}O_2$	112-39-0	32.20	207.08
60% Methyl palmitate + 40% Lauric Acid		-	-	25.50 (exp.)	205.2 (exp.)

2.2. EXPERIMENTAL METHODS

2.2.1. Differential Scanning Calorimetry. Differential scanning calorimetry (DSC) is a widely used method to characterize the thermal properties of PCMs [10, 12, 75-77] among other methods like the differential thermal analysis (DTA) and T-history method [78]. Ramping temperature at constant heating rate (Dynamic Method) is the most common operating mode for DSC [79, 80]. In this study, DSC in dynamic mode is used to determine the thermophysical properties of PCMs such as melting temperature, melting enthalpy, specific heat of samples.

In DSC analysis, the system measures the difference in the amount of heat required to increase the temperature of a material sample (sample pan) and an empty sample (reference pan) as a function of temperature. A schematic diagram of a typical DSC chamber is shown in Figure 2.1.

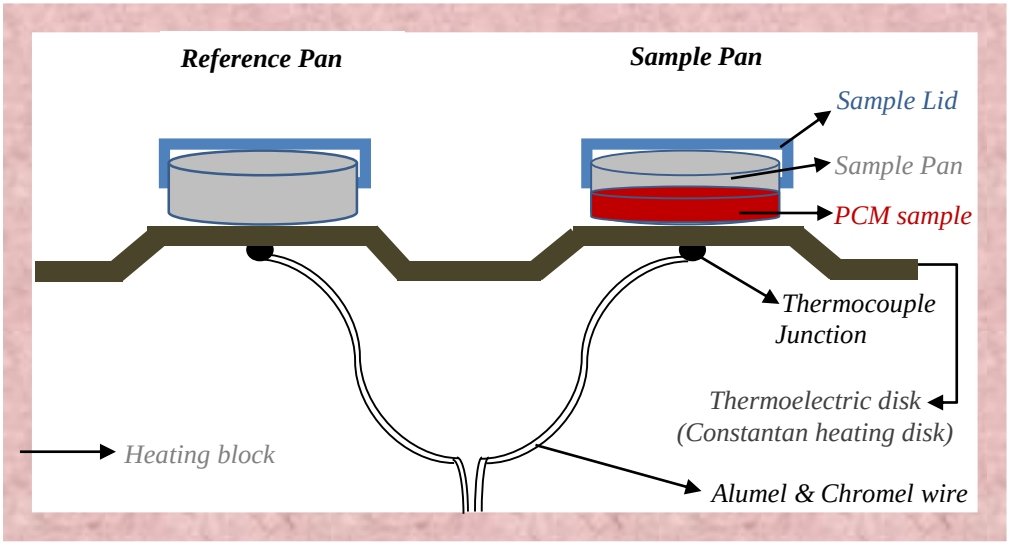

Figure 2.1. Schematic diagram of a typical DSC chamber

The heat applied by the heater block flows radially though the electrical constantan disk toward the reference and sample pan. During thermal events such as transition, the system transfers to or from the sample pan to maintain the same temperature of the reference pan. The DSC measures the sample and reference temperature using the thermocouple junctions. The output electrical potential of the thermocouples is positive if the sample temperature is higher than the reference pan, and negative if the temperature of the reference pan is higher than the sample pan. The differential voltage, which is supplied to the heaters to maintain the same temperature of the sample and reference, is then converted to mW. The heat flow into the sample pan is measured as a function of temperature and the difference from the reference pan represents the specific heat of the PCM sample. The result of DSC measurements is a thermogram curve of heat flux versus temperature. A typical DSC thermogram is shown in Figure 2.2.

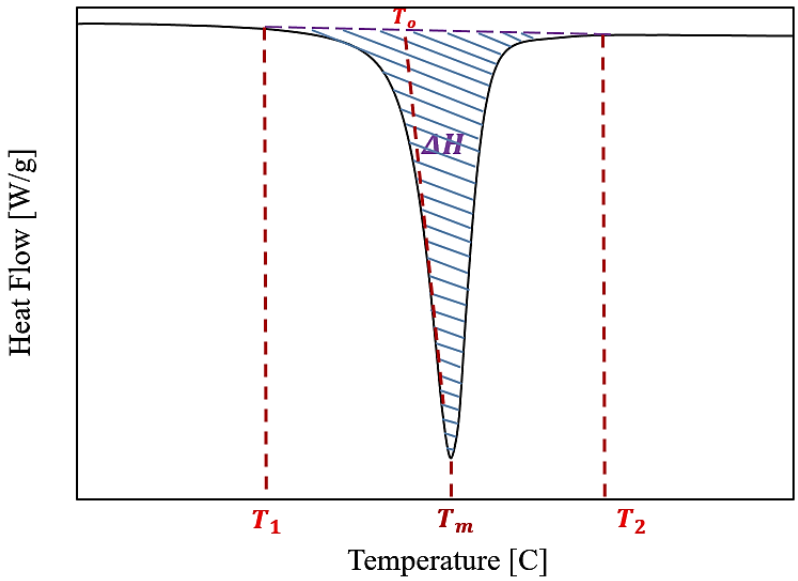

Figure 2.2. Typical characteristics of a DSC thermogram

The blue shaded area (*ΔH)* represents the enthalpy change during transition (total latent heat) of PCM, T_1 and T_2 are the temperature range at which the transition process occurs, T_m: melting temperature, and T_o: is the onset temperature.

2.2.1.1 Enthalpy-sum curves. The DSC thermogram represents the stored heat as a function of temperature. For PCMs where solid-liquid transition occurs, this is equal to the specific heat (C_P) that is the typical output of a colorimeter's measurement [57]. The Enthalpy is obtained by integrating the heat stored in a given temperatures as follows:

$$\Delta H = \int_{T1}^{T2} C_p(T).dT = \int_{T1}^{T2} \frac{\delta Q/dt}{dT/dt}.dT = \int_{T1}^{T2} \frac{\delta Q}{dT}.dT \tag{4}$$

Where ΔH is the latent heat of fusion in units of J/g, C_p is the specific heat capacity at constant pressure in units of J/(g.K), T_1 and T_2 represent the temperature range at which the storage operates, $\delta Q/dt$ is the heat flow in units of *W/g*, and dT/dt is the DSC heating rate in units of ℃*/sec*.

The enthalpy-sum curve is determined from the DSC thermogram results. The enthalpy sum curve -also known as the (enthalpy-temperature) curve- provides an advanced and much better representation of the PCM thermophysical properties when compared to the DSC thermogram curve. The enthalpy-temperature curve gives the ability to characterize the material by one curve only. As shown in Figure 2.3, the melting latent heat (ΔH), total energy storage capacity, melting temperature (T_m), and specific heat capacity of the liquid and solid phases can be directly taken from the curve.

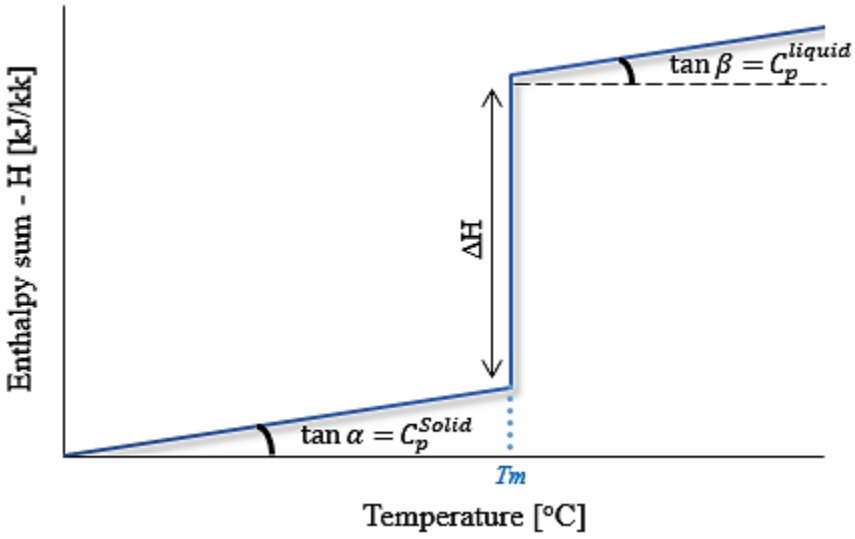

Figure 2.3. The theoretical enthalpy sum as a function of temperature for an ideal latent heat storage material.

Because the area under the thermogram curve between any two temperature points yields an enthalpy change, the enthalpy sum as a function of temperature can be determined using equation 5 as follows:

$$H_{sum}(T_i) = \sum_{k=0}^{i-1} H(T_k) + H(T_i)$$
$$H(T_i) = \int_{T_i}^{T_{i+1}} \frac{\delta Q/dt}{dT/dt}.dT \qquad (5)$$

Where $H_{sum}(T_i)$ is the enthalpy sum or energy storage between the reference's initial temperature (T_o) and the final temperature (T_i), $H(T_i)$ is the enthalpy at a single temperature increment between two T_i and T_{i+1}, $\delta Q/dt$ is the heat flow in units of *W/g*, and dT/dt is the DSC heating rate in units of *℃/sec*.

2.2.1.2 DSC baseline. In order to accurately determine the enthalpy-temperature curve and the specific heat capacity of materials using a DSC, a baseline measurement using two empty pans has to be performed. For accurate results, the DSC pan used for baseline measurements should be the same as the one used for the subsequent DSC the measurement of PCM sample. The baseline measurement is a DSC run using empty sample and reference pans over the entire temperature range using the same heating rate that will be used for the subsequent measurements. The resulted signal is the DSC baseline that has to be subtracted from the heat flow signal of the subsequent PCM measurements. By following this methodology, the heat capacity contribution of only the tested material in the DSC pans will be measured.

2.2.1.3 Specific heat capacity measurements. The specific heat capacity of PCM is an important property than can be determined from the DSC results. A specific methodology has to be carefully followed to determine the accurate specific heat capacity of materials by DSC measurements. The heat capacity of materials can be determined using Equation 6 as follows:

$$C_P(T) = \left[\frac{60E}{Hr}\right]\frac{\Delta y}{m} \tag{6}$$

Where $C_p(T)$ is the specific heat capacity of the tested material at the temperature (T) of interest, E: cell calibration coefficient at the temperature of interest (dimensionless), Hr: the heating rate in °C/min, and 60 is the conversion constant from minutes to seconds. Δy: the deflection in the y-axis between the baseline curve and sample measurement curve at the temperature of interest in mW, and m is the sample mass in mg. For a given set of experimental conditions, the value of ($60E/Hr$) is constant and converts the heat capacity

into a unit of J/g K. For higher accuracy, the value of this quantity can be accurately determined by running a known standard material such as sapphire (Al_2O_3) or indium.

As seen in Figure 2.3, the value of the specific heat capacity can also be determined from the enthalpy-temperature curves. The slope of the sensible heat part (the solid and liquid phase region) in the enthalpy-temperature curve is equal to the specific heat capacity of the tested material.

In general, for a solid to liquid phase change process, the energy stored in an interval of 1°C is equal to the specific heat at a constant pressure and can be found as follows:

$$C_p(T) = \frac{\delta H}{\delta T} \tag{7}$$

In this study, the DSC measurements were performed on a Seiko DSC6200 colorimeter (Seiko Instruments) and DSC2010 (TA instruments) with aluminum sample pans (TA pans #900786.901, TA Lids #900779.901). The temperature repeatability, calorimetric sensitivity, and calorimetric precision for both of the calorimeters is ±0.1°C, 1μW and ±1%, respectively.

The technical specifications for both of the DSCs are shown in table 2.2. Temperature and enthalpy calibrations were carried out using a standard manufacturer-supplied indium sample. The experimental test samples were taken by a calibrated pipette after the PCMs were melted and stirred evenly.

Table 2.2. Technical specifications for the DSC cell

Name	Specification
Type	Heat Flux DSC
Temperature	±0.1°C repeatability
Calorimetric sensitivity	1 μW (rms)
Calorimetric precision	1%
Baseline noise	0.5 μW (rms)

2.2.1.4 DSC data analysis. The melting onset temperature (T_o), melting temperature (T_m) and latent heat or melting enthalpy (ΔH_m) were determined from the DSC thermograms by computer software using MUSE standard analysis (Seiko Instruments) and Universal Analysis 2000 (TA instruments). The temperature at which the PCM starts to melt (T_o) was obtained from the point of maximum slope of the leading side of the transition peak and extrapolating the heat flow base line on the same side. The ΔH_m was calculated as the area under the peak by numerical integration.

2.2.2. Thermal Conductivity Meter (THB1). The study of the thermal conductivity of experimental samples was done using the Transient Hot-Bridge technique using a thermal conductivity measuring instrument (THB1, Linseis Inc., USA [81]) as show in Figure 2.4. A kapton insulated sensor (Sensor/B/MFR) equipped with enforced metal frame with a length of 105 mm and width of 42 mm was used. The instrument uncertainty is better than 2% for thermal conductivity. The sensor is directly inserted into the sample, and acts as a heat source and temperature probe.

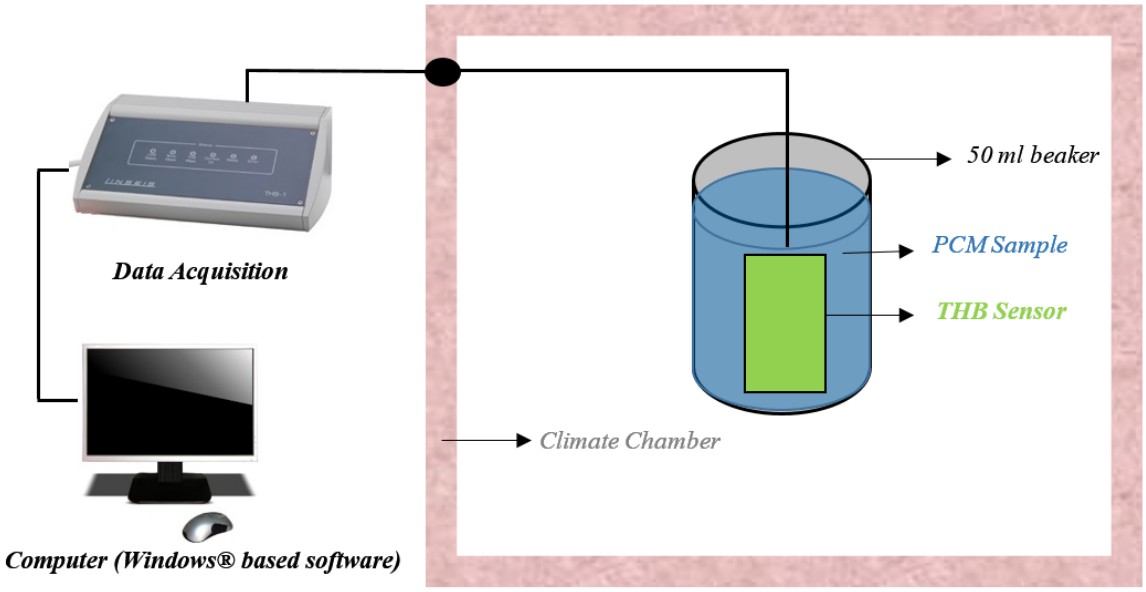

Figure 2.4. Transient Hot Bridge - Thermal Conductivity Meter

An appropriate current of (0.049 A) and an appropriate measurement time of (55 s) were chosen according to the PCM material used. The THB data acquisition unit is connected to a computer to record the data. A computer software (Intuitive Windors® based software) calculated the required thermophysical properties (thermal conductivity, heat capacity, and thermal diffusivity). In order to assure precision and repeatability, the reported values were the average of at least 10 measurements for each sample, or until an uncertainty of 0.003 W/m.K or lower for thermal conductivity was achieved. A delay time of 5 times the measuring time was set between the single measurements to allow the sample to cool down and back to steady state before the next measurement run. Five temperature drift measurements was performed before each run to insure that there was no thermal stratification within the sample.

The sample temperature at which the measurement performed was controlled using a climate chamber (UN260, Memmert GmbH, Germany) as part of the THB1 system. The

chamber has special penetrations for the THB wires and sensor. The experimental sample temperature was taken from the immersed sensor and the temperature was controlled using the climate chamber with a 0.1°C accuracy.

2.2.3. Precision Electronic Balance. The sample mass of the experimental materials was controlled using a precision electronic balance (Mettler MX5, METTLER TOLEDO, Switzerland) at a precision of 0.001mg.

2.2.4. Density Measurements. The density measurements were performed using the conventional volume displacement method. A 10 ml graduated cylinder with 0.1 ml intervals was used. The precision electronic balance was used to measure the sample mass. A temperature controlled cooling unit (FM-62DZ, Whynter Instrument, USA) was used to control the temperature of samples at 10 °C bellow the melting temperature to measure the density of the solid phase. The climate chamber (UN260, Memmert GmbH, Germany) was used to control the sample temperature at 10°C above the melting temperature for measurements of the liquid phase. A measurement uncertainty of better than ±0.7% was obtained using this method.

2.2.5. Thermal Diffusivity Calculations. The thermal diffusivity is an important factor for describing the performance of PCMs in a heat storage system as it governs the diffusion during heat transfer. Therefore, the investigation of thermal conductivity, latent heat, and heat capacity alone is insufficient for predicting the overall heat transfer enhancement of PCMs. Only a few existing studies examined all of these additional thermophysical properties in this detailed manner.

In this study, as the heat capacity of samples was experimentally measured using the DSC, thermal diffusivity can be calculated using Equation 6 as follows:

$$\alpha = \frac{k}{\rho \times C_P} \tag{8}$$

Where α is the measured thermal diffusivity, C_p: the experimental specific heat capacity measured directly from the DSC results, k: experimental thermal conductivity, and ρ: the experimental measured density. Using this method, the uncertainty for thermal diffusivity is expected to not exceed 2.9%.

3. EXPERIMETAL RESULTS AND DISCUSSION

3.1. DSC ANALYSIS OF PCMS

The study aimed to provide a valuable and useful database for PCMs for low temperature thermal energy storage applications. Only a few existing studies provided an overall investigation of thermophysical properties of PCMs in a detailed manner.

3.1.1. DSC Heat Flow Curves. Differential scanning calorimetry (DSC) measurements were carried out to determine thermophysical properties of five PCMs namely, Myristic acid (99% purity), Capric acid (99% purity), Lauryl Alcohol (99% purity), Palmitic acid (99% purity) and Lauric acid (99% purity). The typical result of a DSC measurement is the DSC thermogram (heat flow curve), which directly displays information about the melting onset temperature (T_o), melting temperature (T_m), latent heat of fusion or melting enthalpy (ΔH_m), and temperature range of phase transformation (T_{range}).

Figures 3.1 to 3.5 display the DSC thermograms of Lauryl Alcohol, Capric Acid, Lauric Acid, Myrisitc Acid, and Palmitic Acid, respectively, at sample mass of 7.5mg and a heating rate of 3°C/min. The figures display heat flow results starting at about 20-25°C bellow the expected melting temperature and up to 20-25°C above the melting temperature. However, the actual DSC measurements were started from approximately -5°C for most of the samples and kept constant at that temperature for about 3 minutes to remove the thermal and temperature history from previous cycles. Moreover, the samples of each material were first heated until fully melted before they were prepared in a DSC sample pan.

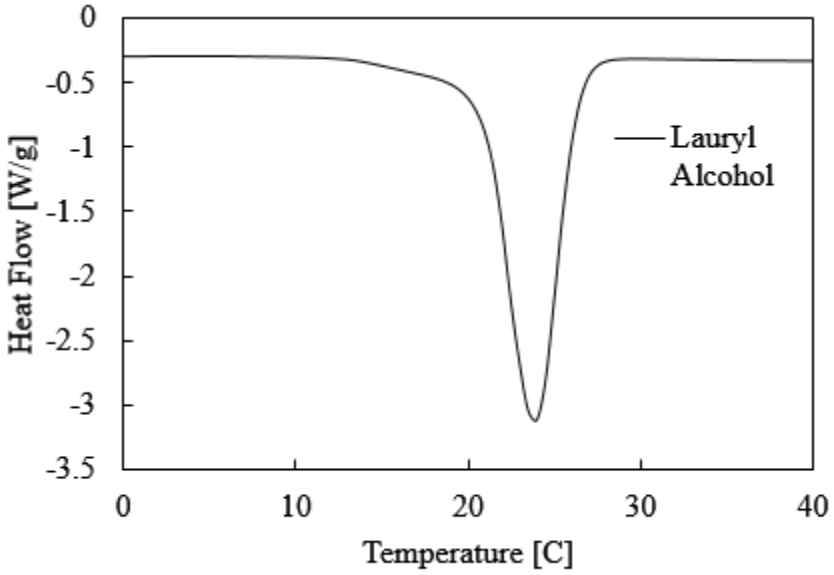

Figure 3.1. Results of DSC measurement for Lauryl Alcohol

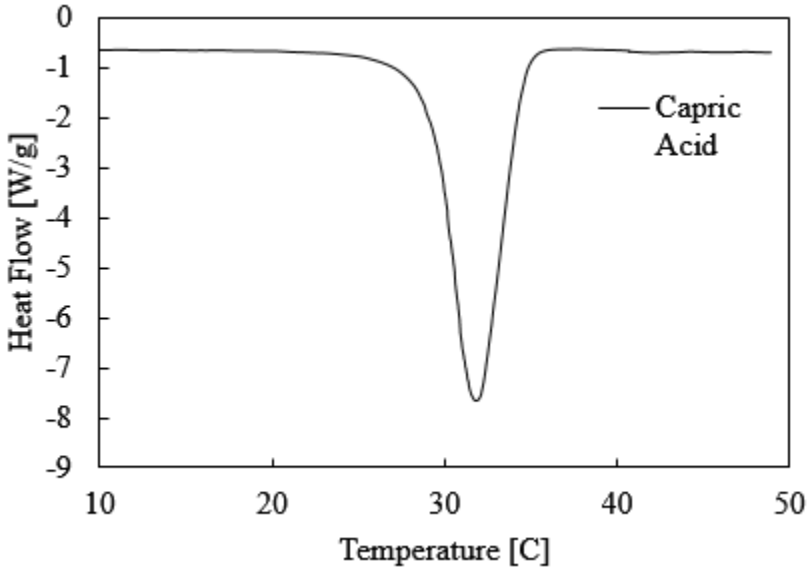

Figure 3.2. Results of DSC measurement for Capric Acid

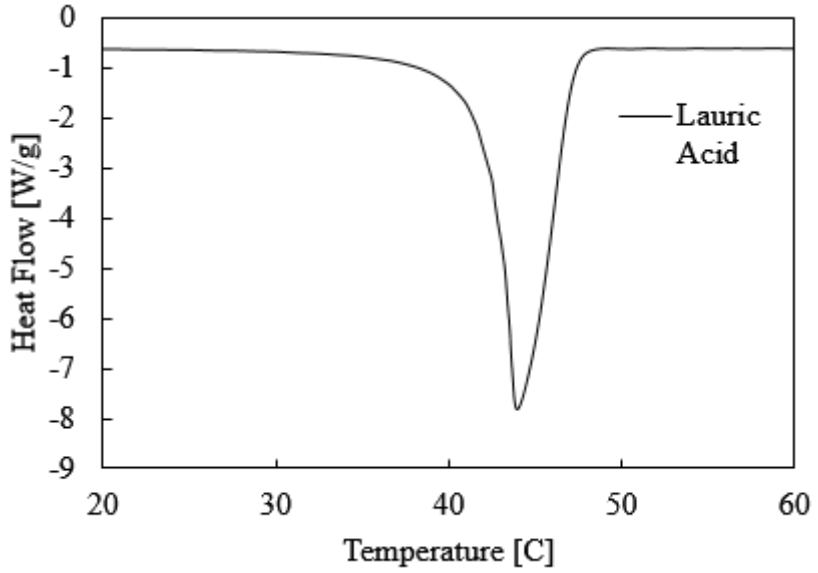

Figure 3.3. Results of DSC measurement for Lauric Acid

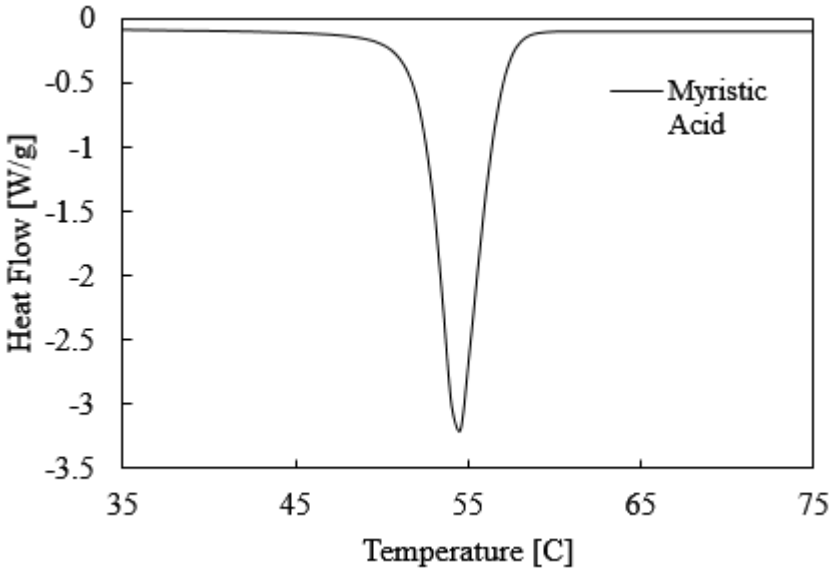

Figure 3.4. Results of DSC measurement for Myristic Acid

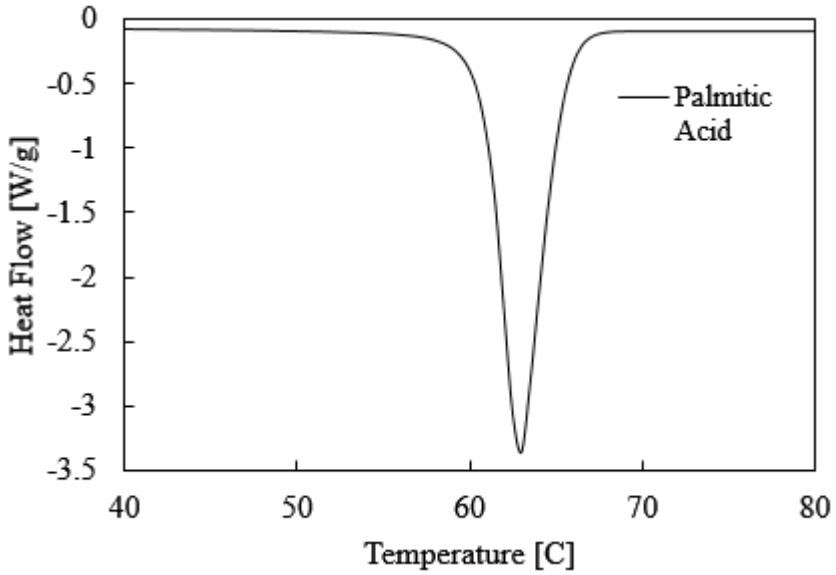

Figure 3.5. Results of DSC measurement for Palmitic Acid

Figure 3.1 displays the DSC curve of lauryl Alcohol. The melting temperature and onset temperature were observed at 20.88°C and 23.83°C, respectively. The latent heat of fusion was found to be 216.5 J/g. For Capric Acid as shown in Figure 3.2, the melting temperature and onset temperature was observed at 29.19°C and 31.82°C, respectively. The latent heat of fusion was found to be 162.2 J/g. The DSC curve for Lauric Acid in Figure 3.3 indicates a melting temperature and onset temperature of 42.72°C and 43.98°C, respectively. The latent heat of fusion was found to be 180.8 J/g. For Myristic Acid based on Figure 3.4, the melting temperature and onset temperature is 51°C and 54.21°C, respectively. The latent heat of fusion is 198.5 J/g. The DSC curve for Palmitic Acid in Figure 3.5 shows that the melting temperature and onset temperature are 60.28°C and 62.93°C. The latent heat of fusion was found to be 209.3 J/g.

For a TES system, it is important that the PCM material goes into a complete phase transition. In other words, if the phase change process has not been completed, the system

will fail to store or release the total value of the heat of fusion. Therefore, the melting temperature range of phase transformation is one of the most important parameters in determining the PCM performance in a TES system. For that reason, the onset melting temperature, full width at half maximum (*FWHM)* for melting peak, and temperature range of phase transformation (T_{range}) for the experimental PCMs are shown in Table 3.1 along with their melting temperature ($T_{m,}$) and latent heat of fusion (ΔH_m).

Table 3.1. Characteristic of melting phase transition of PCMs

PCM	T_o °C	T_m °C	$FWHM$ °C	T_{range} °C	ΔH_m J g^{-1}
Lauryl Alcohol	20.88	23.83	3.25	15.60	216.5
Capric Acid	29.19	31.82	2.91	12.61	162.2
Lauric Acid	42.72	43.98	2.70	13.42	180.8
Myristic Acid	51.00	54.21	2.52	12.23	198.5
Palmitic Acid	60.28	62.93	2.62	13.27	209.3

A PCM with a narrow melting temperature range has a better thermal performance because it can completely melt and store its latent heat of fusion in a smaller temperature range.

It should be noted that the onset temperature can be determined accurately using the dynamic DSC method because it is not affected by the applied heating rate or the PCM sample mass, as will be shown and discussed in Section 3.2. However, the endset melting temperature can be shifted to higher or lower values based on the measurement conditions

(heating rate and sample mass). Thereby, the temperature range of phase transformation would also be affected by these measurement conditions. For that reason, a detailed study was conducted in Section 3.2 in order to investigate the effect of these conditions and to find correct measurement conditions at which measurements for PCMs in a DSC can be conducted accurately. The correct measurement conditions were found and applied to evaluate the melting range of phase transformation and other parameters in the next sections.

3.1.2. Enthalpy Sum. The thermophysical properties of PCMs can be evaluated easily using the enthalpy-sum curve, or also known as the enthalpy-temperature curve. Compared to the DSC thermogram, the enthalpy-sum curve provides a much better representation for the experimental data and gives the ability to characterize and compare the materials by one curve only. Moreover, the enthalpy as a function of temperature (enthalpy-sum) is an important data especially for the current computational simulations of TES system.

As shown in Figures 3.6-3.10, the melting latent heat (ΔH), total energy storage capacity, melting temperature (T_m), and specific heat capacity of liquid and solid phase can be directly evaluated from the curve. The slope of the sensible heat part (the solid and liquid phase region) in the enthalpy-temperature curve is equal to the specific heat capacity of the tested material. The heat capacity of the material at a certain temperature can be determined using Equation 6. The enthalpy sum curves were evaluated using the DSC results as discussed in Section 2.2.1.1 using Equations 4, and 5.

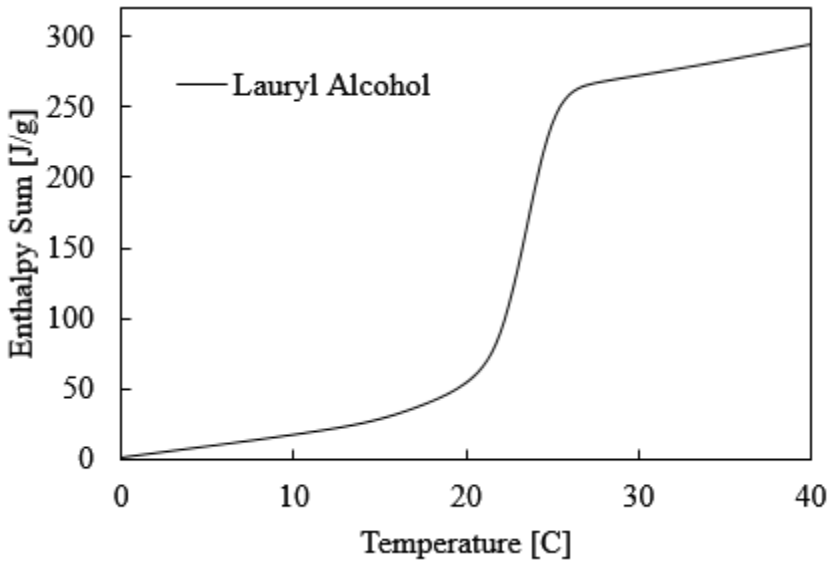

Figure 3.6. Enthalpy sum as a function of temperature obtained for Lauryl Alcohol

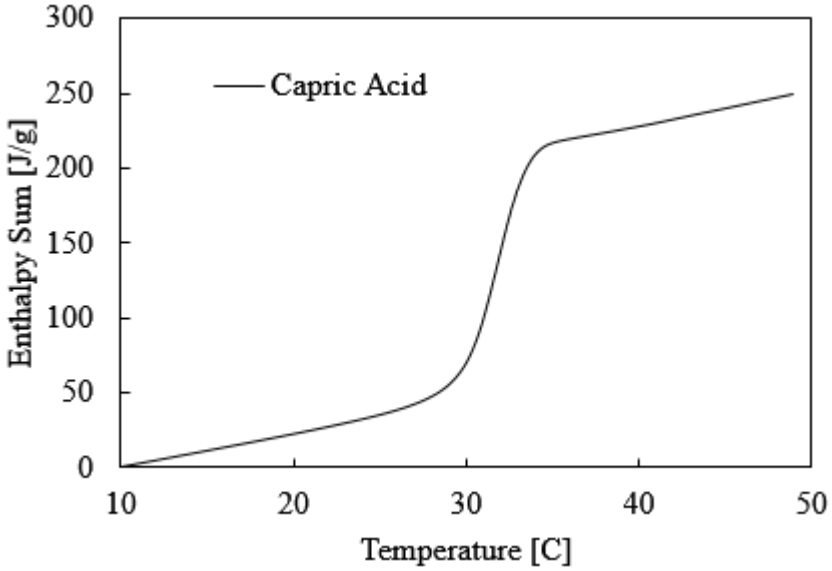

Figure 3.7. Enthalpy sum as a function of temperature obtained for Capric Acid

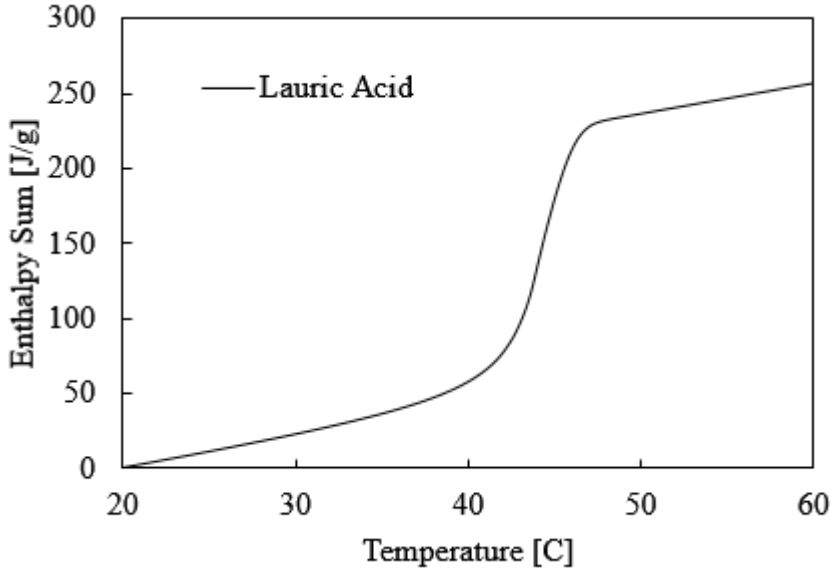

Figure 3.8. Enthalpy sum as a function of temperature obtained for Lauric Acid

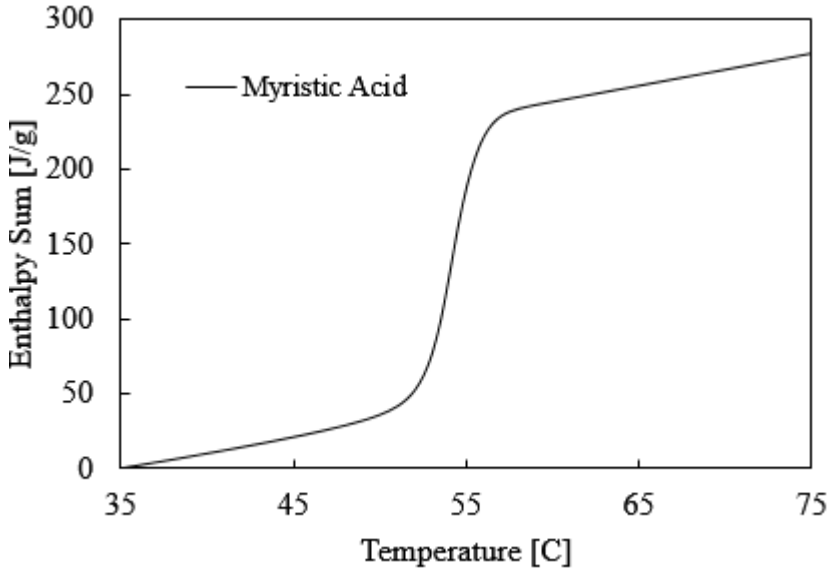

Figure 3.9. Enthalpy sum as a function of temperature obtained for Myristic Acid

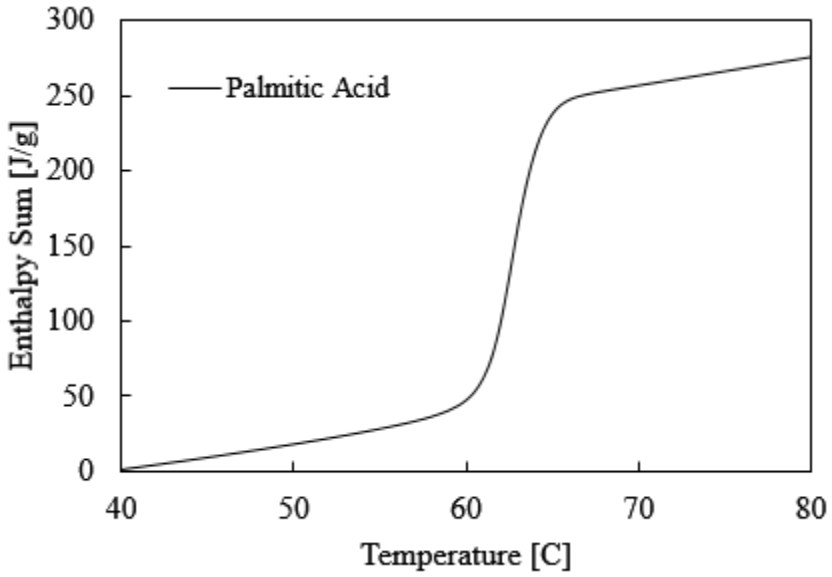

Figure 3.10. Enthalpy sum as a function of temperature obtained for Palmitic Acid

In general, heat storage using ideal PCMs occurs over three distinct steps. Initially, the temperature is raised uniformly from the system starting temperature up to its melting temperature through sensible heating.

Once the melting temperature is reached, the material no longer shows an increase in temperature until it stores its latent heat of fusion while it goes through phase transition from solid to liquid. However, actual PCMs have a very narrow temperature range of phase transformation instead of being attributed to a single temperature.

During phase transition, a very slight increase in temperature is noticed because most of the energy is used to break the molecular or atomic bonds of PCMs by latent heat instead of increasing their temperature [82]. In other words, during phase transition, the energy is rather stored in the PCM's bond structure instead of increasing the temperature.

As the material stores its maximum storage capacity (latent heat of fusion), the material becomes fully melted phase. Further addition of heat is stored through sensible heat in the liquid phase as the temperature raises again uniformly in a rate proportional to the PCM specific heat. Therefore, the total amount of energy stored for a TES system is given by:

$$Q = m\left[\int_{T1}^{Tm} C_{P\_Solid}.dT + \Delta h + \int_{Tm}^{T2} C_{P\_Liquid}.dT\right] \quad (9)$$

Where the first term and last term represent the contributions of sensible heat of the solid and liquid phases, m: mass of PCM, T_1 and T_2 are the temperature range in which the TES process operates, T_m: melting temperature, and Δh: latent heat of fusion.

It is clearly seen that all of the tested PCMs have a comparable total thermal energy storage between 250 J/g to 300 J/g for a temperature range of about ±20°C around the melting temperature. It is also noted that the height of the enthalpy-sum curve within the phase transition region is not only due to the latent heat of fusion, but also accounts for the contribution of the sensible heat since the transition in reality occurs within a temperature range of about ±2°C or ±3°C around the exact melting point seen in the DSC thermogram.

The total energy stored "Enthalpy-sum" is a measure of how much energy can be stored in a 1Kg mass of PCM as it transitions form solid to liquid within a certain temperature range. Therefore, as the TES density of PCM can be described by only one curve (enthalpy-sum), the total energy stored for any of the above tested PCMs within a certain temperature range for any TES system can be calculated using a single equation as follows:

$$E_{stored} = m_{PCM} * [H(T_2) - H(T_1)] \quad (10)$$

Where E_{stored} is the total energy stored in the PCM TES system as sensible heat and latent heat, m_{pcm}: the total mass of PCMs in the TES system, $H(T_2)$: the enthalpy-sum at the upper temperature limit (T_2) of the TES system, and $H(T_2)$: the enthalpy-sum at the lower temperature limit (T_2) of the TES system.

As clearly seen in Figures 3.6-3.10, the largest contribution in the total energy storage is due to the latent heat during phase transitions. However, as considered in the enthalpy-sum curves, the sensible heat contribution should also be taken into account in the design of a TES system; especially when the system works in a temperature range beyond the temperature range of the phase transition (Latent heat region), since the contribution of sensible heat becomes more significant when the working temperature range is wider. The contribution of sensible heat also depends on the specific heat of the PCM.

Figure 3.11 compares the experimental TES capacity for the tested PCMs, namely Palmitic Acid, Myristic acid, Lauric Acid, Capric acid, and Lauryl Alcohol. The theoretical TES capacities of water and concrete are also included to compare sensible heat storage materials with latent heat storage materials (PCMs). The specific heat capacity of concrete rock and water was assumed to be 0.750 kJ/(kg.K) and 4.182 kJ/(kg.K), respectively. As a sensible heat material, water is a standard sensible storage medium, and it can be noted that water has a good TES storage capacity because of its high specific heat. This shows the great importance of improving the heat capacity of PCMs to increase its storage density.

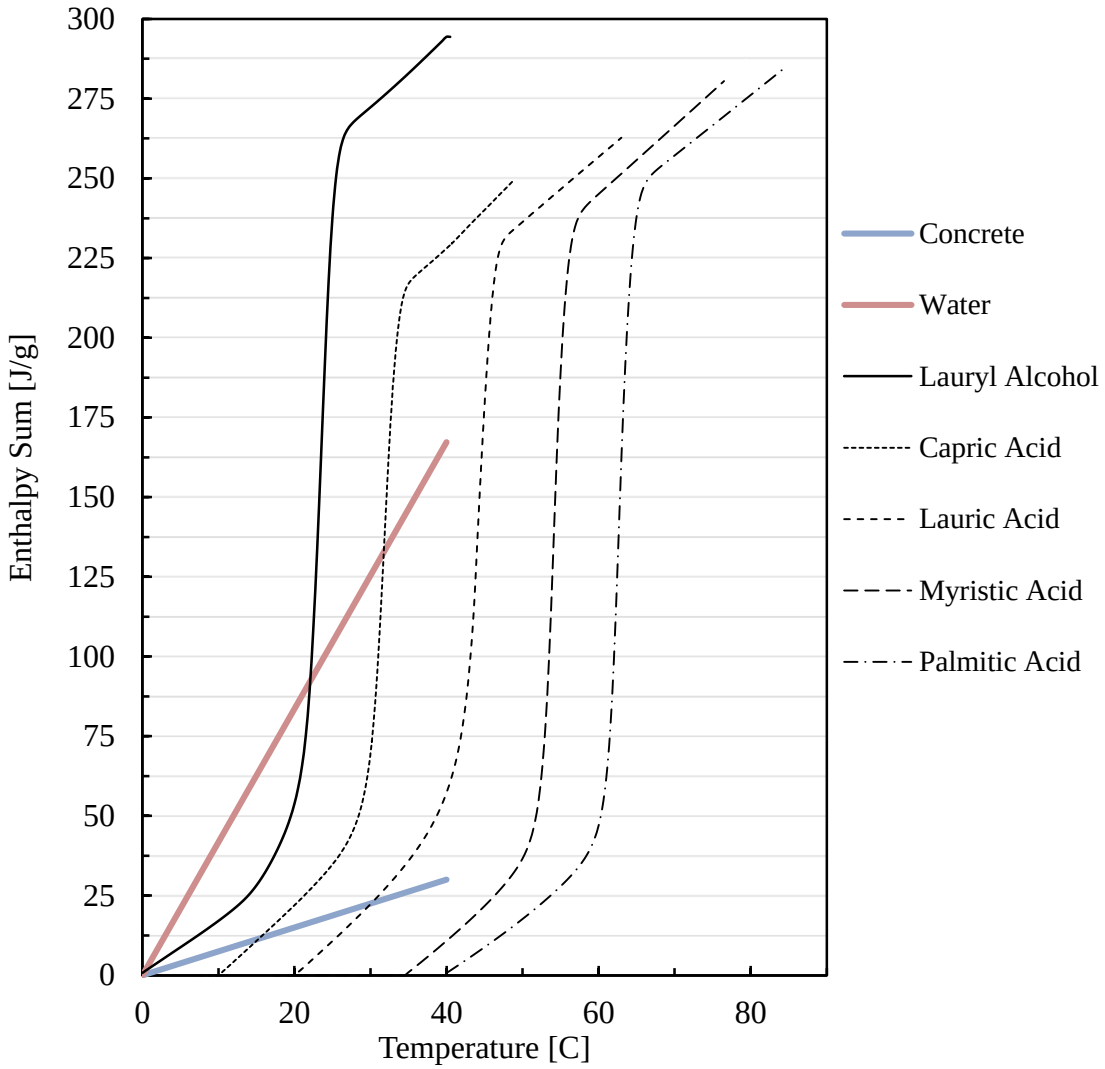

Figure 3.11. Comparison of the thermal energy storage capacity.

3.1.3. Heat Capacity. The specific heat capacity is a key parameter in describing the thermal energy storage during sensible heat process (before and after phase transitions).

The specific heat capacity of PCMs was determined using the enthalpy-sum curve as the slope of the sensible heat part before the phase transition region for the solid phase and after the phase transition region for the liquid phase.

The experimental results for the specific heat capacity (C_p) and the total energy storage density of PCMs through a temperature range of about 20°C around the melting temperature (*TES*) are shown in Table 3.2.

Table 3.2. The specific heat capacity and total energy storage capacity values for PCMs

PCM	C_P^{Sol} J g^{-1} K^{-1}	C_P^{Liq} J g^{-1} K^{-1}	TES J g^{-1}
Lauryl Alcohol	1.667	2.251	294.4
Capric Acid	2.220	2.339	250.1
Lauric Acid	2.056	2.045	262.7
Myristic Acid	1.912	2.009	287.1
Palmitic Acid	1.832	1.906	284.8

3.2. UNCERTAINTY OF THERMAL CHARACTERIZATION OF PHASE CHANGE MATERIAL BY DSC ANALYSIS [83]

The content of this section is an original work published by the author of the current thesis in [83]. Some information may have been omitted or shortened in order to avoid duplicating the information in other chapters or sections.

The Accurate knowledge of the thermophysical properties of PCMs is very crucial for the correct design of commercial storage products. Therefore the temperature range of the phase change transition and the energy storage density must be determined accurately. Those parameters decide the system's capacity, temperature range, and size. As an example, Dolado et al. [79] proved that reducing the uncertainty of the PCM melting temperature from ±1°C to ±0.25°C results in a 25% reduction in the uncertainty of the

average heat exchange rate. PCMs are also widely used in buildings where the temperature change is small during the day [80], and for an effective PCM design in such applications, the uncertainty should be known within ±10% for the specific enthalpy and ±0.5°C for melting temperature [84].

When measurements are performed in a DSC, some errors arise from the measurement of the heat transferred to the calorimeter from the samples [85]. The effect of these uncertainty sources is thus of interest, particularly for PCMs where the melting enthalpy is very high and the thermal conductivity is low [7, 23]. As more applications of PCMs have approached the commercial stage a precise knowledge of the thermophysical properties of PCMs has become more important. The lack of a clear standard for DSC measurements of PCMs has resulted in differing measurements being reported in the literature [7, 23].

The existing standards and methods for calorimetry, which were designed for other materials, can lead to a large errors if applied to PCMs [84]. Results are often systematically shifted to higher or lower values.

In this section, several DSC measurements have been carried out to prove that these differences are not due to the variability of materials, but are due to problems with the measurement mode itself. More specifically, due to the strong influence of heating rate and sample mass on the DSC results for PCMs.

3.2.1. Phase Change Materials. Five heat storage materials, namely Palmitic Acid, Myristic acid, Lauric Acid, Capric acid, and Lauryl Alcohol were tested. These materials were selected based on their melting temperatures (24 - 62 °C), which are suitable for many low temperature heat storage applications, high latent heat, ease of availability, high specific heat, nontoxicity, low cost, and the availability of their thermophysical properties in literature [74]. Table 3.3 shows the PCM's chemical data and values which were collected by the National Institute of Standards and Technology (NIST).

Table 3.3. Compositions and chemical data for the reference PCMs

Name	Scientific Name	Molecular Formula	CAS Number	Melting Temperature [°C]	Melting Enthalpy [J g^{-1}]
Myristic Acid	Tetradecanoic acid	$C_{14}H_{28}O_2$	544-63-8	53.96 ±0.15	197.97 ±0.19
Capric Acid	n-Decanoic acid	$C_{10}H_{20}O_2$	334-48-5	31.19 ±0.37	162.69 ±1.01
Lauryl Alcohol	1-Dodecanol	$C_{12}H_{26}O$	112-53-8	24.00 ±0.09	215.83 ±0.35
Palmitic Acid	n-Hexadecanoic acid	$C_{16}H_{32}O_2$	57-10-3	62.47 ±0.54	211.99 ±2.89
Lauric Acid	Dodecanoic acid	$C_{12}H_{24}O_2$	143-07-7	43.92 ±0.30	181.45 1.18

3.2.2. Experimental Process and Data Analysis. In order to examine the influence of sample mass and heating rate on the accuracy of the results, measurements were carried out for the five selected PCMs. First, measurements were performed using the Seiko DSC6200 for Myristic acid and Capric acid. Each PCM was tested at four different sample masses (2.5, 5, 7.5, and 10mg), and each sample was subjected to four different heating rates (0.5, 1, 3 and, 5°C/min). Palmitic acid and Lauric acid measurements were performed with the Seiko DSC6200 at only a sample mass of 7.5mg at varying heating rates (0.5, 1, 3 and, 5°C/min).

In order to check the reproducibility of the measurements Lauryl Alcohol measurements were performed in a different laboratory using a different DSC instrument (DSC2010, TA instrument) under the same measurements conditions.

Each sample of Lauryl Alcohol was tested at four different sample masses (2.5, 5, 7.5, and 10mg), and each sample was subjected to four different heating rates (0.5, 1, 3 and, 5°C/min).

The phase transition temperature, onset temperature, and the enthalpy of fusion were analyzed at different heating rates and sample weights to show that the experimental results differ considerably at different measurements conditions.

The experimental data was compared with NIST data to reveal the effect of different measurement conditions.

To easily compare the experimental data with the reference data from NIST, all the reference values were considered as a baseline value (*Pref*). The variations between the experimental values (*Pexp*) and the reference values (*Pref*) were presented as a percentage error for each parameter (*P%*), and calculated using Equation 11 as follows:

$$P\% = \left| \left(\frac{P_{exp}}{P_{ref}} - 1 \right) \right| \times 100\% \qquad (11)$$

3.2.3. Results and Discussion. Table 3.4 represents the DSC experimental data for a total of 56 experiments performed for PCMs with various heating rates as a function of the sample mass. The melting onset temperatures, melting temperatures and melting enthalpies are presented.

Table 3.4. DSC experimental measurements of onset temperature, melting temperature, and heat of fusion

Materials		T_o [°C]				T_m [°C]				ΔH_m [J g^{-1}]			
Heat Rate [°C/min] →		***0.5***	***1***	***3***	***5***	***0.5***	***1***	***3***	***5***	***0.5***	***1***	***3***	***5***
Myristic Acid	***2.5mg***	51.07	51.42	51.40	51.90	52.57	52.97	53.66	55.37	191.1	191.3	193.1	193.5
	5 mg	51.45	51.40	51.16	51.49	52.67	52.87	53.62	54.59	193.3	194.3	196.5	197.5
	7.5mg	51.71	51.43	51.00	51.29	52.87	53.32	54.21	54.87	193.4	194.7	198.5	199.1
	10 mg	51.64	50.79	51.22	51.34	52.87	53.65	54.76	55.55	194.0	196.1	198.5	199.8
Capric Acid	***2.5mg***	29.5	29.27	29.15	29.59	30.16	30.27	30.64	31.28	156.3	157.9	159.0	161.2
	5 mg	29.19	29.22	29.27	29.17	30.19	30.44	31.10	31.52	158.8	159.7	161.2	162.3
	7.5mg	29.51	29.31	29.19	29.56	30.42	30.85	31.82	32.28	161.4	161.7	162.2	165.5
	10 mg	29.54	29.74	29.47	28.92	30.64	31.18	32.10	32.30	161.7	162.8	164.2	165.8
Lauryl Alcohol	***2.5mg***	20.55	20.89	20.98	22.01	21.87	22.34	23.05	23.57	202.2	208.2	215.1	218.1
	5 mg	20.90	20.83	20.9	21.08	21.87	22.34	23.38	23.70	204.6	212.1	215.4	218.5
	7.5mg	20.88	20.78	20.88	21.03	22.13	22.94	23.83	24.51	206.2	213.8	216.5	218.8
	10 mg	20.88	20.88	20.82	20.82	22.04	22.63	23.90	24.89	207.1	214.2	219.4	221.0
Palmitic Acid	***7.5mg***	60.83	60.50	60.28	63.50	61.69	62.08	62.93	63.87	205.8	207.7	209.3	214.7
Lauric Acid	***7.5mg***	40.64	40.78	42.72	40.79	42.56	42.78	43.98	44.35	177.3	178.0	180.8	183.4

Figures 3.12-3.16 display the DSC heat flow curve for five PCMs chosen to display the shapes of the peaks determined in dynamic mode at different heating rates and sample masses. The figures show that the test data and peak shapes vary significantly at different measurement conditions for all the samples. The shape of the DSC curve and the thermal behavior of PCMs in a DSC depend significantly on the heating rate and sample mass. As the onset temperature (T_o) values are not affected significantly, the melting process starts at the same temperature for all cases but continues its evolution over a wider range of temperatures for higher heating rates or sample masses. For example, as one can see in

Figure 3.16, the end of the phase change peak is shifted from 26.2°C (2.5mg) to about 29.3°C (10mg). It is also noted that the melting peak temperature (T_m) increases when increasing the heating rate or sample mass.

The lower heating rates of 0.5°C/min and 1°C/min provide a good resolution for determining the phase transition temperature. However, the sensitivity of the latent heat measurement is lower, especially for small sample masses of 2.5mg. The increase in latent heat sensitivity with increased heating rate or sample mass is caused by a much larger heat flow signal associated with a very small corresponding increase in signal noise. It is therefore important to choose an optimum heating rate and sample mass to maintain good sensitivity and resolution at the same time.

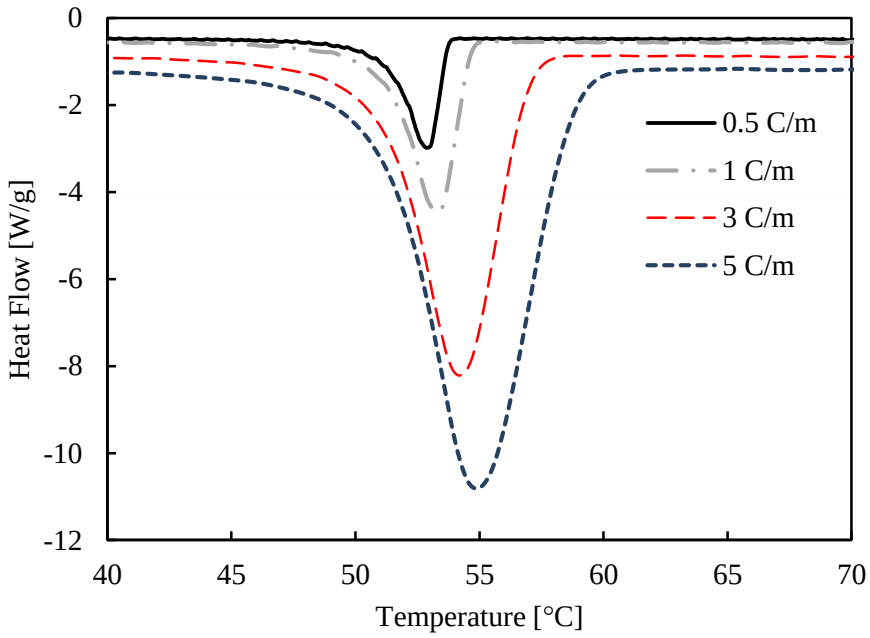

Figure 3.12. Results of dynamic DSC measurements of 7.5 mg of Myristic Acid at various heating rates

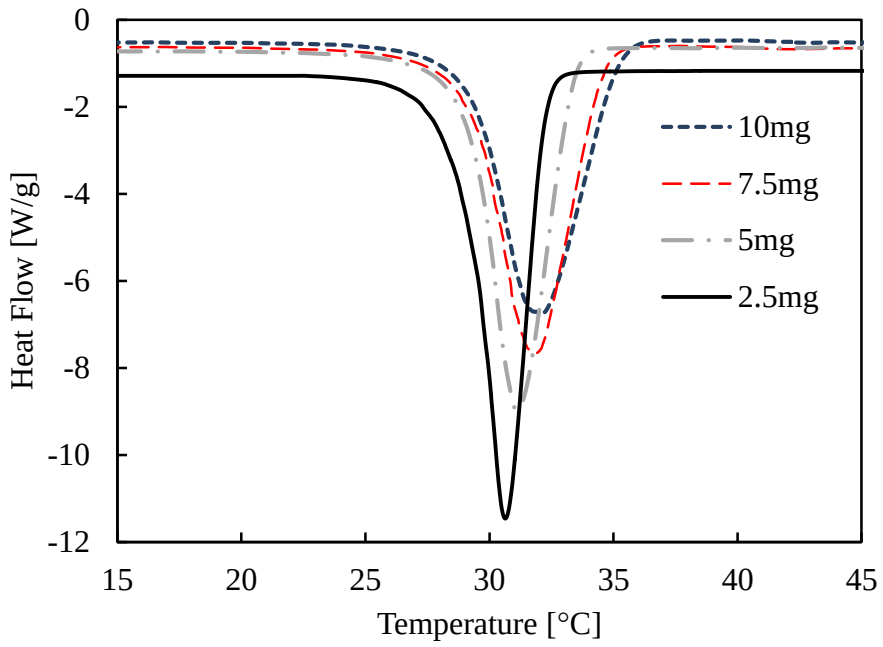

Figure 3.13. Results of dynamic DSC measurements of Capric Acid at 3°C/min at various samples mass

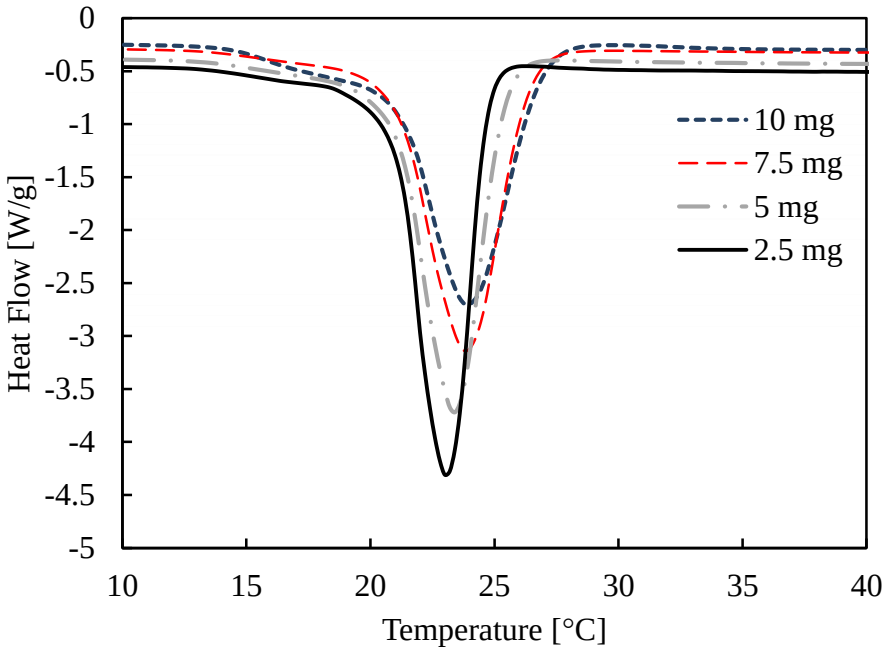

Figure 3.14. Results of dynamic DSC measurements of Lauryl Alcohol at 3°C/min at various samples mass

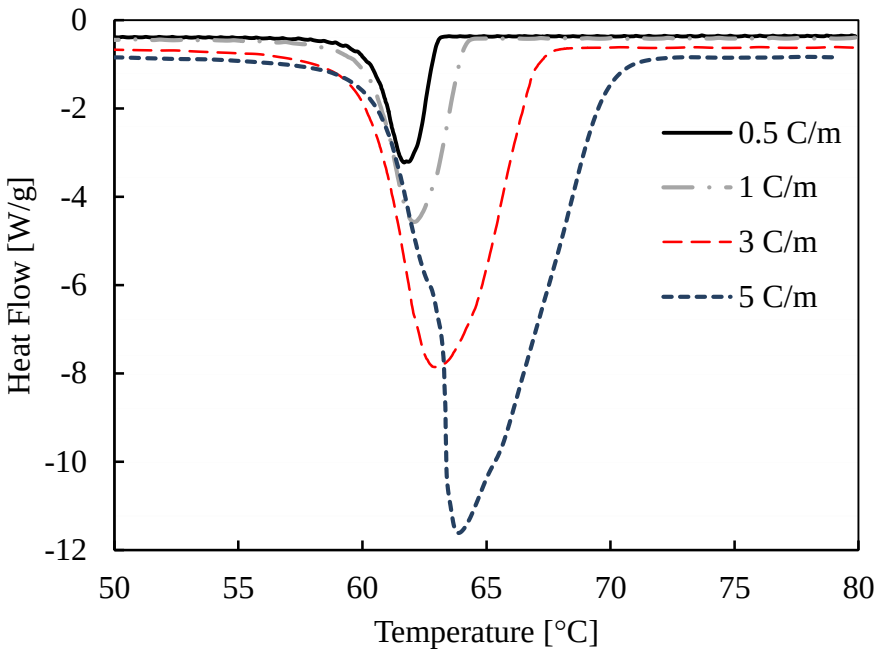

Figure 3.15. Results of dynamic DSC measurements of 7.5 mg of Palmitic Acid at various heating rates

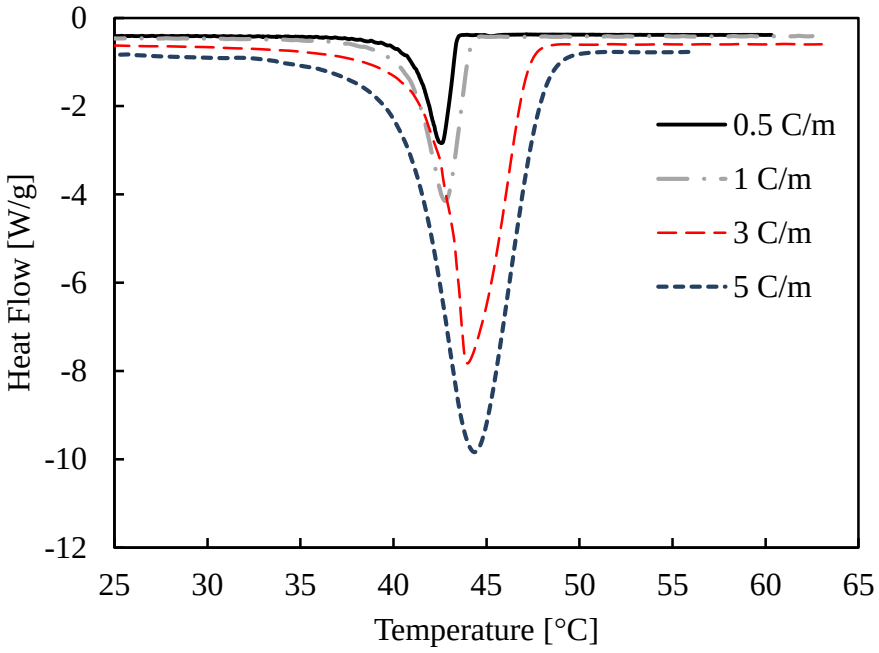

Figure 3.16. Results of dynamic DSC measurements of 7.5 mg of Lauric Acid at various heating rates

Figure 3.17 displays the melting temperatures for five PCMs (Myristic acid, Capric acid, Palmitic Acid, Lauric Acid, and Lauryl Alcohol) at varying heating rates and sample masses. The main finding was a significant difference in T_m between measurements. Figure 3.17-a shows the melting temperature results of PCMs of the same sample mass (7.5 mg) at varying heating rates. Figure 3.17-b shows the melting temperature results for PCMs at the same heating rate (3°C/min) but varying sample masses. As clearly seen in Figure 3.17, the melting temperatures significantly increase with the increase in heating rate or sample mass. For example, T_m for Capric Acid was observed at 30.64°C for a sample mass of 2.5 mg at 3°C/min heating rate, and shifted to higher temperatures with higher sample mass to 31.10, 31.82 ,and 32.10 °C at 5, 7.5, and 10 mg, respectively

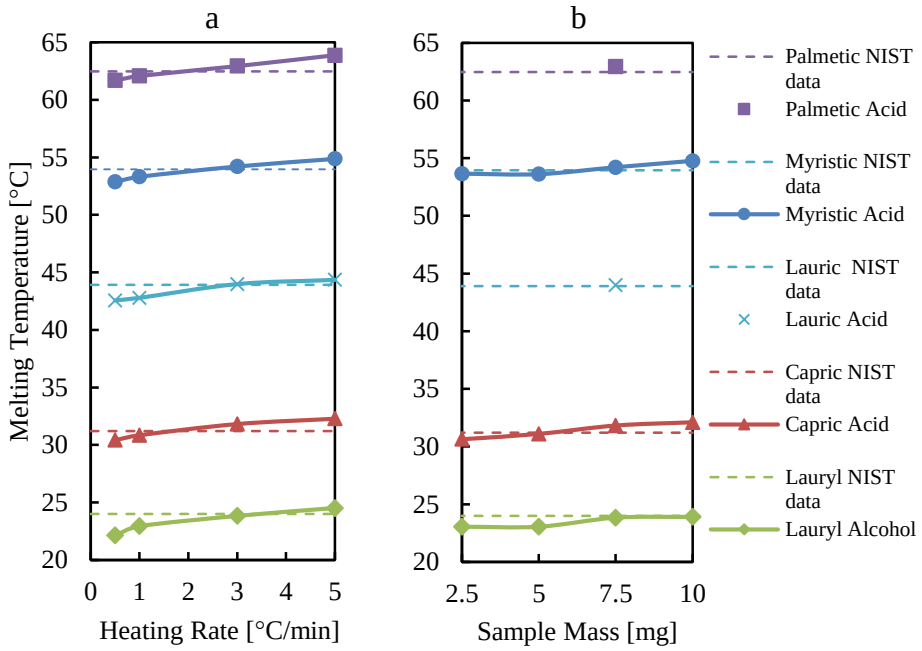

Figure 3.17. The effect of the varying heating rate (a) and sample mass (b) on the measured melting temperature

. It can be seen in Table 3.4 that a similar behavior in T_m is observed when varying the heating rate for other constant sample masses (2.5, 5, and 10mg).

The same trend can also be observed when varying the sample mass under other constant heating rates (0.5, 1, and 5°C/min). Samples with low heating rates (0.5°C/min) deviate strongly from the NIST reference values, especially at lower sample masses of 2.5mg.

Figure 3.18 illustrates the trend in ΔH_m values under varying heating rates and sample masses for five PCMs (Myristic acid, Capric acid, Palmitic Acid, Lauric Acid, and Lauryl Alcohol).

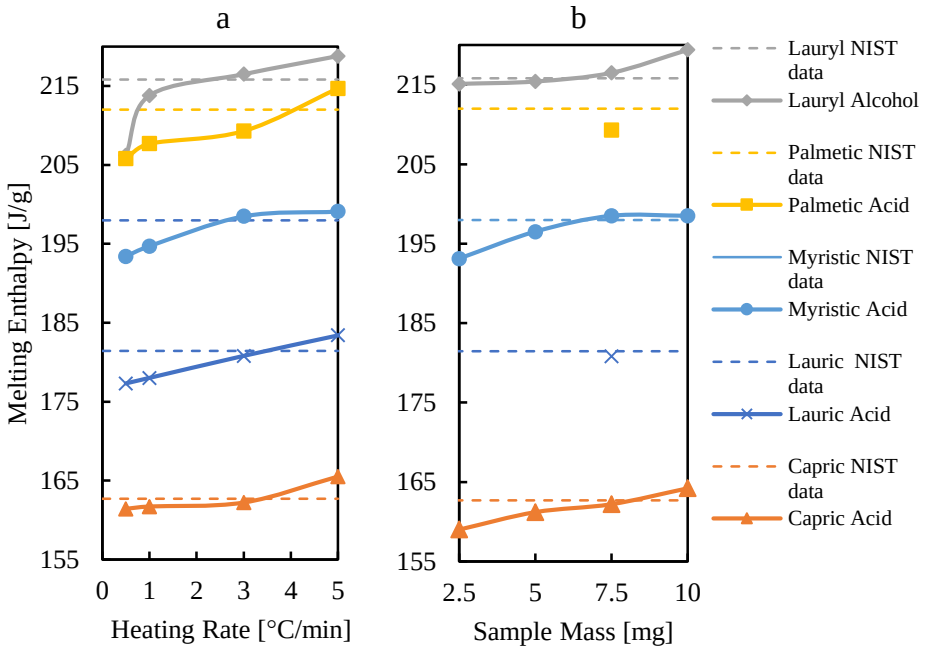

Figure 3.18. The effect of varying heating rate (a) and sample mass (b) on the measured melting enthalpy

In Figure 13.18-a, results for PCMs of the same sample mass (7.5mg) at varying heating rates are compared. In Figure 3.18-b, the experimental results for PCMs at the same heating rate (3°C/min) but varying sample masses are compared. For higher heating rates and sample masses, a slight increase in ΔH_m was observed. In general, the enthalpy values do not diverge too much from the reference NIST values with varied measurement conditions, with the exception of lower masses (2.5mg). At lower masses, the values deviate strongly, especially at low heating rates. When compared to T_m, The increase in ΔH_m shows a lower dependency on the heating rate and sample mass.

The average variation of all the ΔH_m measurements from the NIST reference values are only within ±1.78%, whereas the average absolute change for T_m is within ±0.87°C. This is considered to be a significant error for PCM applications, in which the melting temperature must be determined with a very high accuracy due to its very important role in the system's behavior. On the other hand, a ±1.78% uncertainty for the melting enthalpy is within the typical uncertainty of the DSC method [86, 87]**.** However, as is clearly seen in Table 3.5, even lower uncertainties can still be achieved if correct measurement conditions are chosen carefully.

The clear trend of peaks shifting toward higher temperatures with an increased sample mass or heating rate can be explained by the internal thermal gradient inside the PCM samples. The thermal gradient in the crucible is created as the constant heating rate is supplied, and the effect increases with an increasing heat rate or sample size. This thermal gradient effect is very strong for PCMs in particular because PCMs have a high thermal energy storage combined with a low thermal conductivity and heat diffusivity [23]. As a consequence, a gradient of temperature is developed throughout the material and the

temperature is not uniform throughout the sample. The measured temperature by the DSC sensor, which is in direct contact with the specimen surface, is higher than the average sample temperature - especially at higher heating rates and sample mass. In this situation, a thermal lag exists between the thermocouples and the sample, and the instrument response becomes slow. Since the temperature difference between the average sample temperature and DSC sensor is due to the time necessary for the heat flux to dissipate through the sample, lower heating rates and sample masses, up to a certain limit, can help to reduce these effects.

When measurements on PCMs are performed in a DSC some sources of error arise from the heat transferred to the calorimeter from the samples, especially for materials of high enthalpy storage [88, 89]. With materials like PCMs in particular, the effect of these uncertainty sources becomes much more significant. As mentioned above, the shift in transition temperatures is very high for substances like PCMs, in which the heat diffusivity and thermal conductivity are very low. PCMs tend to melt over wider range of temperatures, and the shift in transition event is significant under varying measurements conditions.

This effect is less significant for other materials, especially for pure materials like indium samples. For measurements by Poel and Mathot [90] of indium samples studied at varying heating rates and sample masses, the maximal increase in indium melting temperatures was only within ΔT=0.5°C. These samples were studied within the same range of interest for the current study in terms of heating range (1-5°C/min) and sample mass of (1 to 8 mg), and a maximal increase of only 0.4°C for melting temperature was observed when sample mass increases from 1 mg to 8 mg at heating rage of 5°C/min. On

the contrary, as seen in Table 3.4 for PCMs, the change in melting temperatures in some cases has reached a value of ΔT=3.8°C, as was in the case of Myristic acid when heating rate increased from 0.5 to 5°C/min with a sample mass of 2.5 mg.

A possible explanation for the slight increase in melting enthalpy at an increased heating rate or sample mass is that at higher heating rates and samples mass, as seen in Table 3.6, the transition occurs over a wider range of temperature due to the internal thermal gradient. Therefore liquid PCM may exist at higher temperatures than the melting temperature, resulting in some sensible heat being included in the latent heat measurement. Hence melting is measured to be at a higher temperature with a higher heat of fusion.

Explained in another way as supported by Kasap's [91] observations, the increase of melting enthalpies with higher DSC heating rates or sample masses is due to the instrument sensitivity and resolution. For smaller sample mass or heating rate, the instrument's resolution is improved at the cost of its sensitivity.

The DSC sensitivity can be expressed by the maximum heat flux value corresponding to the peak height [92, 93]. This effect of heating rate and sample mass on the DSC resolution and sensitivity is confirmed experimentally in Figure 3.19. The sensitivity of the calorimeter is found to be directly proportional to the sample mass and heating rate.

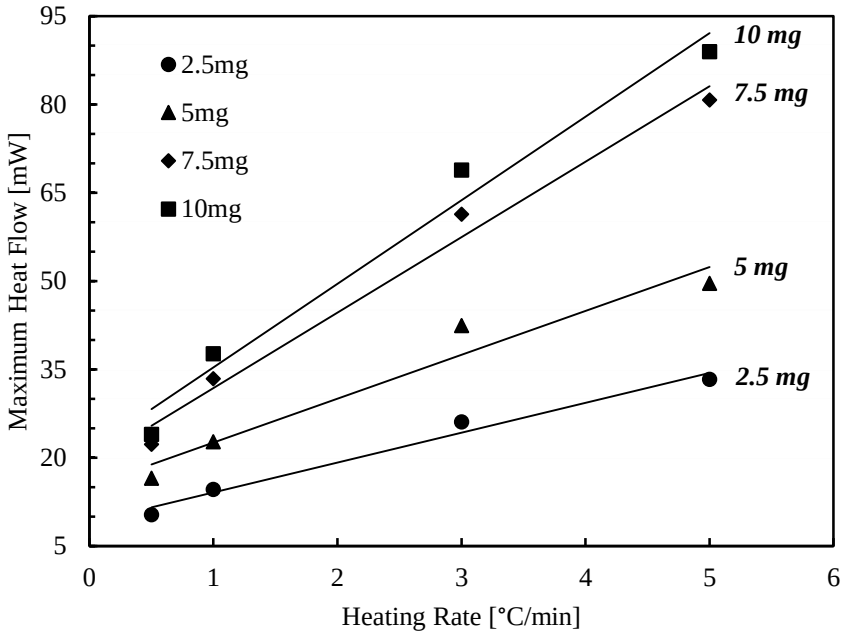

Figure 3.19. Maximum heat flux for varying heating rates and sample masses of Myristic acid

Figure 3.20 shows the experimental heat flow response to varying heating rate for the same material. At lower heating rates, a low rate of enthalpy change is obtained. In other words, the endothermic reaction of phase transition is expanded over a longer period of time. For example at a heating rate of 5°C/min, the phase transition from solid to liquid occurs in less than 6 minutes, compared to about 11 minutes at a lower heating rate of 0.5°C/min. because the heat flux measurement is lower for the lower heating rate, the measurement uncertainty is higher and the instruments sensitivity is lower. Supported by these observations and according to the literature [94], a lack of accuracy results.

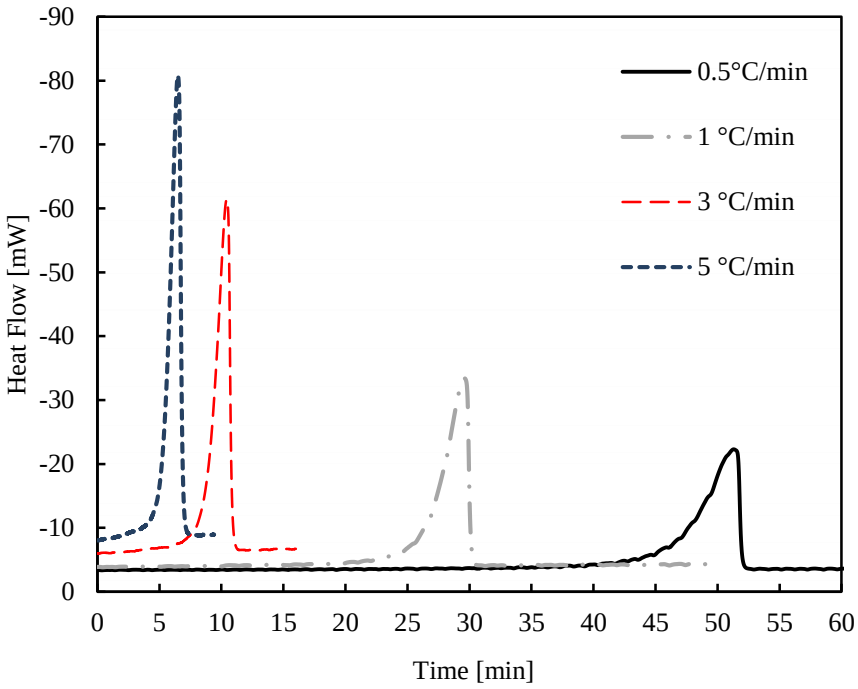

Figure 3.20. Effect of heating rate on the DSC resolution and sensitivity

It can be concluded that with an increase in the heating rate or sample mass, transition temperatures and enthalpy values are systematically shifted to higher values. Also, it is suggested that very large samples and high heating rates are not recommended, since a temperature gradient is developed through the sample and the rate of heat transferred by conduction must be taken into account. Therfore, the thermal lag effect on transition events becomes much more significant. Lower heating rates and sample masses can help to reduce the thermal gradient effect and help to distinguish two separate transition peaks in some cases. However, use of slow heating rates or very small sample masses results in a simultaneous decrease in the DSC sensitivity due to the weaker signal. This causes a decreased accuracy in the enthalpy determination. Furthermore a very slow

heating rate increases the time needed for experiments, and the results for very small samples may not be representative of the bulk material.

Table 3.5 shows the absolute variation for the experimental melting temperature and the percentage variation for the melting enthalpy by applying Equation 11. The variation of experimental data was compared to the NIST reference values. To provide much more representative data related to the heating rate and sample mass, the average deviation of T_m and ΔH_m for all the PCMs combined together at varying heating rates and sample's mass is presented in Table 3.6. The average deviation was calculated by taking the average of the deviation of the individual results for all of the measurements. It is seen that uncertainties in T_m and ΔH_m values are relatively high at very low heating rates. As previously mentioned, This can be explained by the decreased (signal to noise) ratio at very small heating rates [95] and by the decreased sensitivity with lower heating rates [91, 93]. A comparatively high heating rate is recommended for an accurate determination of the enthalpy but only up to a certain limit where the thermal gradient effect is minimal.

Table 3.5. The variation for the experimental melting temperature and melting enthalpy of all the PCMs from the NIST referene data

Heat Rate [°C/min] →	$\pm T_m$				$P_{\Delta Hm}$			
	0.5	***1***	***3***	***5***	***0.5***	***1***	***3***	***5***
2.5mg	±1.52	±1.19	±0.60	±0.64	4.57%	3.28%	1.69%	1.41%
5 mg	±1.47	±1.17	±0.35	±0.42	3.32%	1.81%	0.62%	0.57%
7.5mg	±1.17	±0.71	±0.31	±0.87	2.55%	1.42%	0.50%	1.21%
10mg	±1.20	±0.56	±0.60	±1.20	2.22%	0.59%	0.95%	1.75%

Table 3.6. The average variation for the experimental melting temperature and enthalpy of all the measurements from the NIST reference data

Heat Rate [°C/min] →	$P_{Tm+\Delta Hm}$			
	0.5	***1***	***3***	***5***
2.5mg	4.60%	3.30%	1.70%	1.42%
5 mg	3.35%	1.84%	0.63%	0.59%
7.5mg	2.58%	1.44%	0.51%	1.24%
10mg	2.25%	0.62%	0.97%	1.79%

Considering the average deviation of all the measurements of T_m and ΔH_m, it can be suggested that the most accurate results were obtained at heating rate and sample mass of 3°C/min and 7.5 mg respectively. At this measuring condition, the deviation in T_m and ΔH_m from the NIST reference values did not exceed ±0.31 and 0.50% for the melting temperature and heat of fusion, respectively. This suggests that this range of heating rate and sample mass is an appropriate choice to combine an accurate results for both of the melting enthalpy and melting temperature at the same time. For example, at this measurement condition a maximal difference of only ±0.64°C (0.21%) in T_m and 1.27% in ΔH_m was observed compared to the NIST reference values. Moreover, a sample size of 7.5 mg allows the bottom of most of the available standards pans to be completely covered with a thin layer of sample. At this measurements condition, a very good agreement with the NIST reference data is observed, and the shift in thermal events was minimal. Moreover, the averaged uncertainty in the determination of both T_m and ΔH_m combined together is only 0.32%.

A high heating rate mode helps to obtain a better accuracy for the melting enthalpy, but at the cost of decreased resolution and an increase in the thermal gradient effect and thermal lag. It is suggested that a smaller sample mass be used when DSC measurements

are performed at a high heating rate to reduce the drawbacks of the high heating rate and attain a high accuracy at the same time. Using a smaller sample mass when an increased heating rate is applied reduces the expected increase in the internal thermal gradient throughout the sample, avoiding any extra thermal lag arising and maintaining the DSC resolution. According to Pijpers et al. [96], if the heating rate is increased by a factor (*Y*), the sample mass has to be reduced by the same factor (*Y*). In this way, an important aim is achieved: the measuring time is shortened by using the high heating rate, higher accuracy is attained, and the drawbacks associated with the higher heating rate are avoided at the same time.

It must be mentioned that the correct choice of DSC measurements conditions is very crucial with PCMs. When incorrect results such as the transition temperature range are used in the design of a PCM storage system, the phase change process may not be completed and the system will fail to store or release the total value of the heat of fusion. Accurate determination of phase transition parameters helps to design the system with an appropriate capacity, temperature range and, size.

3.3. THERMAL CONDUCTIVITY OF PCMS

The study of the thermal conductivity of the experimental samples was done by the Transient Hot-Bridge technique using a thermal conductivity measuring instrument (THB1, Linseis Inc., USA [81]). Table 3.7 shows the reported thermal conductivity values of 10 measurements and their average for each PCM material. The thermal conductivity of the PCMs was tested at about 10°C above their experimental melting temperature.

Table 3.7. Thermal conductivity for the selected PCMs

Test	Lauryl Alcohol	Capric acid	Lauric Acid	Myristic Acid	Palmitic Acid
1	outlier	0.1598	outlier	0.169	outlier
2	0.1697	0.1597	outlier	outlier	0.1755
3	outlier	0.1602	outlier	outlier	0.1724
4	0.1686	0.1604	0.1633	0.1694	0.1691
5	outlier	0.1607	0.1632	0.1676	outlier
6	0.1708	0.1566	0.1638	0.1669	0.1733
7	0.1696	0.161	0.1636	0.1665	outlier
8	0.1696	0.161	0.1639	0.1665	0.1682
9	0.1695	0.1611	0.1637	0.1666	0.1687
10	0.1693	0.1566	0.1630	0.1666	0.1699
Avg	0.1696	0.1597	0.1635	0.1674	0.1710
Std	±0.0006	±0.0016	±0.0003	±0.0011	±0.0025

The thermal conductivity for the measured PCMs was very low as generally expected in organic PCMs. However, the enhancement of the thermal conductivity of the PCMs has been studied by many researchers [11, 12, 17, 82, 97-104] using several types of Nano-additives and metallic fillers.

3.4. DENSITY

The density for selected PCMs was measured and summarized in Table 3.8. The density of the solid phase was measured at about 10°C below the experimental melting

temperature and at about 10°C above the experimental melting temperature for the liquid phase.

Table 3.8. The experimental density for the selected PCMs

Test	ρ_{Solid} g/ml	Uncertainty g/ml	ρ_{Liquid} g/ml	Uncertainty g/ml
Lauryl Alcohol	0.8868	±0.0044	0.8337	±0.0045
Capric acid	0.8916	±0.0049	0.8486	±0.0050
Lauric Acid	0.8885	±0.0052	0.8562	±0.0048
Myristic Acid	0.8663	±0.0059	0.8165	±0.0059
Palmitic Acid	0.8512	±0.0054	0.8164	±0.0059

It was noted that the selected PCMs which belong to the organic PCMs have an acceptable decrease in their density when they melts. Therefore, their volume expansion during phase transformation from solid to liquid are minimal and not expected to cause any problems when the materials are encapsulated in containers or sheets for any applications. For that reason, these kinds of PCMs are considered to be very attractive for TES applications, because the required empty space that is equivalent to thier volume expansions is very small.

3.5. THERMAL DIFFUSIFITY

The thermal diffusivity of the selected PCMs was measured using Equation 8. The experimental heat capacity, density, and thermal conductivity were used to calculate the

thermal diffusivity of solid and liquid phases. Reviewing the available literature revealed that the difference in thermal conductivity between the liquid phase and solid phase for PCMs was not significant and the difference was within an average of 8% [6, 12, 17, 97-99, 105]. In this study, the thermal conductivity of liquid phase was experimentally determined. Therefore, the thermal diffusivity for the liquid phase can be determined directly. However, In order to determine the thermal diffusivity for the solid phase, the thermal conductivity for the solid phase was assumed to be equal to its value for the liquid phase. The THB1 meter is capable of measuring the thermal conductivity for liquid and solid samples. However, the thermal expansion of PCMs when they solidify around the sensor caused some air gaps to be exist between the surface of the THB1 sensor and the PCM material, which caused a disturbance for the heat signal of the sensor. Therefore, full contact between the sensor and the solid PCM was not possible and the instrument was not able to measure the solid phase thermal conductivity. The value was assumed to be equal for its value for the liquid sate. Table 3.9 summarizes the thermal diffusivity results for the selected PCMs.

Table 3.9. The thermal diffusivity for MP and LA and their eutectic mixture

Test	α_{Solid} mm^2/s	α_{Liquid} mm^2/s
Lauryl Alcohol	0.115	0.090
Capric acid	0.081	0.080
Lauric Acid	0.090	0.093
Myristic Acid	0.101	0.102
Palmitic Acid	0.110	0.110

3.6. EXPERIMENTAL INVESTIGATION OF THE THERMAL PERFORMANCE OF NOVEL EUTICTIC MIXTURE OF Gel-PCM FOR TES IN BUILDINGS

The U.S. Energy Information Administration (EIA) publishes a monthly energy review of the recent and historical energy statistics. The total energy consumption by the residential and commercial building sectors was estimated to be 41% of the total U.S energy consumption ("Monthly Energy Review", 2016). Heating and cooling requirements alone account for 58% of the total energy consumption in the residential and building sectors [1]. Therefore, the use of PCMs for thermal regulation and thermal energy storage in buildings provides an elegant solution for more efficient energy use. Despite the great efforts devoted to study a variety of its applications, the thermal energy storage using phase change materials is very challenging, and some targets cannot be met with the existing materials. This study involves a systematic and rational approach to discover novel enhanced energy storage materials that hold promises to achieve attributes that other materials cannot achieve.

The first goal was to discover a new PCM consisting of a eutectic binary mixture as a promising candidate for thermal regulation and TES applications. The next goal was to make a novel eutectic mixture characterized by a solid to (Gel) phase transformation with an enhanced thermal performance. The proposed eutectic mixture consists of a (Methyl Palmitate and Capric acid) PCMs as the thermal energy storage components. This eutectic mixture was further enhanced by a Solid to (Gel) phase transformation feature using Methyl hydroxyethyl cellulose as a thickening or gelling agent at an appropriate composition for each. Moreover, the thermal performance of the prepared gel-PCM was further enhanced with Nano-graphene platelets (NGPs).

The PCM materials were selected based on the ease of availability and low cost for commercial applications, as well as their desirable thermophysical properties and, most important, the suitable melting temperature of their final composition (Gel eutectic mixture modified by NGPs). In order to guarantee an excellent thermal performance, the eutectic mixture has to possess a high latent heat of fusion with a suitable melting temperature for thermal regulation and thermal storage in building applications.

Basically, thermal energy storage using phase change materials is accomplished through solid to liquid phase transformations. However, for many thermal energy storage applications such as buildings, medical applications, solar panels, or transportation containers for instance, the PCM in its liquid phase has many disadvantages such leakage and the undesired weak structural strength.

PCMs have been used in buildings structure for thermal regulations, reducing energy consumption, and reducing the indoor temperature swing. To achieve these objectives, PCMs in buildings are used in many ways either by incorporating them through gypsum mixture, cement paste, and mortar [104, 106, 107] or by using PCM in the wallboards, ceiling tiles, or floors of buildings.

In addition to the problem of PCM leakage, many studies [100, 108-110] also reported that the use of PCMs in cement paste, mortar, and gypsum mixture, significantly decrease the compressive strength and structural strength when these structures were incorporated with PCM content. Li et al. [111] reported that previous studies have mainly been focused on the preparation of from-stable or shape-stabilized PCM composites but without considering the expected PCM leakage when the material melts. Their results showed that the leakage of PCM from cement mixture was found to be significant when

the PCM was incorporated with the cement paste composite without the use of modifier or gelling agent. The PCM leakage ratio from the PCM/Cement composite when PCM melted was 57.3%, which is considered to be very high and causes a large decrease in the thermal energy storage capacity of the PCM composite. Moreover, incorporating pure PCMs was found to have a significant effect on the composite structural strength. Therefore, it's very important to provide a form-stable or shape-stabilized PCM composite by using an appropriate gelling or thickening agent.

The proposed PCM gelled mixture can be incorporated in the wallboards, ceiling tiles, floors, or the material structure of buildings and conditioning units in order to reduce temperature swing and energy consumption. Moreover, the gelled PCM mixture is expected to have many benefits by preventing leakage, reducing fluidity of the PCM, and providing the required structural strength. Additionally, gelled PCM is expected to improve the stability over multiple cycles, increase the viscosity, prevent phase segregation and separation, and also work as a crosslinked medium when Nano-additives are used and prevent them from sinking in to the bottom by holding the material together.

3.6.1. Preparation of MP-LA Binary Eutectic Mixture. This section investigates the thermal characterization of a eutectic binary mixture of Methyl Palmitate (MP) and Lauric Acid (LA) as a promising candidate for thermal regulation and TES applications.

3.6.1.1 Materials. Methyl Palmitate (MP) and Lauric Acid (LA) were supplied by Sigma Aldrich. A binary eutectic mixture of 60% MP and 40% LA was prepared. The chemical data of the pure PCMs and their thermal properties are listed in Table 3.10 [74].

Table 3.10. The chemical data of the pure PCMs used for the eutectic mixture

Name	Molecular weight [g mol^{-1}]	Molecular Formula	CAS Number	Melting Temperature [°C]	Melting Enthalpy [J g^{-1}]
Methyl Palmitate	270.4507	$C_{17}H_{34}O_2$	112-39-0	32.20	207.06
Lauric Acid	200.3178	$C_{12}H_{24}O_2$	143-07-7	43.92	181.12

3.6.1.2 Preparation of the binary eutectic mixture. The investigation of eutectic mixtures is usually done by several experiments until an ideal PCM mixture with a certain mass percentage is found at a certain melting temperature with a single desirable "sharp" melting peak and high enthalpy.

Therefore, In order to obtain the required results, several experiments must be performed to find an optimum mixture and composition. This process is time consuming and requires a lot of work. In comparison, the initial predicting of the molar percentage, phase change temperature, and latent heat of fusion can be done by theoretical prediction of the material phase diagram.

The phase change temperature, latent heat of fusion, and their optimum mixing ratio for a binary mixture can be determined by thermodynamic calculations by Schroder-Van Laar equation [112] using Equation 12:

$$T_m = \frac{\Delta H_i}{\frac{\Delta H_i}{T_i} - R \ln X_i} \quad , i = A \ , B \tag{12}$$

Where ΔH_i is the latent heat of fusion for PCM components A and B in units of J/mole, T_m is the melting temperature of the eutectic mixture in units of Kelvin, T_i is the melting temperature of the pure PCM components A and B. X_i is the mole ratio of

components A and B. R is the universal gas constant 8.315 J/(mole.K). Therefore, the phase diagram of the eutectic mixture can be plotted using Equation 11 directly.

Supported by the model proposed by Zhang et al. [113], the latent heat of fusion for the binary eutectic mixture can be calculated using Equation 13 as follows:

$$H_m = T_m \sum_{i=1}^{n} \left[\frac{X_i H_i}{T_i} + X_i (C_{P,i}^{Liq} - C_{P,i}^{Sol}) \ln \frac{T_m}{T_i} \right] \quad , i = A \ , B \tag{13}$$

Where $C_{P,i}^{Liq}$ and $C_{P,i}^{Sol}$ is the specific heat at constant pressure of the component "i" at the solid and liquid phase, respectively. If the molecular weight of the PCM component is big enough, the sensible heat part in the equation can be ignored and the latent heat of fusion can be calculated within an error of less than 4% using Equation 14 as follow:

$$H_m = T_m \sum_{i=1}^{n} \frac{X_i H_i}{T_i}, \quad i = A \ , B \tag{14}$$

Figure 3.21 illustrates the evaluated phase diagram for the proposed MP-LA binary mixture at different molar ratios. Points A and B stand for the melting temperature of pure PCM components, LA and MP, receptively. With the increase in the MP concentration, the melting point of LA gradually decreases until it reaches point E along the line AE. A similar behavior for the pure MP occurred with the increase in the LA concentration along line BE. At point E (Eutectic Point), both of the PCM components melt simultaneously at the same time and temperature, and the phase change transformation occurs in a single sharp peak. The theoretical eutectic point (E) for this binary mixture is observed at MP/LA molar ratio of 60/40.

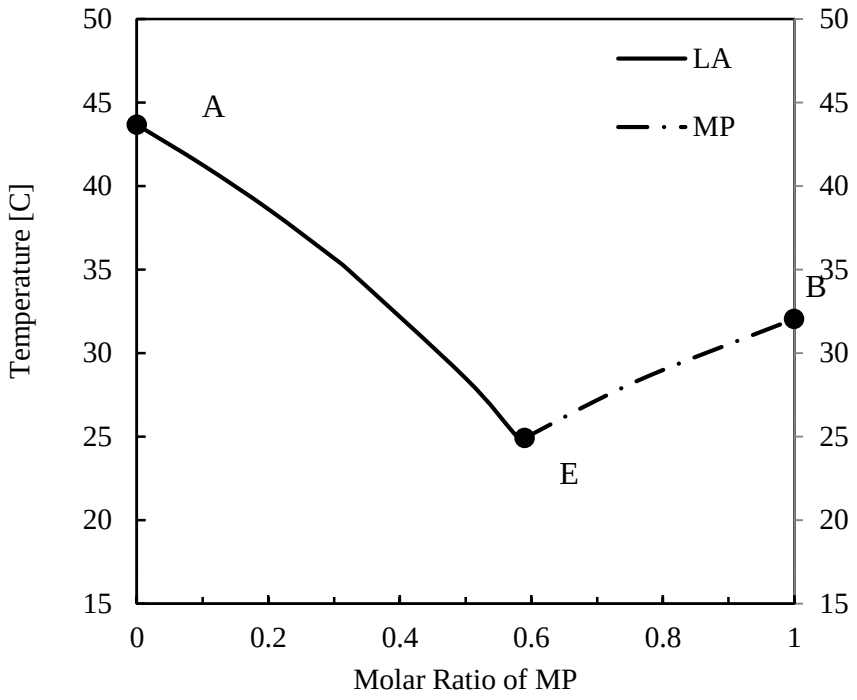

Figure 3.21. The experimental phase diagram for the MP-LA eutectic system

It can be concluded that the initial theoretical prediction of the molar ratio, phase change temperature, and latent heat of fusion using Equation 13, due to the dispersion of MP in LA, is expected to produce an ideal PCM eutectic mixture that melts at 24.8°C with a latent heat of 203.1 J/g, at a molar ratio of 60/40.

3.6.1.3 DSC thermal analysis. In order to verify the predicted eutectic mixture and its thermal behavior, the eutectic mixture of Methyl Palmitate in Lauric Acid at a molar ration of 60/40 has been experimentally investigated in a DSC. The MP-LA binary mixture was prepared by mixing the PCM materials at about 25°C above their theoretical predicted melting temperature (mixed at 50°C) and stirring them for 15 minutes.

The DSC melting curve of the binary eutectic mixture is shown in Figure 3.22. The DSC thermal analysis showed that the binary eutectic mixture of Methyl Palmitate (MP)

and Lauric Acid (LA) showed a single narrow melting phase change peak melting temperature at 25.5°C, and the latent heat of fusion was 205.2 J/g. The experimental values were in good agreement with the theoretical values with a relative error of 0.23% and 1.0% for melting temperature and latent heat of fusion, respectively. This proves that the Schroeder-Van Laar equation for binary mixture can be applied to PCM eutectic mixtures with a low level of uncertainty and provides a powerful tool to save time and money when predicting the eutectic composition of PCMs. Figure 3.23 shows the enthalpy-sum curve for the eutectic mixture.

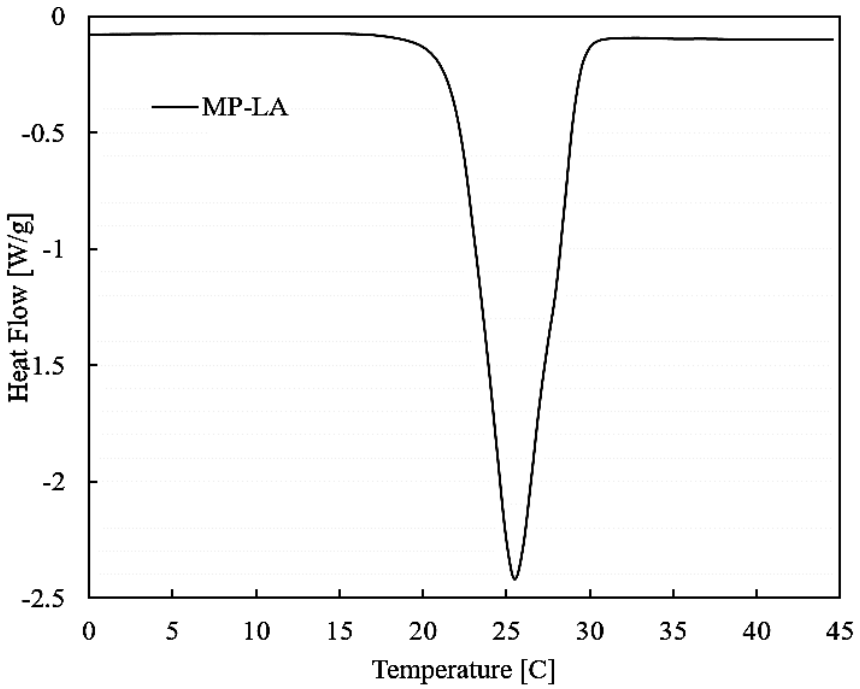

Figure 3.22. Results of DSC measurement for the MP-LA eutectic mixture.

The DSC experimental results for melting onset temperature (T_o), melting temperature ($T_{m,}$), latent heat of fusion (ΔH_m), full width at half maximum (*FWHM)* for melting peak, and temperature range of phase transformation (T_{range}) are listed in Table 3.11.

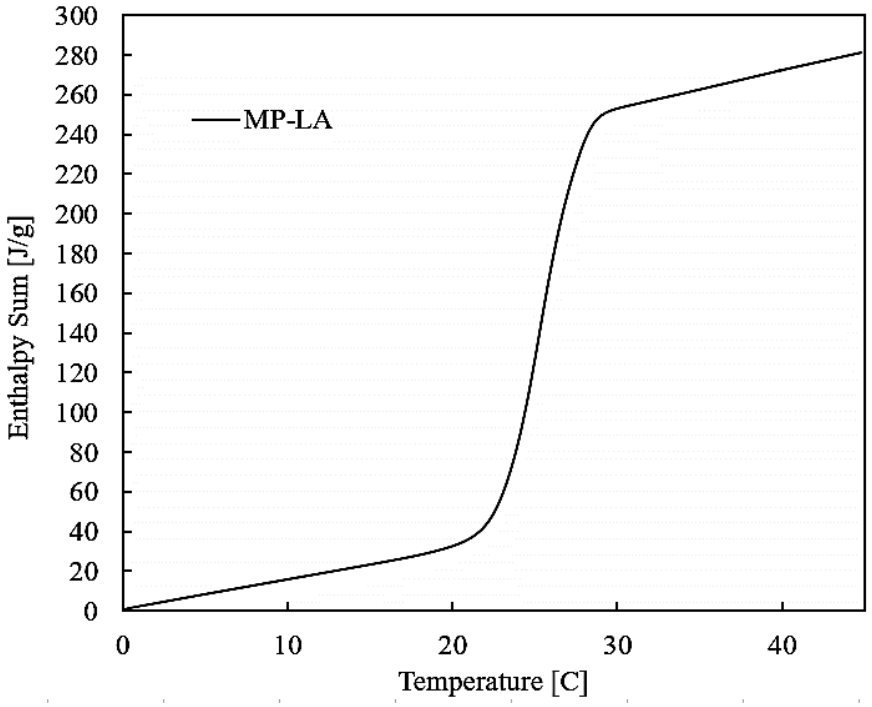

Figure 3.23. Enthalpy-sum curve for the MP-LA eutectic mixture

Figure 3.23 displays the evaluated enthalpy-sum as function of temperature for the MP-LA eutectic mixture. Using the data of the enthalpy-sum curve, the results for the specific heat capacity (C_p) for liquid and solid phase, and the total energy storage density of PCMs through a temperature range of ±20°C around the melting temperature (TES) were evaluated and are listed in Table 3.11.

Table 3.11. The experimental thermophysical properties for the eutectic mixture.

PCM	C_P^{Sol} J g^{-1} K^{-1}	C_P^{Liq} J g^{-1} K^{-1}	T_o °C	T_m °C	$FWHM$ °C	T_{range} °C	ΔH_m J g^{-1}	TES J g^{-1}
MP	1.704	2.015	25.10	29.06	3.99	12.50	202.2	301.2
LA	2.056	2.045	42.72	43.98	2.70	13.42	180.8	262.7
60MP/40LA	1.513	1.952	21.98	25.50	4.25	15.17	205.2	285.0

The determination of the thermophysical properties proves that this eutectic PCM can be considered as a promising PCM for thermal regulation in buildings particularly, due to its suitable melting temperature of 25.5 °C, the high latent heat of fusion of 205.2 J/g, and high thermal energy storage capacity of 277.5J /g.

As a eutectic mixture. The Methyl Palmitate and Lauric Acid mixture has an acceptable transition temperature range when compared to the pure Methyl Palmitate and Lauric Acid.

3.6.1.4 Thermal conductivity. The thermal conductivity of MP, LA and their MP-LA eutectic mixture was studied using the Hot-Bridge technique using a thermal conductivity measuring instrument (THB1, Linseis Inc., USA [81]).

Table 3.12 shows the reported values of 10 measurements and their for the MP-LA eutectic mixture or until an uncertainty of 0.003 W/m.K or lower for thermal conductivity was achieved. The thermal conductivity if the MP, LA, and their eutectic mixture was measured at about 10°C above their experimental melting temperature at about 35 °C.

Table 3.12. Thermal conductivity of MP and LA and their eutectic mxiture (W/m.K).

Test	MP	LA	60MP/40LA
1	outlier	outlier	0.1727
2	0.1795	outlier	outlier
3	0.1793	outlier	0.1731
4	0.1782	0.1633	0.1730
5	0.1762	0.1632	0.1729
6	outlier	0.1638	Outlier
7	outlier	0.1636	0.1729
8	0.1783	0.1639	0.1727
9	0.1789	0.1637	0.1727
10	0.1788	0.1630	0.1728
Avg	0.1785	0.1635	0.1729
Std	0.0010	0.0003	0.0001

3.6.1.5 Density. The density for MP, LA, and their eutectic mixture is measured and summarized in Table 3.13. The density of the solid phase was measured at about 10°C below the experimental melting temperature and at about 10°C above the experimental melting temperature for the liquid phase.

Table 3.13. The experimental density for MP, LA and their eutectic mixture

Test	ρ_{Solid} g/ml	Uncertainty g/ml	ρ_{Liquid} g/ml	Uncertainty g/ml
MP	0.8621	±0.0049	0.8238	±0.0045
LA	0.8885	±0.0052	0.8562	±0.0048
60MP/40LA	0.8877	±0.0047	0.8406	±0.0043

It was noted that the eutectic mixture showed an acceptable decrease in density when it melted. Therefore, its volume expansion during the phase transformation from solid to liquid was minimal and not expected to cause any problems when the material is encapsulated in containers or sheets for TES applications.

3.6.1.6 Thermal diffusivity. The thermal diffusivity for MP, LA, and their eutectic mixture was measured using Equation 8. The measured heat capacity, density, and thermal conductivity were used to calculate the thermal diffusivities for the solid and liquid phases of the eutectic mixture. Table 3.14 summarizes the thermal diffusivity results for MP, LA and their eutectic mixture.

Table 3.14. The thermal diffusivity for MP and LA and their eutectic mixture

Test	α_{Solid} mm^2/s	α_{Liquid} mm^2/s
MP	0.122	0.108
LA	0.090	0.093
60MP/40LA	0.129	0.105

The thermal diffusivity of the MP/LA eutectic binary mixture was found to be 0.129 mm^2/s for the solid phase and 0.105 mm^2/s for the liquid phase. Compared to the thermal diffusivity of the pure methyl palmitate and lauric acid, the thermal diffusivity of the MP/LA eutectic mixture has an average value for both of the liquid sate and the solid state.

3.6.2. Preparation and Enhanced Thermal Performance of Novel (Solid to Gel) Binary Eutectic PCM Modified by Nano-Graphene Platelets. The vast majority of studies have been focused on enhanced PCMs with nanomaterials or other additives. However, these enhanced materials make it difficult to reach a reasonable balance between the increase in thermal conductivity and the large drop of other thermal properties such as heat capacity and latent heat of fusion which directly effects the thermal storage capacity and performance of the system.

A great effort has been focused on achieving that balance. First, a suitable thickening and gelling material was used in this study to improve the structural strength, increase the viscosity, provide a homogeneous mixture when nanomaterials are added, and prevent the leakage of the prepared PM/LA binary eutectic mixture. Second, graphene was selected as a promising additive in terms of enhancing the thermal performance of PCMs. Graphene is expected to not only enhance thermal conductivity significantly but also to enhance the heat capacity of PCMs so that the contribution of the sensible heat process to the total energy storage becomes more significant.

In general, problems may occur when using nano-additives that are suspended in pure PCMs. these materials may sink to the bottom, and incongruent melting and phase separation may occur especially when eutectic mixtures are used. Moreover, it is difficult to form a stable homogeneous mixture between the PCM and additives. However, by discovering a Gel PCM, this semi form-stable PCM in its gel phase acts as a crosslinked material that holds the whole material together when it melts. For that reason, the gelling agent in this study has the benefits of preventing the Nano-additives from sinking to the bottom when fabricated or kept in containers to be used in any TES system.

The proposed modified eutectic PCM composite is expected to increase the structural strength, prevent any possibilities of phase separation or leakage, and help to achieve a homogeneous mixture when Nano-additives are suspended. Additional desirable effects can be achieved when using a gel PCM such as increased heat capacity and thermal conductivity based on the gelling material and PCM that are used. Therefore, the proposed PCM gelled mixture is expected to be an ideal TES material to be used in wallboards, ceiling tiles, floors, material structure of buildings, and the conditioning units in order to reduce temperature swing and energy consumption.

3.6.2.1 Materials. In this study, Methyl hydroxyethyl cellulose (MHE-Cellulose) was chosen as a gelling/thickining material for the proposed MP-LA binary eutectic mixture. The properties of the MHE-Cellulose provided by the manifacturer (Sigma Aldrich) are shown in Table 3.15.

Table 3.15. Chemical data of MHE-Cellulose gelling agent

Name	Molecular Formula	CAS number	Viscosity
Methyl 2-hydroxyethyl cellulose (MHE-C)	$C_2H_6O_2x \cdot CH_4Ox$	9032-42-2	15,000-20,500 cP at 2wt.% in water

Nano graphene platelets (NGPs) have been selected as a possible candidate for the proposed MP-LA binary eutectic mixture due to its high thermal conductivity. thier unique morphology is comprised of a short stack of graphene platelets in the planar form as shown

in Figure 3.24. Beside its high thermal conductivity, these types of NGPs have a very unique characteristic by increasing the flame retardancy [114], which is a very important and desirable property for PCMs when used in applications such as residential houses and buildings. Moreover, the unqiue structure of NGPs as nano-layers from an efficient heat conduction link compared to many types of nanoparticles or CNTs.

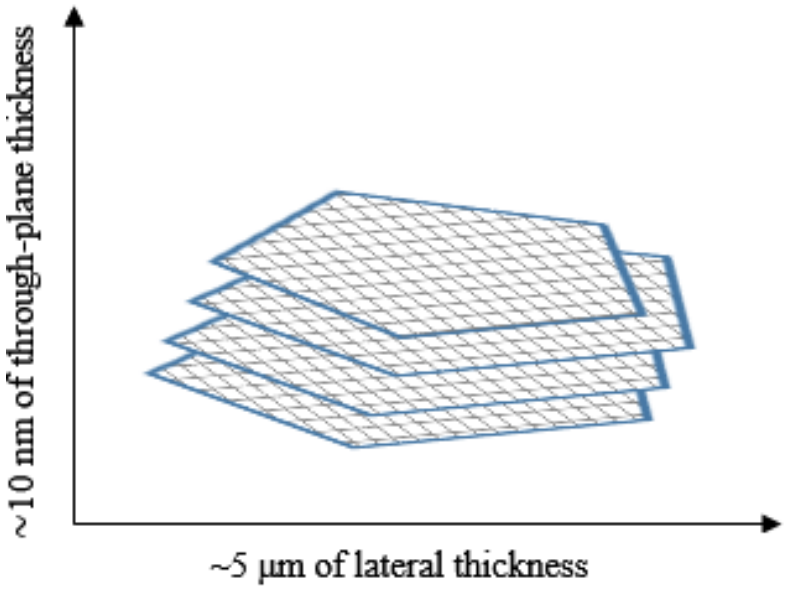

Figure 3.24. Schematic diagram for a short stack of Nano Graphene Platelets (NGPs).

The selected NGPs have an average through plane thickness of 10 nanometers, a lateral thickness of ≤5 micrometers, and a specific surface area of 15 m^2/g. The characteristics of NGPs provided by the manufacturer (Angstron) are shown in Table 3.16

Table 3.16. Properties of the experimental Nano Graphene Platelets (NGPs).

Name	Visual	Density	Surface Area	Through Plane Thick	Lateral Thickness
Graphene nanoplatelets	Fluffy, light powder	≤ 2.20 g/cm^3	≥ 15 m^2/g	10 nm	≤ 5 μm

3.6.2.2 Preparation of modified MP-LA binary eutectic mixture. The prepared experimental samples of the MP-LA binary eutectic mixture were heated up to 25°C above their melting temperature (up to 50°C). MHE-Cellulose was added to the MP-LA mixture as a gelling agent at a sample weight of 10% and stirred for 30 minutes.

After that, NGPs was added in order to increase the thermal conductivity to the MP-LA and MHE-Cellulose mixture at different sample weights (1%, 3%, 5%, and 10%) and stirred for 30 minutes.

3.6.2.3 Results and discussion. The DSC results for the binary eutectic mixture PCM (MP-LA) and Gelled PCM (MP-LA/MHE-Cellulose) are summarized in Table 3.17, and the DSC thermogram is shown in Figure 3.26.The DSC thermal analysis shows that the addition of MHE-Cellulose gelling did not cause any phase sepeartion or incongruent melting.

As seen in table 3.17, the prepared gelled PCM shows a single narrow melting phase change peak melting temperature at 24.06°C and a latent heat of 159.9 J/g. This suggested that the addition of 10 wt% of (MHE-Cellulose) gelling agent slightly decreased the melting temperature and latent heat of the eutectic PCM by 5.6% and 22.1%, respectively.

Table 3.17. DSC results for the gelled eutectic mixture (MP-LA/MHE-C).

PCM	T_o °C	T_m °C	$FWHM$ °C	T_{range} °C	ΔH_m J g^{-1}
MP-LA	21.98	25.50	4.25	15.17	205.2
MP-LA/MHE-C	21.09	24.06	2.91	19.94	159.9

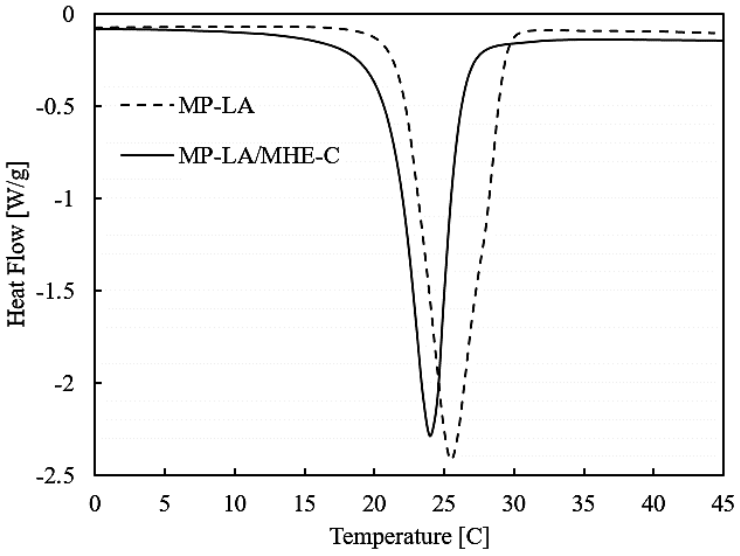

Figure 3.25. DSC measurement for MP-LA/MHE-C eutectic mixture

Figure 3.26 displays the DSC curves of the MP-LA eutectic mixture with the addition of NGPs MP-LA/MHE-C/NGP) at different concentrations (1%, 3%, 5%, and 10%) and compares them to pure (MP-LA) and to the gelled (MP-LA/MHE-C) eutectic mixture; while the data for the PCM weight fraction (*wt%*), melting onset temperature (T_o), melting temperature ($T_{m,}$), full width at half maximum (*FWHM)* for melting peak, temperature range of phase transformation (T_{range}), and latent heat of fusion (ΔH_m) are listed in Table 3.18.

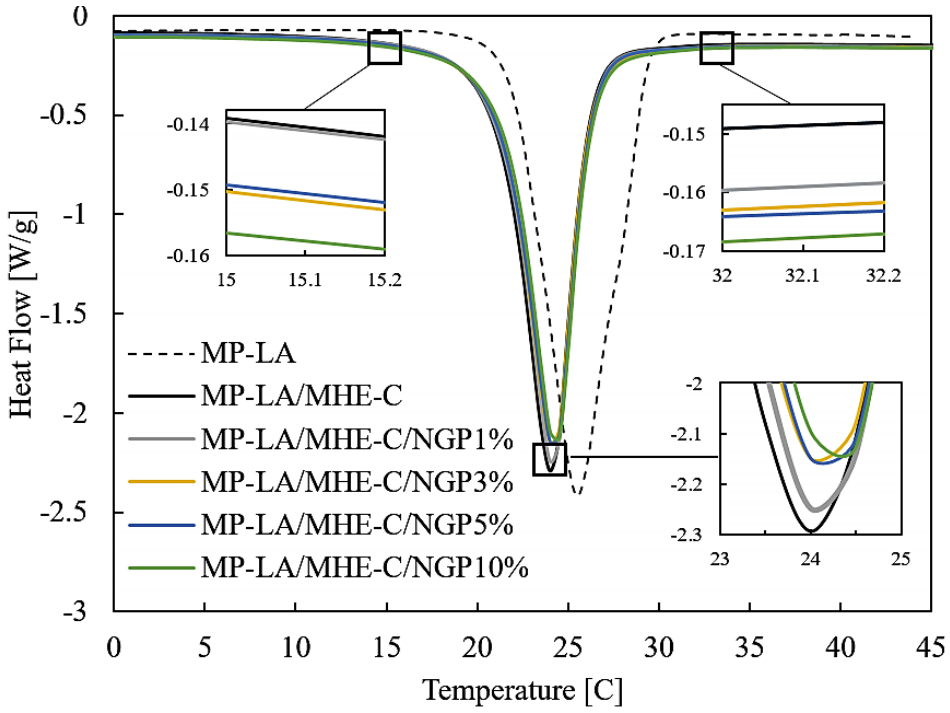

Figure 3.26. DSC results for gelled eutectic PCM modified by NGPs

Table 3.18. DSC data for gelled Eutectic PCM modified by NGPs.

PCM	$PCM\ wt\%$	T_o °C	T_m °C	$FWHM$ °C	T_{range} °C	ΔH_m J g^{-1}
MP-LA	100%	21.98	25.5	4.25	15.17	205.2
MP-LA/MHE-C	90.0%	21.09	24.06	2.91	19.94	159.9
MP-LA/MHE-C/NGP1%	89.1%	21.26	24.13	2.87	19.79	156.1
MP-LA/MHE-C/NGP3%	87.3%	21.18	24.16	2.86	21.10	150.5
MP-LA/MHE-C/NGP5%	85.7%	21.2	24.21	2.88	21.54	150.5
MP-LA/MHE-C/NGP10%	81.8%	21.40	24.29	2.79	21.03	147.6

A slight increase in the melting temperature was observed with the addition of NGPs on the gelled eutectic mixture (MP-LA/MHE-C). The melting temperature increased

by only 0.23°C when NGPs at a mass fraction of 10% were added to the (MP-LA/MHE-C) gelled eutectic mixture. However, this increase in melting temperature of (MP-LA/MHE-C/NGP) in each step for the increase in NGP mass fraction was very close to the repeatability of DSC thermocouples (±0.1°C). Therefore, it can be suggested that no major effect was observed on the melting temperature with the addition of NGPs. Many studies [11, 82, 101-103, 115] have reported a change in melting temperature of PCM composites when additives were added for thermal conductivity enhancement. However, unless this change is significantly higher than the DSC thermocouple resolution, the change in PCM phase change temperature should not be explained or related to the addition of these additives, but due to other factors associated with the instrument itself. For this study, the slight increase in the measured melting temperature can be explained by the increase in thermal conductivity and thermal diffusivity of PCM samples with the increase of the NGP mass fraction. As discussed in our work [83] and in section 4.2.3, with the increase of thermal conductivity of the samples, the internal thermal gradient inside the PCM samples becomes lower. For that reason, the thermal lag between the thermocouples and the sample becomes lower too, and the instrument response increases. Therefore, as a result of this decrease in the internal thermal gradient, the measured melting temperature slightly increases.

The main objective here when NGPs are added is to enhance the thermal conductivity of the PCM mixture. However, when any additive materials are added to the PCM mixture, it is expected that the measured latent heat of PCM will decrease, why? Because the additive materials occupy a certain mass fraction in the whole PCM mixture, they cause a reduction in the PCM (MP-LA) mass fraction, which is responsible for the

absorption of thermal energy as a latent heat. As a result of this decrease in latent heat, the total thermal energy storage is expected to decrease by the same value. However, as seen in the enthalpy-curve results in Figure 3.27, the effect of NGP additives on the total energy storage capacity is very weak. In Table 3.19, the total thermal energy storage (TES) capacity for a temperature range of ±25℃ and ±15℃ around the melting temperature for the modified MP-LA/MHE-C/NGP eutectic mixture with different NGP mass fractions was found to be comparable to its value for the pure MP-LA eutectic mixture.

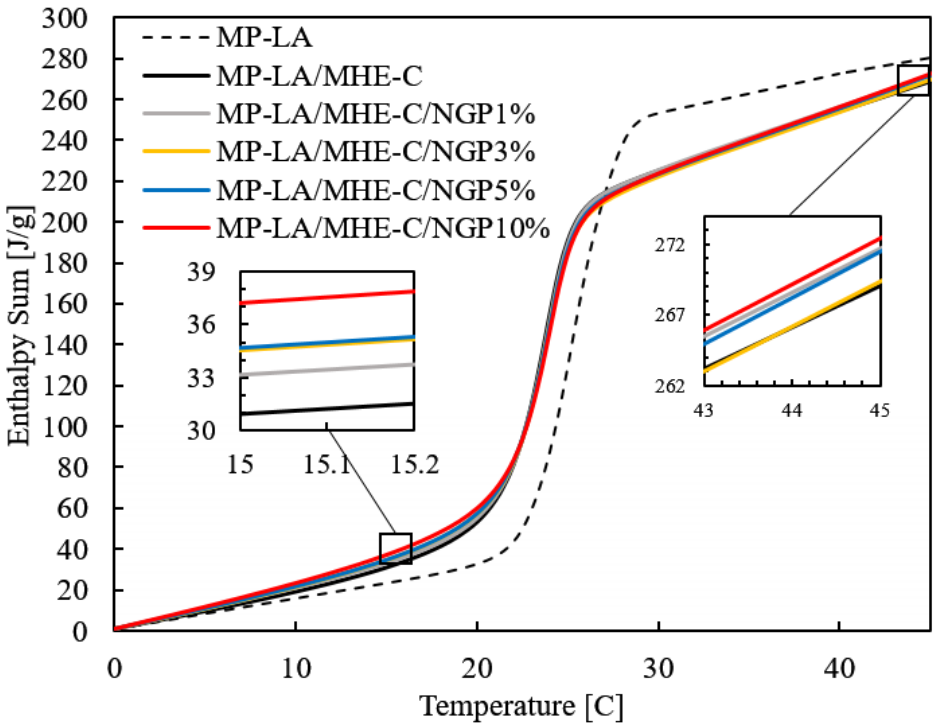

Figure 3.27. Enthalpy-sum curve for gelled eutectic PCM modified by NGPs.

As listed in Table 3.19, when the MHE-C gelling agent was added, the total TES was reduced by only 1.2% and 8.1% for a temperature range of 25°C and 15°C,

respectively. In contrast. when compared to the effect of the gelled eutectic mixture (MP-LA/MHE-C) on the total TES, the addition of NGPs was found to cause no further decrease in the total TES for the a range of ±15℃ around the melting temperature, and the TES was even enhanced (compared to the TES of gelled eutectic mixture) within a range of ±25℃ around the melting temperature.

Table 3.19. The total TES for gelled Eutectic PCM modified by NGPs

PCM	PCM $wt\%$	ΔH_m J g^{-1}	$Change$ $in\ \Delta H_m$	$TES_{\pm 15}$ J g^{-1}	$Change$ $in\ TES_{\pm 15}$	$TES_{\pm 25}$ J g^{-1}	$Change$ $in\ TES_{\pm 25}$
MP-LA	100%	205.2	-	256.2	-	285.0	-
MP-LA/MHE-C	90.0%	159.9	-22.08%	235.4	-8.1%	281.5	-1.2%
MP-LA/MHE-C/NGP1%	89.1%	156.1	-23.93%	235.2	-8.2%	284.9	0.0%
MP-LA/MHE-C/NGP3%	87.3%	150.5	-26.66%	233.3	-8.9%	283.9	-0.4%
MP-LA/MHE-C/NGP5%	85.7%	150.5	-26.66%	233.6	-8.8%	286.4	+0.5%
MP-LA/MHE-C/NGP10%	81.8%	147.6	-28.07%	234.1	-8.6%	287.3	+0.8%

When NGPs were added, the change in TES for a temperature range of 25°C was found to be positive (compared to the gelled eutectic mixture) and equal to (0.0%, 0.4%, 0.5%, and 0.8%) when NGP was added at mass fraction of (1, 3, 5, and 10%), respectively. Such observations are desirable and occur because energy storage occurs over a range of temperatures. The increase in heat capacity with the addition of NGPs leads to an increase in the thermal energy storage caused by the increase in the sensible heat contribution. This increase in the sensible heat contribution compensates for the decrease in melting enthalpy when the mass fraction of PCM decreases with the addition of NGP additives. The increase

in the sensible heat contribution toward the total TES is very important, especially when the PCM works within higher temperature ranges.

The main goal when NGPs were added was to enhance the poor thermal conductivity for the prepared MP/LA eutectic mixture. However, by looking at figure 3.29 and figure 3.30, where the total thermal energy storage, latent heat contribution, and sensible heat contribution for the prepared PCMs are listed, It can be concluded that although the addition of NGPs decreases the pure PCM mass fraction, which in turn decreases the latent heat of enthalpy, but the total thermal energy storage was not affected, but was slightly increased for the temperature range of ±25°C (Figure 3.29). Their effect was also negligible on the TES (a maximum decrease of about 8.9% only) for the temperature range of ±15°C.

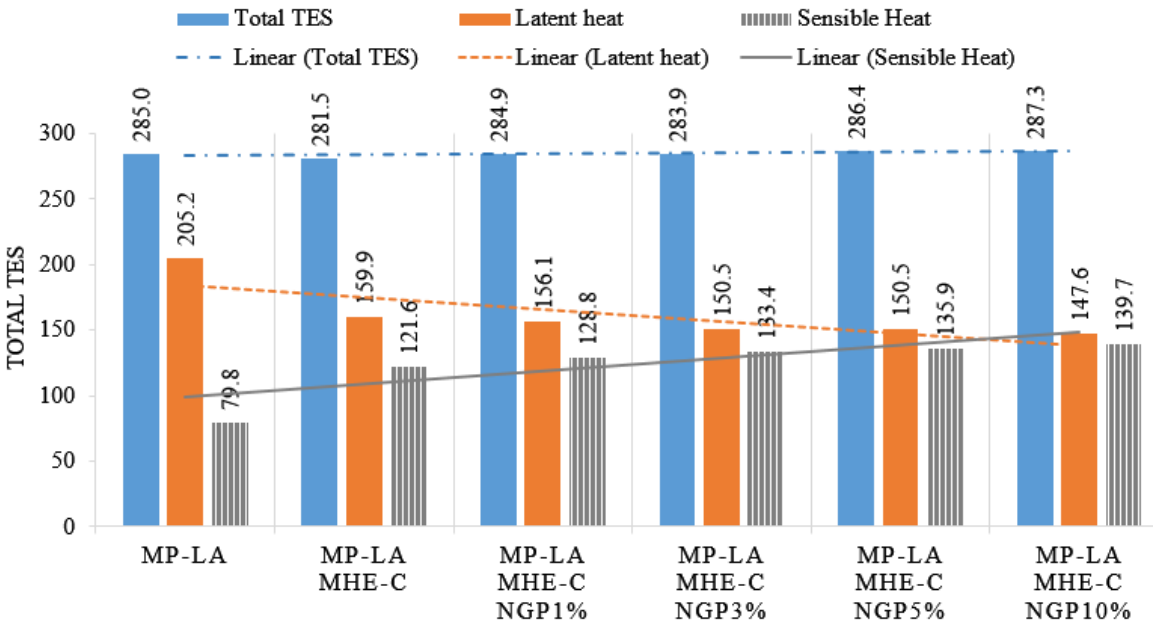

Figure 3.28. Effect of NGPs on the total thermal energy storage (±25°C), latent heat contribution, and sensible heat contribution in units of J/g.

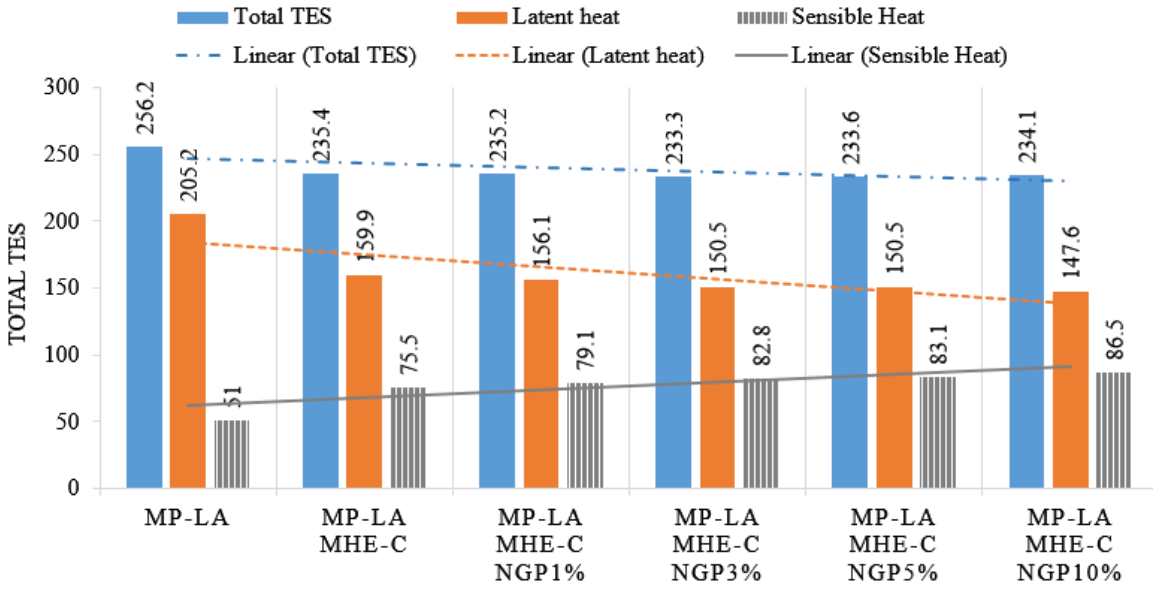

Figure 3.29. Effect of NGPs on the total thermal energy storage (±15°C), latent heat contribution, and sensible heat contribution in units of J/g.

Table 3.20 shows the effect of the NGP mass fraction and MHE-Cellulose on the specific heat capacity of the PCM eutectic mixture. It can be noted that the specific heat capacity was increased significantly for both the solid state and liquid state in varying degrees based on the NGP mass fraction. When MHE-Cellulose was added at a mass fraction of 10% to the MP-LA binary eutectic mixture, the specific heat capacity increased by 24.72% and 47.49% for the solid state and melted state, respectively. It can be observed that the increase in specific heat for the melted state PCM (47.49% increase), at which the gel phase exists, was significantly higher than the increase of specific heat at the solid phase (24.72% increase). Several studies showed that the heat capacity of a material can be enhanced by enhancing its crystallinity [116, 117]. For instance, Shin et al, [117] showed an enhancement of up to 54% in the specific heat capacity by dispersing an additive of

silica ($SiO_{2)}$ in a molten salt PCM eutectic mixture. Therefore, the significant increase in the specific heat capacity when the MHE-Cellulose gelling agent was added is not only related to the specific heat capacity of these additives but is also attributed to the enhanced crystallinity of the prepared PCM eutectic mixture.

Table 3.20. Specific heat capacity of gelled Eutectic PCM modified by NGPs

PCM	C_P^{Sol} J g^{-1} K^{-1}	C_P^{Liq} J g^{-1} K^{-1}	$Change\ in\ C_P^{Sol}$	$Change\ in\ C_P^{Liq}$
MP-LA	1.513	1.952	-	-
MP-LA/MHE-C	1.887	2.879	24.72%	47.49%
MP-LA/MHE-C/NGP1%	2.051	3.055	35.56%	56.51%
MP-LA/MHE-C/NGP3%	2.126	3.121	40.52%	59.89%
MP-LA/MHE-C/NGP5%	2.135	3.222	41.11%	65.06%
MP-LA/MHE-C/NGP10%	2.302	3.216	52.15%	64.75%

When NGPs were added to the MP-LA gelled eutectic mixture (MP-LA/MHE-C) with a mass fraction of (1%, 3%, 5%, and 10%), the specific heat capacity when compared to the pure MP-LA binary eutectic mixture was further enhanced by (35.56%, 40.52%, 41.11%, and 52.15%) for the solid state, and by (56.54%, 59.89%, 65.06%, and 64.75%) for the liquid state. This significant increase in heat capacity with the addition of NGPs increased the amount of energy that can be stored as sensible heat. This is very important particularly when the PCMs works beyond its phase transition period, especially when the discharge in the previous cycle was not enough to reach the phase transition range (latent heat region).

Whereas the detailed thermal conductivity measurements are listed in Table 3.21, the summary of these measurements is listed in Table 3.22 and shows the impact of NGPs on thermal conductivity.

Table 3.21. Thermal conductivity measurements for gelled eutectic PCM modified by NGPs

Test	MP-LA	MP-LA/ MHE-C	MP-LA MHE-C NGP1%	MP-LA MHE-C NGP3%	MP-LA MHE-C NGP5%	MP-LA MHE-C/NGP10%
1	0.1727	outlier	outlier	outlier	outlier	outlier
2	outlier	outlier	0.2175	0.2352	outlier	0.3294
3	0.1731	0.1631	0.2185	0.2352	outlier	outlier
4	0.173	0.1632	0.2187	0.2324	0.2623	0.3254
5	0.1729	0.1649	0.2188	0.2354	0.2640	0.3274
6	outlier	0.1664	0.2181	0.2364	0.2643	outlier
7	0.1729	0.1669	0.2181	0.2368	0.2636	0.3263
8	0.1727	0.1688	0.2180	0.2366	0.2645	0.3278
9	0.1727	outlier	0.2188	outlier	0.2646	0.3281
10	0.1728	outlier	0.2183	outlier	0.2639	0.3265
Avg	0.1729	0.1656	*0.2183*	*0.2354*	*0.2639*	*0.3273*
Std	0.0001	±0.002	*0.000*	*0.001*	*0.001*	*0.001*

Table 3.22 shows the impact of NGPs on the thermal conductivity for the gelled eutectic mixture. First, the thermal conductivity of the eutectic mixture decreased from 0.1729 to 0.1656 when MHE-C was added as a gelling agent. This can be explained by the low thermal conductivity of methyl Hydroxyethyl cellulose. However, the thermal

conductivity can be significantly increased by adding NGPs. The largest influence of NGPs on thermal conductivity occurs at the highest mass fraction. This increase is considered to be very significant when compared to other additives due to the large specific surface area of NGPs.

The thermal conductivity for the modified PCM (MP-LA/MHE-C/NGP) with mass fractions of (1, 3, 5, and 10%) for NGPs increased by (31.9%, 42.2%, 59.4%, and 97.7%), respectively, when compared to that of the gel PCM eutectic mixture (MP-LA/MHE-C).

Table 3.22. Effect of NGPs on the thermal conductivity of gelled Eutectic PCM.

PCM	K W m^{-1} K^{-1}	$Change\ in\ K$
MP-LA	0.1729	-
MP-LA/MHE-C	0.1656	-
MP-LA/MHE-C/NGP1%	0.2183	31.9%
MP-LA/MHE-C/NGP3%	0.2354	42.2%
MP-LA/MHE-C/NGP5%	0.2639	59.4%
MP-LA/MHE-C/NGP10%	0.3273	97.7%

A linear relationship between the NGP mass fraction (x) and thermal conductivity (*K*), is obtained from Figure 3.30 as follows in Equation 15:

$$K = 1.4602x + 0.1866 \quad (15)$$

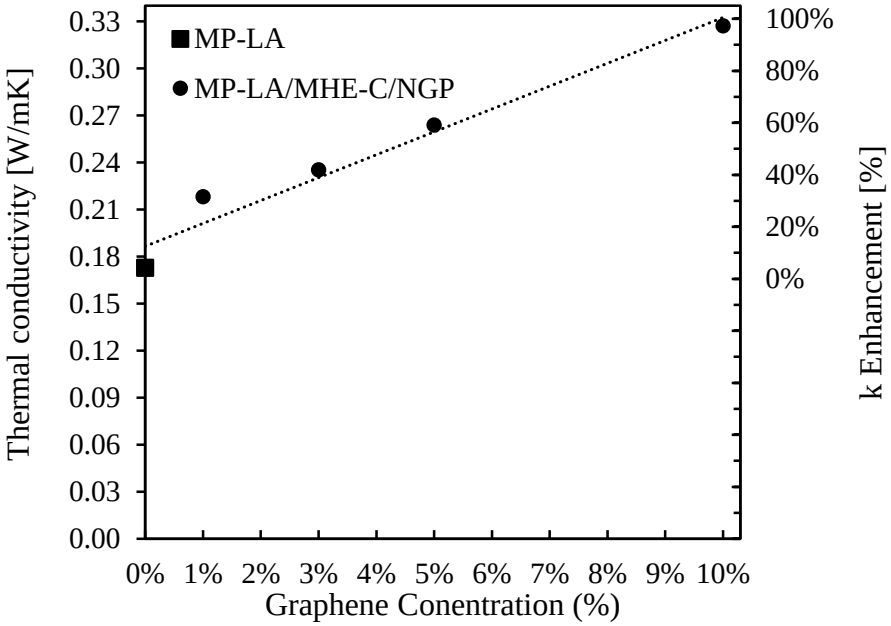

Figure 3.30. Thermal conductivity enhancement of PCM with NGPs.

Looking at the impact of NGPs on thermal conductivity, it can be concluded that the addition of NGPs provides the required balance between the thermal conductivity enhancement and the thermal energy storage capacity. As discussed above, this balance was achieved by increasing the heat capacity which in turn increased the total thermal energy storage and compensate for the reduction in latent heat. At the same time, a significant increase in thermal conductivity was achieved by adding NGPs, and is directly proportional to the mass fraction of these additives. Moreover, the addition of NGPs was found to have no significant effect on melting temperature.

In Table 3.23, the density for the prepared eutectic mixture is compared to its value for the gelled eutectic mixture and the density for each of the corresponding NGPs mass fractions. When compared to the MHE-Cellulose gelling agent, the addition of NGPs was found to have a higher effect on density. This is attributed to the high density of NGPs of

about 2.2 g/cm^3 as seen in table 3.16. The prepared gelled PCM modified with NGPs maintained the acceptable decrease in density upon melting. Therefore, its volume expansion during phase transformation from solid to liquid was minimal and not expected to cause any problems when the PCM is encapsulated in containers or sheets for any applications.

Table 3.23. Density of gelled Eutectic PCM modified by NGPs.

Test	ρ_{Solid} g/ml	$Change\ in\ density$	ρ_{Liquid} g/ml	$Change\ in\ density$
MP-LA	0.8877	-	0.8406	-
MP-LA/MHE-C	0.8930	0.60%	0.8470	0.76%
MP-LA/MHE-C/NGP1%	0.9092	2.42%	0.8575	2.01%
MP-LA/MHE-C/NGP3%	0.9345	5.27%	0.8839	5.15%
MP-LA/MHE-C/NGP5%	0.9284	4.58%	0.9078	4.78%
MP-LA/MHE-C/NGP10%	1.0185	15.86%	0.9714	16.75%

The effect of MHE-Cellusose and NGPs on thermal diffusivity is listed in Table 3.24. It was noted that the addition of MHE-Cellulose gelling agent decreased the thermal diffusivity of MP-LA by 24% for liquid state, and 35.2% for gel or liquid state. The reduction in thermal diffusivity with the addition of MHE-Cellulose was attributed to the fact that this gelling agent enhanced the ability of PCM material to store energy rather than diffusing it. The results for heat capacity enhancement (24% for solid and 47% for liquid) and thermal conductivity reduction (4%) clearly support this observation. However, thermal diffusivity of the prepared eutectic gelled PCM (MP-LA/MHE-C) increased again

when NGPs were added. When compared to the thermal diffusivity of MP-LA/MHE-C, the addition of NGPs at mass fractions of (1, 3, 5, and 10%) increased the thermal diffusivity by (19.12%, 20.57%, 35.48%, and 42.05%) for the solid state, and by (22.17. 25.65%, 32.84%, and 54.28%) for the liquid state.

Table 3.24. Thermal diffusivity of gelled Eutectic PCM modified by NGPs.

Test	α_{Solid} mm^2/s	$Change\ in\ diffusivity$	α_{Liquid} mm^2/s	$Change\ in\ diffusivity$
MP-LA	0.129	-	0.105	-
MP-LA/MHE-C	0.098	-	0.068	-
MP-LA/MHE-C/NGP1%	0.117	19.12%	0.083	22.71%
MP-LA/MHE-C/NGP3%	0.118	20.57%	0.085	25.65%
MP-LA/MHE-C/NGP5%	0.133	35.48%	0.090	32.84%
MP-LA/MHE-C/NGP10%	0.140	42.05%	0.105	54.28%

Therefore, it can be concluded that the final composition of the prepared MP-LA with the addition of MHE-Cellulose as a gelling agent and NGP as a thermal modulator had a satisfactory thermal performance for all of the studied thermal properties, such as, total energy storage capacity, thermal conductivity, and specific heat capacity.it also had a minimal effect on the melting temperature.

3.7. A SUMMARY OF THE THERMO-PHYSICAL PROPERTIES OF PCMS

A summary of the thermophysical properties of PCMs is listed in Table 3.25.

Table 3.25. Summary of the thermophysical properties of PCMs

PCM	C_p^{liq} J/g.K	C_p^{liq} J/g.K	T_o °C	T_m °C	FWHM °C	T_{range} °C	ΔH_m J g^{-1}	TES J g^{-1}	K W/mK	ρ_{Solid} g/ml	ρ_{Liquid} g/ml	α_{Solid} mm^2/s	α_{Liquid} mm^2/s
Lauryl Alcohol	1.667	2.251	20.88	23.83	3.25	15.60	216.5	294.4	0.169	0.886	0.833	0.115	0.090
Capric Acid	2.220	2.339	29.19	31.82	2.91	12.61	162.2	250.1	0.159	0.891	0.848	0.081	0.080
Lauric Acid	2.056	2.045	42.72	43.98	2.70	13.42	180.8	262.7	0.163	0.888	0.856	0.090	0.093
Myristic Acid	1.912	2.009	51.00	54.21	2.52	12.23	198.5	287.1	1.674	0.866	0.816	0.101	0.102
Palmitic Acid	1.832	1.906	60.28	62.93	2.62	13.27	209.3	284.8	0.171	0.851	0.816	0.110	0.110
MP-LA	1.513	1.952	21.98	25.50	4.25	15.17	205.2	285.5	0.172	0.877	0.840	0.129	0.105
MP-LA/MHE-C	1.887	2.879	21.09	24.06	2.91	19.94	159.9	281.5	0.165	0.893	0.847	0.098	0.068
MP-LA/MHE-C/NGP1%	2.051	3.055	21.26	24.13	2.87	19.79	156.1	284.9	0.218	0.909	0.857	0.117	0.083
MP-LA/MHE-C/NGP3%	2.126	3.121	21.18	24.16	2.86	21.10	150.5	283.9	0.235	0.934	0.883	0.118	0.085
MP-LA/MHE-C/NGP5%	2.135	3.222	21.20	24.21	2.88	21.54	150.5	286.4	0.263	0.928	0.907	0.133	0.090
MP-LA/MHE-C/NGP10%	2.302	3.216	21.40	24.29	2.79	21.03	147.6	287.3	0.327	1.018	0.971	0.140	0.105

4. CONCLUSION

Seven heat storage materials were selected for this study, namely Myristic acid, Capric Acid, Lauryl Alcohol, Palmitic acid and Lauric acid, and Methyl palmitate. These materials were carefully selected based on their properties to cover wide range of Thermal Energy Storage (TES) applications.

The study provided an overall investigation of thermophysical properties of PCMs in a detailed manner in order to provide a valuable database for TES applications using PCMs. Using the provided experimental data in this work, the thermal behavior of these materials in a TES system can be easily predicted and stimulated. A Differential Scanning Calorimeter (DSC) was used to characterize the PCMs and to determine the latent heat of fusion, phase change (melting) temperature, specific heat capacity, the enthalpy as a function of temperature, and their total TES capacity. The additional thermophysical properties such as thermal conductivity, thermal diffusivity, and density were experimentally determined.

The study experimentally investigated the uncertainty of thermal characterization of PCMs by DSC analysis. The results proved that the sample mass and heating rate must be carefully selected. The various thermal events and effects that occurs when PCMs are tested in a DSC were discussed in detail. The higher heating rates and sample masses were found to shift the observed melting temperature to significantly higher temperatures and significantly widen the temperature range of the melting peaks. A slight increase in the measured latent heat was also observed for higher heating rates and sample masses. The optimum measurement condition was found to be at a heating rate of 3°C/min and a sample mass of 7.5 mg.

A new PCM consisting of a eutectic binary mixture was discovered and found to be a promising PCM for thermal regulation and TES applications, particularly in buildings because of the high latent heat of fusion and suitable phase transition temperature. The Schroeder-Van Laar equation for a binary mixture was used for the initial prediction of this eutectic mixture with a low level of uncertainty, and it saved time and money when predicting the eutectic composition of PCMs. The eutectic mixture consisting of 60% Methyl Palmitate (MP) and 40% Lauric Acid (LA) was prepared and characterized. Experimental DSC results showed a single narrow melting phase change peak melting temperature at 25.5°C, and the latent heat of fusion was 205.2 J/g. The specific heat capacity, enthalpy as function of temperature, and TES capacity, in addition to other thermophysical properties such as thermal conductivity, thermal diffusivity, and density, were experimentally determined.

The PCM eutectic mixture was further enhanced by Methyl hydroxyethyl cellulose as a gelling/thickening agent giving the PCM a gel phase transformation feature. The prepared gel PCM was found to be very promising for thermal regulation, reducing energy consumption, and reducing the indoor temperature swing in buildings. The prepared gelled PCM is expected to have many benefits by preventing leakage, reducing fluidity of PCMs, and providing the required structural strength when PCMs are incorporated through a gypsum mixture, cement paste, and mortar or by using the PCM in the wallboards, ceiling tiles, or floors of buildings. The gel phase of this PCM also works as a crosslinked medium when nano-material additives are added. The thermal performance of the gel-PCM eutectic mixture was characterized and found to have a negligible effect on the melting temperature

with the addition of the Methyl hydroxyethyl cellulose gelling agent. The specific heat significantly increased by 24% for the solid phase and 47% for the liquid phase.

The overall thermal performance of the prepared gel-PCM was further enhanced with Nano-graphene platelets (NGPs) with mass fractions of 1%, 3%, 5%, and 10%. Thermal conductivity, specific heat capacity, and thermal diffusivity in particular were enhanced depending on the mass fraction of NGPs. The corresponding enhancement when 10% of NGPs were added was as follows: thermal conductivity was increased by about 97.7%, the specific heat capacity was increased by 52% for the solid phase and 64% for the liquid phase, and the thermal diffusivity increased by 42% for the solid phase and 54% for the liquid phase. A desirable small volume expansion during phase transformation was observed. Compared to the current known PCMs, the prepared final PCM has an excellent thermal performance and characteristics. The characterization of the final formulation for the proposed gelled PCM modified by NGPs shows that this novel PCM can be readily adapted to large-scale industrial production to help improve the performance of energy systems, particularly in buildings, and providing the possibility of conserving energy effectively.

5. REFERENCES

1. Outlook, A.E., *Energy information administration.* Department of Energy, 2016.

2. Li, J., et al., *Micro-encapsulated paraffin/high-density polyethylene/wood flour composite as form-stable phase change material for thermal energy storage.* Solar Energy Materials and Solar Cells, 2009. **93**(10): p. 1761-1767.

3. Baylin, F., *Low temperature thermal energy storage: A state of the art survey'Solar Energy Research Institute*. 1979, Report No. SERI/RR/-54–164, Golden, Colorado (USA).

4. Ercan, A.O., *Storage of thermal energy.* Energy Storage Systems, Eolss Publishers, 2006.

5. Lane, G.A., *Solar heat storage: Latent heat materials*. Vol. 2. 1986: CRC.

6. Abhat, A., *Low temperature latent heat thermal energy storage: heat storage materials.* Solar energy, 1983. **30**(4): p. 313-332.

7. Sharma, A., et al., *Review on thermal energy storage with phase change materials and applications.* Renewable and Sustainable Energy Reviews, 2007. **13**(2): p. 318-345.

8. Paksoy, H.Ö., *Thermal energy storage for sustainable energy consumption: fundamentals, case studies and design*. Vol. 234. 2007: Springer Science & Business Media.

9. Alkan, C. and A. Sari, *Fatty acid/poly (methyl methacrylate)(PMMA) blends as form-stable phase change materials for latent heat thermal energy storage.* Solar Energy, 2008. **82**(2): p. 118-124.

10. Lazaro, A., et al., *Intercomparative tests on phase change materials characterisation with differential scanning calorimeter.* Applied Energy, 2013. **109**: p. 415-420.

11. Teng, T.-P. and C.-C. Yu, *The Effect on Heating Rate for Phase Change Materials Containing MWCNTs.* International Journal of Chemical Engineering and Applications, 2012. **3**(5): p. 340-342.

12. Mehrali, et al., *Shape-stabilized phase change materials with high thermal conductivity based on paraffin/graphene oxide composite.* Energy Conversion and Management, 2013. **67**: p. 275-282.

13. Heine, D. and A. Abhat. *Investigation of physical and chemical properties of phase change materials for space heating/cooling applications*. in *SUN: Mankind's Future Source of Energy*. 1978.

14. Khudhair, A.M. and M.M. Farid, *A review on energy conservation in building applications with thermal storage by latent heat using phase change materials.* Energy conversion and management, 2004. **45**(2): p. 263-275.

15. Tyagi, V.V. and D. Buddhi, *PCM thermal storage in buildings: a state of art.* Renewable and Sustainable Energy Reviews, 2007. **11**(6): p. 1146-1166.

16. Atkin, P. and M.M. Farid, *Improving the efficiency of photovoltaic cells using PCM infused graphite and aluminium fins.* Solar Energy, 2015. **114**: p. 217-228.

17. Wang, J., et al., *Enhancing thermal conductivity of palmitic acid based phase change materials with carbon nanotubes as fillers.* Solar Energy, 2010. **84**(2): p. 339-344.

18. Oró, E., et al., *Review on phase change materials (PCMs) for cold thermal energy storage applications.* Applied Energy, 2012. **99**: p. 513-533.

19. Akgün, M., O. Aydın, and K. Kaygusuz, *Experimental study on melting/solidification characteristics of a paraffin as PCM.* Energy Conversion and Management, 2007. **48**(2): p. 669-678.

20. Sharma, S.D., H. Kitano, and K. Sagara, *Phase change materials for low temperature solar thermal applications.* Res. Rep. Fac. Eng. Mie Univ, 2004. **29**(1).

21. Lane, G.A., et al. *Heat of fusion systems for solar energy storage*. in *Proc. Workshop on Solar Energy Storage Subsystems for the Heating and Cooling of Buildings*. 1975.

22. Herrick, C. and D. Golibersuch, *Qualitative behavior of a new latent heat storage device for solar heating/cooling systems*. 1977: General Electric Company Corporate Research and Development.

23. Mehling, H. and L.F. Cabeza, *Heat and cold storage with PCM*. 2008: Springer.

24. Zhang, H., et al., *Characterization of sugar alcohols as seasonal heat storage media–experimental and theoretical investigations.* 2014.

25. Pielichowska, K. and K. Pielichowski, *Phase change materials for thermal energy storage.* Progress in Materials Science, 2014. **65**: p. 67-123.

26. Kenisarin, M.M., *High-temperature phase change materials for thermal energy storage.* Renewable and Sustainable Energy Reviews, 2010. **14**(3): p. 955-970.

27. Lane, G., *Macro-encapsulation of PCM.* Report No. oro/5117-8, Dow Chemical Company, Midland, Michigan, 1978. **152**.

28. Zalba, B., et al., *Review on thermal energy storage with phase change: materials, heat transfer analysis and applications.* Applied thermal engineering, 2003. **23**(3): p. 251-283.

29. Dincer, I. and M.A. Rosen, *Energetic, environmental and economic aspects of thermal energy storage systems for cooling capacity.* Applied Thermal Engineering, 2001. **21**(11): p. 1105-1117.

30. Zamengo, M., J. Ryu, and Y. Kato, *Chemical Heat Storage of Thermal Energy from a Nuclear Reactor by Using a Magnesium Hydroxide/Expanded Graphite Composite Material.* Energy Procedia, 2015. **71**: p. 293-305.

31. Lee, Y. and C.W. Forsberg, *Conceptual design of nuclear-geothermal energy storage systems for variable electricity production*. 2011, Massachusetts Institute of Technology. Center for Advanced Nuclear Energy Systems. Nuclear Energy and Sustainability Program.

32. Gomez, J., *High-temperature phase change materials (PCM) candidates for thermal energy storage (TES) applications*. 2011, NREL/TP-5500-51446: National Renewable Energy Laboratory.

33. Alameri, S.A., *A coupled nuclear reactor thermal energy storage system for enhanced load following operation.* 2007.

34. *Affiliated Engineers Inc.* 2016; Available from: http://www.aeieng.com. 28 Mar. 2016.

35. Stritih, U. and V. Butala, *Energy savings in building with a PCM free cooling system.* Strojniški vestnik-Journal of Mechanical Engineering, 2011. **57**(2): p. 125-134.

36. Biwole, P., P. Eclache, and F. Kuznik. *Improving the performance of solar panels by the use of phase-change materials*. in *World Renewable Energy Congress*. 2011.

37. Hendricks, J. and W. Sark, *Annual performance enhancement of building integrated photovoltaic modules by applying phase change materials.* Progress in Photovoltaics: Research and Applications, 2013. **21**(4): p. 620-630.

38. Baetens, R., B.P. Jelle, and A. Gustavsen, *Phase change materials for building applications: a state-of-the-art review.* Energy and Buildings, 2010. **42**(9): p. 1361-1368.

39. Emery, K., et al. *Temperature dependence of photovoltaic cells, modules and systems*. in *Photovoltaic Specialists Conference, 1996., Conference Record of the Twenty Fifth IEEE*. 1996. IEEE.

40. Radziemska, E. and E. Klugmann, *Thermally affected parameters of the current–voltage characteristics of silicon photocell.* Energy Conversion and Management, 2002. **43**(14): p. 1889-1900.

41. Hasan, A., et al., *Increased photovoltaic performance through temperature regulation by phase change materials: Materials comparison in different climates.* Solar Energy, 2015. **115**: p. 264-276.

42. Ma, T., et al., *Using phase change materials in photovoltaic systems for thermal regulation and electrical efficiency improvement: A review and outlook.* Renewable and Sustainable Energy Reviews, 2015. **43**: p. 1273-1284.

43. Chaiyat, N. and T. Kiatsiriroat, *Energy reduction of building air-conditioner with phase change material in Thailand.* Case Studies in Thermal Engineering, 2014. **4**: p. 175-186.

44. Vakilaltojjar, S. and W. Saman, *Analysis and modelling of a phase change storage system for air conditioning applications.* Applied Thermal Engineering, 2001. **21**(3): p. 249-263.

45. Fang, G., S. Wu, and X. Liu, *Experimental study on cool storage air-conditioning system with spherical capsules packed bed.* Energy and Buildings, 2010. **42**(7): p. 1056-1062.

46. Prakash, J., H. Garg, and G. Datta, *A solar water heater with a built-in latent heat storage.* Energy conversion and management, 1985. **25**(1): p. 51-56.

47. Ghoneim, A., *Comparison of theoretical models of phase-change and sensible heat storage for air and water-based solar heating systems.* Solar Energy, 1989. **42**(3): p. 209-220.

48. Bansal, N. and D. Buddhi, *An analytical study of a latent heat storage system in a cylinder.* Energy conversion and management, 1992. **33**(4): p. 235-242.

49. Chaurasia, P. *Phase change material in solar water heater storage system*. in *Proceedings of the 8th international conference on thermal energy storage*. 2000.

50. Bajnóczy, G., et al., *Heat storage by two-grade phase change material.* Chemical Engineering, 1999. **43**(2): p. 137-147.

51. Kaygusuz, K., *Experimental and theoretical investigation of latent heat storage for water based solar heating systems.* Energy conversion and management, 1995. **36**(5): p. 315-323.

52. Zhang, X., *Heat-storage and thermo-regulated textiles and clothing.* Smart fibres, fabrics and clothing, Woodhead Publishing, UK, 2001: p. 34-57.

53. Mondieig, D., et al., *Protection of temperature sensitive biomedical products using molecular alloys as phase change material.* Transfusion and apheresis science, 2003. **28**(2): p. 143-148.

54. Lv, Y., Y. Zou, and L. Yang, *Feasibility study for thermal protection by microencapsulated phase change micro/nanoparticles during cryosurgery.* Chemical Engineering Science, 2011. **66**(17): p. 3941-3953.

55. Wang, C., et al., *Highly sensitive thermal detection of thrombin using aptamer-functionalized phase change nanoparticles.* Biosensors and Bioelectronics, 2010. **26**(2): p. 437-443.

56. Azzouz, K., D. Leducq, and D. Gobin, *Performance enhancement of a household refrigerator by addition of latent heat storage.* International Journal of Refrigeration, 2008. **31**(5): p. 892-901.

57. Azzouz, K., D. Leducq, and D. Gobin, *Enhancing the performance of household refrigerators with latent heat storage: An experimental investigation.* international Journal of Refrigeration, 2009. **32**(7): p. 1634-1644.

58. Gin, B., M. Farid, and P. Bansal, *Effect of door opening and defrost cycle on a freezer with phase change panels.* Energy Conversion and Management, 2010. **51**(12): p. 2698-2706.

59. Subramaniam, P., et al. *Phase change materials for domestic refrigerators to improve food quality and prolong compressor off time*. in *International refrigeration and air conditioning conference at Purdue*. 2010.

60. Ahmed, M., O. Meade, and M.A. Medina, *Reducing heat transfer across the insulated walls of refrigerated truck trailers by the application of phase change materials.* Energy Conversion and Management, 2010. **51**(3): p. 383-392.

61. Kandasamy, R., X.-Q. Wang, and A.S. Mujumdar, *Transient cooling of electronics using phase change material (PCM)-based heat sinks.* Applied Thermal Engineering, 2008. **28**(8): p. 1047-1057.

62. Alrashdan, A., A.T. Mayyas, and S. Al-Hallaj, *Thermo-mechanical behaviors of the expanded graphite-phase change material matrix used for thermal management of Li-ion battery packs.* Journal of Materials Processing Technology, 2010. **210**(1): p. 174-179.

63. Yin, H., et al., *Experimental research on heat transfer mechanism of heat sink with composite phase change materials.* Energy Conversion and Management, 2008. **49**(6): p. 1740-1746.

64. Tan, F. and C. Tso, *Cooling of mobile electronic devices using phase change materials.* Applied thermal engineering, 2004. **24**(2): p. 159-169.

65. Hauer, A., et al., *Advanced Thermal Energy Storage through Phase Change Materials and Chemical Reactions–Feasibility Studies and Demonstration Projects.* IEA, Final Report, 2001.

66. Socaciu, L.G., *Thermal energy storage with phase change material.* Leonardo Electronic Journal of Practices and Technologies, 2012(20): p. 75-98.

67. Ismail, K. and J. Henríquez, *Thermally effective windows with moving phase change material curtains.* Applied Thermal Engineering, 2001. **21**(18): p. 1909-1923.

68. Ling, Z., et al., *Experimental and numerical investigation of the application of phase change materials in a simulative power batteries thermal management system.* Applied Energy, 2014. **121**: p. 104-113.

69. Vasiliev, L., et al., *Latent heat storage modules for preheating internal combustion engines: application to a bus petrol engine.* Applied thermal engineering, 2000. **20**(10): p. 913-923.

70. Blüher, P., *Latentwärmespeicher erhöht den Fahrkomfort und die Fahrsicherheit.* Automobiltechnische Zeitschrift, 1991. **93**(10).

71. Mulligan, J., D. Colvin, and Y. Bryant, *Microencapsulated phase-change material suspensions for heat transfer in spacecraft thermal systems.* Journal of spacecraft and rockets, 1996. **33**(2): p. 278-284.

72. Buddhi, D. and L. Sahoo, *Solar cooker with latent heat storage: design and experimental testing.* Energy Conversion and Management, 1997. **38**(5): p. 493-498.

73. Boulard, T., et al., *Performance of a greenhouse heating system with a phase change material.* Agricultural and forest meteorology, 1990. **52**(3): p. 303-318.

74. Linstrom, P. and W. Mallard, *NIST Chemistry WebBook, NIST Standard Reference Database Number 69*. National Institute of Standards and Technology. 2015, Gaithersburg, MD 20899.

75. Buddhi, D., et al., *A simplification of the differential thermal analysis method to determine the latent heat of fusion of phase change materials.* Journal of Physics D: Applied Physics, 1987. **20**(12): p. 1601.

76. Hasan, A., et al., *Characterization of phase change materials for thermal control of photovoltaics using Differential Scanning Calorimetry and Temperature History Method.* Energy Conversion and Management, 2014. **81**: p. 322-329.

77. Mehling, H., et al. *A new measurement and evaluation method for DSC of PCM samples*. in *Proceedings of Effstock-11th International Conference on Energy Storage, Stockholm, Sweden*. 2009.

78. He, B., V. Martin, and F. Setterwall, *Phase transition temperature ranges and storage density of paraffin wax phase change materials.* Energy, 2004. **29**(11): p. 1785-1804.

79. Dolado, P., et al., *Experimental validation of a theoretical model: uncertainty propagation analysis to a PCM-air thermal energy storage unit.* Energy and Buildings, 2012. **45**: p. 124-131.

80. Castellón, C., et al., *Determination of the enthalpy of PCM as a function of temperature using a heat-flux DSC—A study of different measurement procedures and their accuracy.* Int J Energy Res, 2008. **32**(13): p. 1258–1265.

81. Linseis. *User's Manual of Transient Hot Bridge Analyzer THB*. 2013; Available from: http://www.linseis.com. 28 Mar. 2016.

82. Warzoha, R.J., R.M. Weigand, and A.S. Fleischer, *Temperature-dependent thermal properties of a paraffin phase change material embedded with herringbone style graphite nanofibers.* Applied Energy, 2015. **137**: p. 716-725.

83. Saeed, R.M., et al., *Uncertainty of Thermal Characterization of Phase Change Material by Differential Scanning Calorimetry Analysis.* International Journal of Engineering Research & Technology, 2016. **5**(1): p. 405-412.

84. Mehling, H., H. Ebert, and P. Schossig. *Development of standards for materials testing and quality control of PCM*. in *Proceedings of 7th conference on phasechange-materials and slurries. Dinan, Frankreich*. 2006.

85. Vergnaud, J.-M. and J. Bouzon, *Cure of thermosetting resins: modelling and experiments*. 2012: Springer Science & Business Media.

86. Höhne, G., W. Hemminger, and H.-J. Flammersheim, *Differential scanning calorimetry.* Analytical and Bioanalytical Chemistry, 2004. **380**(3): p. 366-367.

87. Rudtsch, S., *Uncertainty of heat capacity measurements with differential scanning calorimeters.* Thermochimica Acta, 2002. **382**(1): p. 17-25.

88. Brazier, D. and N. Grassie, *Developments in Polymer Degradation*. 1987, Applied Science Publishers: London. p. 27.

89. Armand, J. and J. Vergnaud, *Effect of the value of heating rate in DSC on the kinetic parameters, when there is high enthalpy of reaction.* Thermochimica acta, 1988. **131**: p. 15-27.

90. Poel, G.V. and V.B. Mathot, *High-speed/high performance differential scanning calorimetry (HPer DSC): Temperature calibration in the heating and cooling mode and minimization of thermal lag.* Thermochimica Acta, 2006. **446**(1): p. 41-54.

91. Kasap, S.O., *Principles of electronic materials and devices*. 2006: McGraw-Hill.

92. Braga, C.I., M.C. Rezende, and M.L. Costa, *Methodology for DSC calibration in high heating rates.* Journal of Aerospace Technology and Management, 2011. **3**(2): p. 179-192.

93. Armand, J., et al., *Effect of sample size and heating rate on cure reaction of rubber in DSC.* Thermochimica acta, 1986. **108**: p. 345-356.

94. Bouzon, J. and J.-M. Vergnaud, *Cure of thermosetting resins. Modelling and experiments.* Plastics rubber and composites processing and applications, 1992. **18**(5): p. 277-280.

95. Günther, E., et al., *Enthalpy of phase change materials as a function of temperature: required accuracy and suitable measurement methods.* International Journal of Thermophysics, 2009. **30**(4): p. 1257-1269.

96. Pijpers, T.F., et al., *High-speed calorimetry for the study of the kinetics of (de) vitrification, crystallization, and melting of macromolecules.* Macromolecules, 2002. **35**(9): p. 3601-3613.

97. Goli, P., et al., *Graphene-enhanced hybrid phase change materials for thermal management of Li-ion batteries.* Journal of Power Sources, 2014. **248**: p. 37-43.

98. Renteria, J.D., D.L. Nika, and A.A. Balandin, *Graphene thermal properties: applications in thermal management and energy storage.* Applied Sciences, 2014. **4**(4): p. 525-547.

99. Dincer, I. and M. Rosen, *Thermal energy storage: systems and applications*. 2002: John Wiley & Sons.

100. Zhang, L. and G. Shi, *Preparation of highly conductive graphene hydrogels for fabricating supercapacitors with high rate capability.* The Journal of Physical Chemistry C, 2011. **115**(34): p. 17206-17212.

101. Tao, Y., C. Lin, and Y. He, *Preparation and thermal properties characterization of carbonate salt/carbon nanomaterial composite phase change material.* Energy Conversion and Management, 2015. **97**: p. 103-110.

102. Warzoha, R.J., et al. *Experimental characterization of the thermal diffusivity of paraffin phase change material embedded with herringbone style graphite nanofibers*. in *ASME 2012 Heat Transfer Summer Conference collocated with the ASME 2012 Fluids Engineering Division Summer Meeting and the ASME 2012 10th International Conference on Nanochannels, Microchannels, and Minichannels*. 2012. American Society of Mechanical Engineers.

103. Teng, T.-P. and C.-C. Yu, *Characteristics of phase-change materials containing oxide nano-additives for thermal storage.* Nanoscale research letters, 2012. **7**(1): p. 1-10.

104. Zhang, Z., et al., *Thermal energy storage cement mortar containing n-octadecane/expanded graphite composite phase change material.* Renewable energy, 2013. **50**: p. 670-675.

105. Royon, L., G. Guiffant, and P. Flaud, *Investigation of heat transfer in a polymeric phase change material for low level heat storage.* Energy conversion and management, 1997. **38**(6): p. 517-524.

106. Li, M., Z. Wu, and J. Tan, *Heat storage properties of the cement mortar incorporated with composite phase change material.* Applied Energy, 2013. **103**: p. 393-399.

107. Barreneche, C., et al., *Improvement of the thermal inertia of building materials incorporating PCM. Evaluation in the macroscale.* Applied Energy, 2013. **109**: p. 428-432.

108. Félix, M. and J. Aguiar, *Study of a cement mortar with incorporation of PCM microcapsules.* 2009.

109. Cheng, R., et al., *A new method to determine thermophysical properties of PCM-concrete brick.* Applied Energy, 2013. **112**: p. 988-998.

110. Li, X., J.G. Sanjayan, and J.L. Wilson, *Fabrication and stability of form-stable diatomite/paraffin phase change material composites.* Energy and Buildings, 2014. **76**: p. 284-294.

111. Li, H., et al., *Development of thermal energy storage composites and prevention of PCM leakage.* Applied Energy, 2014. **135**: p. 225-233.

112. Khoo, I.-C. and S.-T. Wu, *Optics and nonlinear optics of liquid crystals*. Vol. 1. 1993: World Scientific.

113. Zhang, Y., Y. Su, and X. Ge, *Prediction of the melting temperature and the fusion heat of (quasi-) eutectic PCM.* Journal of China University of Science and Technology, 1994. **25**(4): p. 474-478.

114. Ran, S., et al., *Char barrier effect of graphene nanoplatelets on the flame retardancy and thermal stability of high-density polyethylene flame-retarded by brominated polystyrene.* Journal of Applied Polymer Science, 2014. **131**(15).

115. Tian, H., et al., *Preparation of binary eutectic chloride/expanded graphite as high-temperature thermal energy storage materials.* Solar Energy Materials and Solar Cells, 2016. **149**: p. 187-194.

116. Shin, D. and D. Banerjee, *Enhancement of specific heat capacity of high-temperature silica-nanofluids synthesized in alkali chloride salt eutectics for solar thermal-energy storage applications.* International journal of heat and mass transfer, 2011. **54**(5): p. 1064-1070.

117. Shin, D. and D. Banerjee, *Enhanced specific heat capacity of nanomaterials synthesized by dispersing silica nanoparticles in eutectic mixtures.* Journal of Heat Transfer, 2013. **135**(3): p. 032801.

VITA

Rami Mohammad Reda Saeed was born on June, 1991, in Irbid, Jordan. He received his Bachelor of Science degree in Nuclear Engineering from Jordan University of Science and Technology, Ramtha, Jordan in July 2014. After graduation, he joined Nuclear Engineering department as a graduate student at Missouri University of Science and Technology. He held a Graduate Assistantship under Dr. Joshua P. Schlegel and worked in the field of phase change materials for thermal energy storage. He received his Master of Science in Nuclear Engineering from Missouri University of Science and Technology, Rolla, USA in May, 2016.